

# A Qualitative and Quantitative Mathematical Analysis of Chalcopyrite Disease within Sphalerite

Der Fakultät für Mathematik und Informatik  
der Universität Leipzig  
eingereichte  
**Habilitationsschrift**  
zur Erlangung des akademischen Grades  
doctor rerum naturalium habilitatus  
Dr. rer. nat. habil.

vorgelegt  
von

Dr. Thomas Blesgen  
aus Bonn

Leipzig, den 19. Februar 2005



# Contents

<b>1</b>	<b>Introduction</b>	<b>1</b>
<b>2</b>	<b>Derivation of the Model</b>	<b>5</b>
2.1	The general mathematical approach . . . . .	5
2.2	A purely reactive system . . . . .	8
2.3	The model for chalcopyrite disease . . . . .	9
2.4	Two further models for simulations relying on data bases of the free energy . . . . .	14
2.5	Dimensionality analysis . . . . .	16
2.6	Free energy inequality for the isothermal system . . . . .	18
2.7	The non-isothermal case . . . . .	21
2.8	More general forms of the surface energy . . . . .	23
<b>3</b>	<b>Existence and Uniqueness Results for the derived Models</b>	<b>25</b>
3.1	Preliminaries . . . . .	26
3.2	The weak formulation of the problem . . . . .	27
3.3	A semi-implicit time discretisation . . . . .	28
3.4	Structural Assumptions . . . . .	28
3.5	Existence of solutions to the time discrete scheme . . . . .	29
3.6	Uniform estimates . . . . .	32
3.7	Global existence of solutions for polynomial free energy . . . . .	35
3.8	Uniqueness of the solution . . . . .	36
3.9	Logarithmic free energy . . . . .	39
3.10	Uniform estimates . . . . .	42
3.11	Higher integrability for the logarithmic free energy . . . . .	43
3.12	Global existence of solutions for logarithmic free energies . . . . .	45
3.13	The limit equations . . . . .	47
3.14	Proof of existence of solutions to Model III . . . . .	49

<b>4</b>	<b>Computational Methods</b>	<b>53</b>
4.1	General numerical solution technique . . . . .	54
4.2	A table lookup principle for the free energy . . . . .	56
4.3	The harmonic free energy approximation . . . . .	57
4.4	Free energy computation with GULP . . . . .	60
4.5	Molecular dynamics computations of the free energy . . . . .	68
4.6	Quantum mechanical computations . . . . .	69
<b>5</b>	<b>Numerical Simulations</b>	<b>79</b>
5.1	Verification of the algorithms . . . . .	79
5.1.1	Two simple analytic tests for Model I . . . . .	79
5.1.2	Analysis of the different parts of the entropy . . . . .	81
5.2	The dependence of GULP data on atomistic lattice configurations	82
5.3	Numerical results for Model I . . . . .	84
5.4	Extension of Model I to linear elasticity . . . . .	86
5.5	Finite element computations with the tabulated free energy . . . . .	91
5.6	Free energy minimisation for Model III . . . . .	94
<b>6</b>	<b>Discussion of the Results and Outlook</b>	<b>95</b>
<b>A</b>	<b>Notations</b>	<b>99</b>
<b>B</b>	<b>Mathematical Symbols</b>	<b>102</b>
B.1	Function spaces . . . . .	102
B.2	Vector- and tensor notations . . . . .	103
	<b>References</b>	<b>104</b>

Ce à quoi l'un s'était failli, l'autre est arrivé et ce qui était inconnu à un siècle, le siècle suivant l'a éclairci, et les sciences et les arts ne se jettent pas en moule mais se forment et figurent en les maniant et polissant à plusieurs fois [...] Ce que ma force ne peut découvrir, je ne laisse pas de le sonder et essayer et, en retasant et pétrissant cette nouvelle matière, la remuant et l'eschaufant, j'ouvre à celui qui me suit quelque facilité et la lui rends plus souple et plus maniable. Autant en fera le second au tiers qui est cause que la difficulté ne me doit pas désespérer, ni aussi peu mon impuissance...

Where someone failed, another has succeeded; what was unknown in one century, the next has discovered; science and the arts do not grind themselves into uniformity, but gain shape and regularity by carving and polishing repeatedly [...] What my own strength has not been able to uncover, I cease not from working at and trying out and, by reshaping and solidifying this new material, in moulding and heating it, I bequeathe to him who follows some facility and make it the more supple and malleable for him. The second will do the same for the third, which is why difficulty does not make me despair, nor of my own weakness...

MONTAIGNE, LES ESSAIS

There is a theory that states that whenever someone will find out what the universe is and why it is here, it will instantly disappear and be replaced by something even more bizarre and inexplicable. There is another that states that this has already happened.

DOUGLAS ADAMS



# Chapter 1

## Introduction

In the present work we are concerned with the so-called chalcopyrite disease within sphalerite. This is a well-known and extensively-discussed problem arising in geology. The quantitative description of this process helps to get a precise understanding of the time scales involved of magma ascending from earth's core and might lead to better predictions for earth quakes and volcano eruptions.

Characteristic for chalcopyrite disease is the presence of a mellon-type structure close to the boundary of a rock sample.

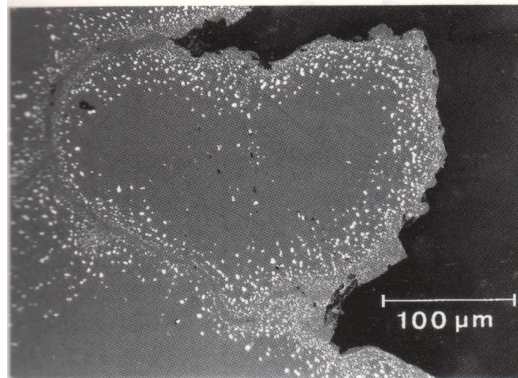


Figure 1.1: Reflecting light image of a rock sample with chalcopyrite disease, black matrix: sphalerite, white grains: chalcopyrite

The common understanding is that these structures develop during a long time period in the range of several hundred thousand years. Since no experimentalist would be so patient, mineralogists studied chalcopyrite disease under altered conditions in the laboratory with increased temperature (kept isothermally between  $T = 550^{\circ}\text{C}$  and  $T = 700^{\circ}\text{C}$ ). The reports of the original experiments are collected in [12] and [13]. By the increase of  $T$  (and sufficiently high sulphur fugacity, see below) the process is accelerated and the characteristic pattern formation is observed after several weeks ( $T = 700^{\circ}$ ) or months ( $T = 550^{\circ}$ ).

In the crystallographic experiment, the sphalerite sample is surrounded by sulphur gas and copper powder is spread at its surface. This setup becomes clear after understanding how the crystal lattice is rearranged.

Chalcopyrite disease is caused by gradients of the chemical potential induced by an increase of external sulphur fugacity. Hereby, the primary  $\text{Fe}^{2+}$  is oxidised to  $\text{Fe}^{3+}$  and reacts with copper diffusing into the Fe-containing sphalerite crystal to chalcopyrite ( $= \text{CuFeS}_2$ ). During the process, gas  $\text{S}^{2-}$  molecules attach to the crystal surface. Since roughly speaking the formation of chalcopyrite phases can only take place after a sufficient amount of Cu has diffused into the matrix, the generic mechanism has been called *diffusion induced segregation* or shortly DIS.

As oxidation is the key to the formation of the chalcopyrite phase, the Fe atoms play a central role as antagonist to copper. If the Fe concentration is below a certain threshold, no DIS will occur. If the sulphur fugacity is weaker, the experiments produce either a simple diffusion front or end up with an alloy, as documented in the reports [13] on further experiments on DIS with the related system  $\text{ZnS-CuInS}_2$ .

Fig. 1.2 shows how the reorganisation of the sphalerite lattice close to the crystal boundary takes place. A more detailed picture of this process will be available in Chapter 4, summarised in particular in Fig. 4.1. The migration of Zn is not displayed in Fig. 1.2. The picture is wrong inasmuch as a perfect structure without impurities is shown, we will come back to this matter later.

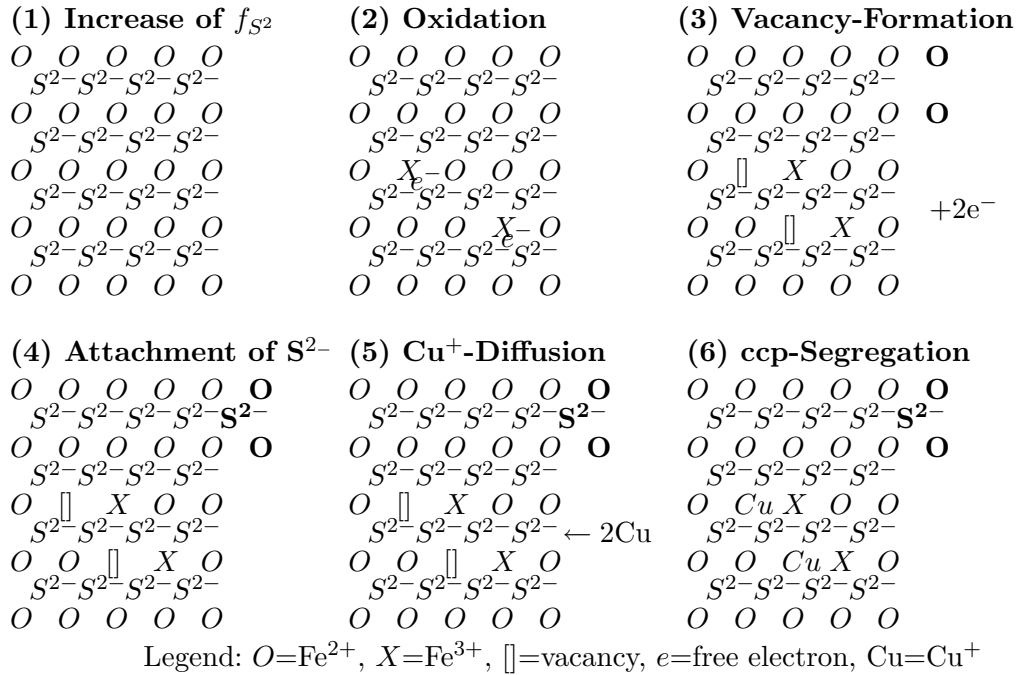


Figure 1.2: The effect of increased sulphur fugacity on the ZnS lattice

The mathematical analysis of chalcopyrite disease presented in this work is based on partial differential equations and a thermodynamical description and will try to understand the physics underlying these examinations with the goal to make simulations close to the ideal experimental conditions. The model developed will represent chalcopyrite disease on a medium spatial scale, the microstructure will not be resolved. The main idea pursued in this work is to insert expressions of the free energy gained from ab initio calculations into (standard) finite element computations and to compare the results to simulations of a continuum thermodynamical model.

Beside this main subject, the thermodynamics of reactive systems undergoing phase changes are studied. Two principal properties of such systems are elaborated that allow to find an expression that generalises the classical reaction formula of systems without phase changes.

The text is organised in the following way. In Chapter 2 the theoretical background of the mathematical approach is set up. In the first place, the main model for chalcopyrite disease within sphalerite as a system of partial differential equations is derived together with a simplified model that corresponds to the level of approximation when ab-initio computations are used. Additionally a dimensionality analysis is performed and the validity of the second law of thermodynamics is shown, also for a generalised non-isothermal model.

Chapter 3 is devoted to an uniqueness and global existence result. The analysis is based on an implicit time discretisation (except for the reaction term that is treated explicitly) and applies direct methods in the calculus of variations. Uniform estimates allow to pass to the limit of the continuous model.

Chapter 4 is an assembly of computation techniques and explains in particular the harmonic approximation, molecular dynamics simulations and finally quantum mechanical computations to get estimated values of the Helmholtz free energy of the real segregation process. Furthermore it shortly summarises the general finite element approach and numerical solution techniques.

The results of several numerical experiments together with some program validations and an analysis of the algorithm are presented in Chapter 5. We finish with a critical evaluation of the results and an outlook.

Acknowledgments:

At this point it is my great pleasure to express my thanks to Prof. S. Luckhaus for several fruitful discussions and to Prof. M. Dove for his support without whom the simulations presented in this work would not have been possible. Furthermore I would like to thank Dr. M. Calleja for his fast help with a particular computer problem.



## Chapter 2

# Derivation of the Model

### 2.1 The general mathematical approach

We aim in this chapter at the discussion of reaction-diffusion equations for a system that simultaneously undergoes phase changes. A simple introduction to reactive systems (without phase changes) can be found in [41], a collection of mathematical models for phase change problems (without reactions) is the excellent text book [71]. In [51], a general theory is developed, but the thermodynamic quantities do not depend on an inner phase parameter  $\chi$ .

The starting point of the mathematical discussion are the reaction-diffusion equations in the general form

$$\partial_t c_i = \operatorname{div}(J_i) + r_i = \left( \sum_l \frac{\partial}{\partial x_l} J_{i,l} \right) + r_i, \quad i = 1, \dots, 4. \quad (2.1)$$

Here,  $c_i = c_i(x, t)$  denotes the relative number of species  $i$ ,  $i = 1, \dots, 4$  per available lattice point at time  $t$  and space point  $x \in \Omega$ ,  $\Omega$  a (time-independent) domain in  $\mathbb{R}^D$ ,  $1 \leq D \leq 3$ . By  $0 < T_0 < \infty$  we denote a stop time and by  $\Omega_{T_0} := \Omega \times (0, T_0)$  a cylinder in space-time.

We introduce the notations

$$c_1 \approx \text{Fe}^{3+}, \quad c_2 \approx \text{Fe}^{2+}, \quad c_3 \approx \text{Cu}^+, \quad c_4 \approx \text{Zn}^{2+}, \quad c_5 \approx \text{vacancies}.$$

$c_1$  satisfies  $c_1 = \frac{N_{\text{Fe}^{3+}}}{N_{\text{Me}}}$ , where  $N_{\text{Fe}^{3+}}$  is the number of  $\text{Fe}^{3+}$  atoms and  $N_{\text{Me}}$  is the number of metal ion sites. Similar relationships hold for  $c_2$ ,  $c_3$  and  $c_4$ . We will not model the attachment of S molecules at the lattice surface and assume that the concentration of S is identically 0.5. Sometimes, we will denote this constant by  $c_S$ . It is an essential property of this formulation that there is no equation for  $c_5$ , but the vacancy concentration is obtained implicitly by the conservation of mass:  $c_5 = 1 - \sum_{i=1}^4 c_i - c_S = \frac{1}{2} - \sum_{i=1}^4 c_i$ .

In Eq. (2.1),  $r_i$  denote the reaction terms and  $J_i$  the fluxes of metal ions of species  $i$ . The reaction terms model the jumps of the electrons, see the reaction scheme (2.20). A first ansatz is  $r = (r_1, -r_1, 0, 0)$  and

$$r_1 = k(c_2^2 - \kappa c_1 c_e),$$

where  $k > 0$  and  $k\kappa > 0$  are the reaction rates and  $c_e$  denotes the electron density. If we assume that all sulphur positions are occupied by  $S^{2-}$ , by the condition of electric neutrality we can compute

$$\begin{aligned} c_e &= 2c_S - 3c_1 - 2c_2 - c_3 - 2c_4 \\ &= 1 - 2(c_1 + c_2 + c_3 + c_4) - c_1 + c_3 \\ &= 2c_5 - c_1 + c_3. \end{aligned} \quad (2.2)$$

In the presence of phase transitions the rates may not be chosen to be constants. This will be the topic of later sections.

The constitutive relation for the mass fluxes is assumed to be of the isotropic Onsager form

$$J_i = \sum_{j=1}^4 L_{ij} \nabla \mu_j, \quad 1 \leq i \leq 4, \quad (2.3)$$

where  $L$ , the mobility, is a symmetric positive semi-definite  $4 \times 4$  tensor and

$$\mu_j = \frac{\partial f}{\partial c_j}$$

denotes the chemical potential. To simplify the existence theory of Chapter 3 we will assume in the sequel that  $L$  is positive definite.

For most of this work, we will consider the case where the temperature  $T$  is held constant. This reflects the conditions established in the mineralogical experiments as explained in the introduction. A short discussion of the non-isothermal situation is collected in Section 2.7.

Let  $f$  denote the Helmholtz free energy density of the system, consisting of  $f_1, f_2$  with  $f_1$  for chalcopyrite,  $f_2$  for sphalerite. Hence, the two different phases or lattice orders are characterised by two different free energies, and  $f$  is the convex hull of  $f_1$  and  $f_2$ .

For order-disorder phase transitions, we make the first ansatz

$$f_l = f_l(c) = k_B T \sum_{i=1}^5 \beta_i^l c_i \ln c_i + \sum_{i=1}^3 E_i c_i + \left( \sum_{i=1}^4 \alpha_i c_i \right)^2, \quad l = 1, 2. \quad (2.4)$$

The elastic coefficients  $\alpha_i$  do not change for both phases, only the  $\beta_i^l$  differ. The convex terms  $c_i \ln c_i$  are motivated by considerations from statistical mechanics on the system entropy by counting the different configurations. The expression  $\sum_{i=1}^3 E_i c_i$  is an enthalpic term and a consequence of the presence of the Fe-reaction. This is thoroughly discussed in the subsequent section.

The expression  $(\sum_{i=1}^4 \alpha_i c_i)^2$  is a consequence of Hooke's law. The constants  $\alpha_i$  correspond to the ion radii and measure the volume response when replacing  $Zn^{2+}$  by other metal ions. In (2.4), the  $\beta_i^1, \beta_i^2$  are positive constants and  $k_B$  is the Boltzmann constant.

The ansatz  $\sum_{i=1}^5 c_i \ln c_i$  of Formula (2.4) is well known in the material sciences. It is true whenever the transitions are random pairwise interactions. For the crystallographic experiments, this has been confirmed for the high temperature transitions of chalcopyrite, [12]. Furthermore Eq. (2.4) is a very reasonable term

for a numerical computation, since (2.4) implies infinite slope of  $Df_l$  if one component  $c_j$  approaches 0 or 1. This guarantees, see [59],

$$c_j \in (0, 1) \quad \text{in } \Omega, t > 0 \quad (2.5)$$

and  $c_j$  has physical meaning. As there is no maximum principle for systems of equations, without the logarithmic terms in (2.4), the condition (2.5) may be violated even if  $c_j \in (0, 1)$  holds for  $t = 0$ .

At this stage, a control mechanism for the segregation process is added. The following principle is well known. We introduce a function  $\chi = \chi(x, t) \in [0, 1]$ , in the following called 'phase parameter', that measures the volume fraction of the chalcopryrite phase; e.g.  $\chi(x_0, t_0) = 0$  means that for  $t = t_0$  in  $x_0 \in \Omega$  only the sphalerite phase is present,  $\chi(x_0, t_0) = \frac{1}{2}$  that the system is in  $x_0$  in an intermediate state with no dominant phase.

Let  $\gamma > 0$  be a small constant, denoting the square of the thickness of the interface between sphalerite and chalcopryrite phase. We define the density of the mixing entropy  $s_M$  as

$$s_M(\chi) = W(\chi) + \frac{\gamma}{2} |\nabla \chi|^2, \quad (2.6)$$

with

$$W(\chi) := \chi \ln \chi + (1 - \chi) \ln(1 - \chi). \quad (2.7)$$

Since  $f := \text{conv}(f_1, f_2)$ , we will consider  $f$  as the convex combination of  $f_1$  and  $f_2$ . Because  $s_M$  is subtracted from the entropy density  $s$ , the thermodynamic relation  $f = e - Ts$  thus implies

$$f(c, \chi) := \chi f_1(c) + (1 - \chi) f_2(c) + T s_M(\chi). \quad (2.8)$$

The phase parameter  $\chi$  is governed by the modified Allen-Cahn equation

$$\tau \partial_t \chi = -\partial_\chi \left( \frac{f}{T} \right) = \gamma \Delta \chi - \omega(c, \chi), \quad (2.9)$$

where  $\gamma \Delta \chi$  comes from the first variation of  $-\int_\Omega \frac{\gamma}{2} |\nabla \chi|^2$  w.r.t.  $\chi$  and  $\tau$  is a scaling parameter to adjust the different time scales between mass diffusion and growing of the chalcopryrite phase, see also Eq. (2.39).

The driving force  $\omega$  in (2.9) is given by

$$\omega(c, \chi) := \ln \left( \frac{\chi}{1 - \chi} \right) + m(c). \quad (2.10)$$

The value  $m(c)$  accounts for the growing of chalcopryrite in copper rich regions and is gained implicitly by  $\tau \partial_t \chi = -\partial_\chi (f/T)$ . Since so far the final formula for  $f$  has not been derived, we will postpone the discussion of this term and of the mechanism responsible for the growing of chalcopryrite in copper rich regions. The final definition of  $\omega$  is given in (2.28).

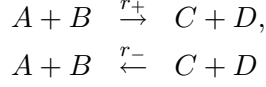
We want to incorporate the electron jumps by including reaction terms in the model. Particular care must be taken because the reactions are represented in the free energy by enthalpic terms which in turn modify the chemical potentials. Especially there is an intrinsic connection between the form of the reaction terms, the ansatz for the free energy and the second law of thermodynamics, which simplifies for isothermal systems to showing that  $\partial_t F \leq 0$ , where  $F = \int_\Omega f$ .

All this will become clear after the discussion of the following toy problem.

## 2.2 A purely reactive system

We consider a purely reactive system without diffusion.

Let the domain  $\Omega$  comprise of substances  $A$ ,  $B$ ,  $C$  and  $D$  subject to the reactions



with positive rates  $r_+$ ,  $r_-$ . Let  $\tilde{c}_1$ ,  $\tilde{c}_2$ ,  $\tilde{c}_3$  and  $\tilde{c}_4$  denote the concentration of substances  $A$ ,  $B$ ,  $C$  and  $D$  where we assume

$$\sum_{i=1}^4 \tilde{c}_i = 1. \quad (2.11)$$

In the language of partial differential equations, as carefully explained in the text book [41], the above reactions can be rewritten in the form

$$\partial_t \tilde{c}_1 = \partial_t \tilde{c}_2 = -r_+ \tilde{c}_1 \tilde{c}_2 + r_- \tilde{c}_3 \tilde{c}_4, \quad (2.12a)$$

$$\partial_t \tilde{c}_3 = \partial_t \tilde{c}_4 = +r_+ \tilde{c}_1 \tilde{c}_2 - r_- \tilde{c}_3 \tilde{c}_4. \quad (2.12b)$$

From statistical mechanics we infer

$$r_+ = \exp\left(\frac{\tilde{E}_1 + \tilde{E}_2 - \tilde{E}_S}{k_B T}\right), \quad (2.13a)$$

$$r_- = \exp\left(\frac{\tilde{E}_3 + \tilde{E}_4 - \tilde{E}_S}{k_B T}\right), \quad (2.13b)$$

where  $\tilde{E}_1 + \tilde{E}_2$  is the energy level before the reaction  $A + B \rightarrow C + D$ ,  $\tilde{E}_3 + \tilde{E}_4$  the energy level after the reaction.  $\tilde{E}_S$  is the activation energy or saddle point energy that has to be exceeded to start the reaction.

For the free energy we make the ansatz

$$\tilde{F}(\tilde{c}) = \int_{\Omega} k_B T \sum_{i=1}^4 \tilde{c}_i \left( \ln \tilde{c}_i + \frac{\tilde{E}_i}{k_B T} \right) \quad (2.14)$$

where the last term defines the system enthalpy, see for instance [35].

Now we will show the following properties of  $\tilde{F}$ :

$$\partial_t \tilde{F}(\tilde{c}(t)) = 0 \quad \text{iff} \quad \partial_t \tilde{c}_i = 0, \quad 1 \leq i \leq 4, \quad (2.15a)$$

$$\partial_t \tilde{F}(\tilde{c}(t)) \leq 0, \quad (2.15b)$$

$$\tilde{F}(\tilde{c}(t)) \text{ is critical} \quad \text{iff} \quad \partial_t \tilde{c}(t) = 0. \quad (2.15c)$$

In order to show (2.15a), (2.15b), after setting

$$R := -r_+ \tilde{c}_1 \tilde{c}_2 + r_- \tilde{c}_3 \tilde{c}_4 = \partial_t \tilde{c}_1 = \partial_t \tilde{c}_2 = -\partial_t \tilde{c}_3 = -\partial_t \tilde{c}_4,$$

elementary computations yield

$$\begin{aligned} \partial_t \tilde{F}(\tilde{c}) &= \int_{\Omega} k_B T R \left[ \ln \left( \frac{\tilde{c}_1 \tilde{c}_2}{\tilde{c}_3 \tilde{c}_4} \right) + \frac{\tilde{E}_1 + \tilde{E}_2 - \tilde{E}_S}{k_B T} - \frac{\tilde{E}_3 + \tilde{E}_4 - \tilde{E}_S}{k_B T} \right] \\ &= \int_{\Omega} k_B T R \ln \left[ \left( \frac{\tilde{c}_1 \tilde{c}_2}{\tilde{c}_3 \tilde{c}_4} \right) \left( \frac{r_+}{r_-} \right) \right]. \end{aligned} \quad (2.16)$$

We observe

$$\ln\left(\frac{\tilde{c}_1\tilde{c}_2 r_+}{\tilde{c}_3\tilde{c}_4 r_-}\right) = 0 \quad \text{iff} \quad \tilde{c}_1\tilde{c}_2 r_+ = \tilde{c}_3\tilde{c}_4 r_-$$

and together with (2.16) we find (2.15a).

Eq. (2.16) directly implies the free energy inequality (2.15b). To see this, let us consider the two mutual exclusive cases:

$$(A) \quad R \geq 0 \quad \iff \quad \tilde{c}_3\tilde{c}_4 r_- \geq \tilde{c}_1\tilde{c}_2 r_+ \quad \iff \quad \ln\left(\frac{\tilde{c}_1\tilde{c}_2 r_+}{\tilde{c}_3\tilde{c}_4 r_-}\right) \leq 0,$$

$$(B) \quad R < 0 \quad \iff \quad \tilde{c}_3\tilde{c}_4 r_- < \tilde{c}_1\tilde{c}_2 r_+ \quad \iff \quad \ln\left(\frac{\tilde{c}_1\tilde{c}_2 r_+}{\tilde{c}_3\tilde{c}_4 r_-}\right) > 0.$$

This discussion reveals the natural structure of the problem,

$$((\ln(\tilde{c}_1\tilde{c}_2 r_+) - \ln(\tilde{c}_3\tilde{c}_4 r_-))(\tilde{c}_3\tilde{c}_4 r_- - \tilde{c}_1\tilde{c}_2 r_+) \leq 0, \quad (2.17)$$

from which we unconditionally infer  $\partial_t \tilde{F}(\tilde{c}(t)) \leq 0$ .

Of course, this canonical structure of the problem goes along with Ansatz (2.14) for the free energy. Hence, the definition of the free energy, the definition of the reaction terms and the estimate of  $\partial_t \tilde{F}$  have to be discussed as a whole!

A critical point  $\tilde{c}$  of  $\tilde{F}$  is characterised by

$$\ln \tilde{c}_l + \frac{\tilde{E}_l}{k_B T} + 1 = 0 \quad \text{for} \quad 1 \leq l \leq 4. \quad (2.18)$$

This implies  $\partial_t \tilde{c}_i = 0$ ,  $1 \leq i \leq 4$  because from (2.18) it follows with (2.13)

$$\ln(\tilde{c}_1\tilde{c}_2 r_+) = -2, \quad (2.19a)$$

$$\ln(\tilde{c}_3\tilde{c}_4 r_-) = -2 \quad (2.19b)$$

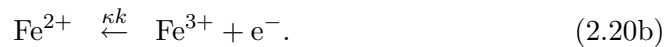
and when subtracting (2.19b) from (2.19a) we find

$$\ln\left(\frac{\tilde{c}_1\tilde{c}_2 r_+}{\tilde{c}_3\tilde{c}_4 r_-}\right) = 0.$$

The last identity implies at once  $\partial_t \tilde{c}_i = 0$ ,  $1 \leq i \leq 4$ . The other implication in (2.15c) is shown similarly.

## 2.3 The model for chalcopyrite disease

Eq. (2.17) reveals the underlying structure of reaction-diffusion equations and we are now in the position to discuss the reaction terms and give a complete description of the model. The swift jumps of the electrons are integrated into the model by two reactions which are



Here,  $\text{e}^-$  is a free lattice electron and  $k$ ,  $\kappa k$  are reaction rates. A formula for  $c_e$  has already been found with (2.2).

If we follow another time the standard approach to model the reactions (2.20) analogous to Eq. (2.12), we end up with

$$r_1 = k(c_2^2 - \kappa c_1 c_e). \quad (2.21)$$

Unfortunately, this is wrong in our case! For the vindication of the inventors of this formula it should be said that (2.21) was not stated for reactive systems that simultaneously undergo phase changes. With the knowledge of the general structure (2.17) we can obtain a consistent formulation of  $r$  that generalises (2.21). In this generalisation, the rates will also depend on  $\chi$ .

Before we can find the final reaction formula, two further modifications of the model are in place. First we remind that the oxidation of Fe is caused by swift shifts of the electrons and occurs thus much faster than any other process, i.e. faster than diffusion. Hence, it is reasonable to assume that this oxidation is instantaneous. The best way to mathematically formulate the reaction term is by introducing a fast variable

$$d_1 = c_1$$

that for fixed  $c_1 + c_2$  describes the free electrons, introducing the slow variables

$$d_2 = c_1 + c_2, \quad d_3 = c_3, \quad d_4 = c_4$$

and by splitting System (2.1) asymmetrically into one stationary elliptic equation for  $d_1$  and three time dependent parabolic equations for  $d_2$ ,  $d_3$  and  $d_4$ .

Even though the formulation in  $d$  variables is the most natural one for the reaction term, we will not use it here because it is somewhat clumsy for the other expressions, in particular with regard to  $(d_2 - d_1) \ln(d_2 - d_1)$  in the definition of  $f$ . At least we will replace the equation for  $c_1$  by a stationary elliptic equation.

Secondly, due to electric neutrality, we postulate

$$c_5 = \frac{1}{2}c_1. \quad (2.22)$$

This condition was found experimentally in [14] long before a mathematical model had been developed. Eq. (2.22) is the key to finding a consistent formulation for the reaction term. There is one difficulty here because (2.22) tells us that the movement of the vacancies is on the same fast time scale as the movement of the free electrons. We will bypass this problem by demanding  $\partial_t c_5 = 0$  in the derivation of the reaction term in (2.26). All crystallographic measurements verify Relation (2.22), but the quick electron jumps are beyond the resolution horizon of today's methods.

As main consequence of (2.2) and (2.22) we find

$$c_e = c_3. \quad (2.23)$$

To end up with the reaction terms having the same structure as in (2.17), the logarithms have to have the same factors. Hence we assume

$$\beta_1^l + \frac{\beta_5^l}{2} = \beta_2^l = \beta_3^l = \beta_4^l =: b^l, \quad l = 1, 2.$$

The final form of the free energy (2.4) is thus

$$f_l(c) = k_B T b^l \sum_{i=1}^4 c_i \ln c_i + \sum_{i=1}^3 c_i E_i + \left( \sum_{i=1}^4 \alpha_i c_i \right)^2, \quad l = 1, 2. \quad (2.24)$$

Combined, (2.8) and (2.24) define the free energy  $F$ .

$$\begin{aligned} F(c, \chi) &= \int_{\Omega} f(c, \chi) \\ &= \int_{\Omega} \left[ k_B T b_{\chi} \left( \sum_{i=1}^4 c_i \ln c_i \right) + \sum_{i=1}^3 c_i E_i + \left( \sum_{i=1}^4 \alpha_i c_i \right)^2 \right. \\ &\quad \left. + \frac{\gamma T}{2} |\nabla \chi|^2 + T W(\chi) \right]. \end{aligned} \quad (2.25)$$

Here and henceforth we use the abbreviation  $b_{\chi} := \chi b^1 + (1 - \chi) b^2$ .

The rates fulfill

$$\begin{aligned} r_+ &= k\kappa = \exp\left(\frac{E_1 + E_3 - E_S}{k_B T}\right), \\ r_- &= k = \exp\left(\frac{2E_2 - E_S}{k_B T}\right). \end{aligned}$$

By a handwaving argument, we can give a quick motivation for the correct reaction term by considering again a purely reactive system, this time with phase changes. If we consider the oxidation process alone (without diffusion!) we have

$$\partial_t c_4 = \partial_t c_5 = 0 \quad (2.26)$$

and from  $\partial_t c_1 = \partial_t c_3$  and  $\sum_{i=1}^5 c_i = 1$  we infer  $\partial_t c_2 = -2\partial_t c_1$ . It is emphasised that  $\partial_t c_5 = 0$  tells us about the different time scales of oxidation and movement of vacancies. With these constraints we compute  $\partial_t F(c(t), \chi(t))$  for the free energy (2.25), where we can drop  $(\sum_{i=1}^4 \alpha_i c_i)^2$  (the estimation of this term is possible in the same way as in Section 2.6 under the natural assumption (2.50)) on the ion radii.

We find

$$\begin{aligned} \partial_t F(c(t), \chi(t)) &= \int_{\Omega} \left[ k_B T b_{\chi} \partial_t c_1 \ln \left( \frac{c_1 c_3}{c_2^2} \right) \right. \\ &\quad \left. + \frac{E_1 + E_3 - E_S}{k_B T} - \frac{2E_2 - E_S}{k_B T} - (\partial_t \chi)^2 \right] \\ &= \int_{\Omega} \left[ k_B T b_{\chi} \partial_t c_1 \ln \left( \frac{c_1 c_3 (r_+)^{1/b_{\chi}}}{c_2^2 (r_-)^{1/b_{\chi}}} \right) - (\partial_t \chi)^2 \right]. \end{aligned}$$

The consistent form of the reaction term that replaces (2.21) is hence

$$r_1 = r_3 = -\frac{1}{2} r_2 = (k)^{1/b_{\chi}} \left( c_2^2 - \kappa^{1/b_{\chi}} c_1 c_3 \right), \quad r_4 = 0. \quad (2.27)$$

$b^1$  and  $b^2$  should be in the magnitude of 1 and for  $b^1 = b^2$  there would be no  $\chi$  dependence. For  $b^1 = b^2 = 1$  we fall back to standard formulas of the reaction term.

A precise justification of (2.27) will be given in Section 2.6.

It remains to discuss the control mechanism for the chalcopyrite phase. Definition (2.25) together with  $\tau\partial_t\chi = -\partial_\chi(f/T) = \gamma\Delta\chi - \omega(c, \chi)$  gives rise to the setting

$$\omega(c, \chi) = W'(\chi) + k_B(b^2 - b^1) \left( \sum_{i=1}^4 c_i \ln c_i + \bar{\alpha} \right). \quad (2.28)$$

Here,  $\bar{\alpha} > 0$  is a temperature-dependent constant. Additive constants occur in (2.25) because one can only measure the change  $\delta F$  of  $F$  when varying a quantity  $q$ , commonly temperature or volume, within some interval  $(q_0, q_1)$ , finding the expression  $\int_{q_0}^{q_1} \delta F$  for  $F$ .

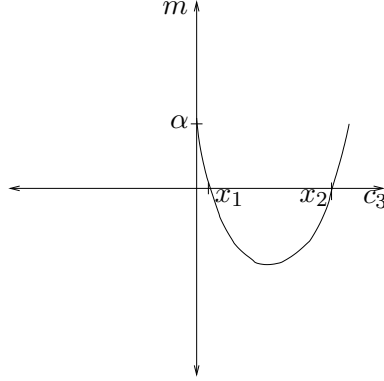


Figure 2.1: Plot of  $m(c_3)$

To understand the principle of the control mechanism, we first freeze  $c_1$ ,  $c_2$  and  $c_4$  and consider

$$\omega(c_3, \chi) = W'(\chi) + m(c_3)$$

with

$$m(c_3) = \beta c_3 \ln c_3 + \alpha$$

for constants  $\alpha > 0, \beta > 0$ , see Fig. 2.1.

The mechanism thus obtained is similar to the one commonly used in phase field models, see [46], where  $c_3$  plays the role of temperature. From convexity of  $m(c_3)$  and from the magnitude of  $\alpha$  and  $\beta$ , we get the existence of  $x_1, x_2 \in (0, 1)$ ,  $x_1 < x_2$  with  $m(c_3) > 0$  for  $c_3 \in (0, x_1) \cup (x_2, 1)$  and  $m(c_3) < 0$  for  $c_3 \in (x_1, x_2)$ . Consequently for  $c_3 < x_1$ , the sphalerite phase is preferred, whereas for  $x_1 < c_3 < x_2$ , chalcopyrite can form. In practice, the branch  $c_3 > x_2$  is never reached, and the chalcopyrite phase once it has formed does not destabilise at a later time.

The expression (2.28) is symmetric w.r.t. the variables  $c_1, \dots, c_4$  and so the mechanism just explained also applies to the other variables. Yet there is unsymmetry here which comes from the initial values for  $c$  and from the constraint  $\frac{3}{2}c_1 + c_2 + c_3 + c_4 = \frac{1}{2}$ . The penetration of  $c_3$  into the crystal causes for suitable  $\bar{\alpha}$  a change of sign of  $\sum_i c_i \ln c_i - \bar{\alpha}$  and consequently the chalcopyrite phase becomes preferable.

We will quickly determine possible values for  $\bar{\alpha}$ . We have to solve

$$\sum_{i=1}^4 c_i \ln c_i \rightarrow \max / \min$$

subject to

$$\frac{3}{2}c_1 + c_2 + c_3 + c_4 = \frac{1}{2}.$$

We introduce a Lagrange multiplier  $\lambda \in \mathbb{R}$ , define

$$h(c, \lambda) := \sum_{i=1}^4 c_i \ln c_i + \lambda \left( \frac{3}{2}c_1 + c_2 + c_3 + c_4 - \frac{1}{2} \right),$$

and search for the unconstrained extremals of  $h$  in  $\mathbb{R}^5$ . We find at once that every extremal point  $(c_1, c_2, c_3, c_4, \lambda)$  satisfies  $c_2 = c_3 = c_4 =: \hat{c}$  and  $c_1 + 2\hat{c} = \frac{1}{3}$ . Additionally, a short computation yields that  $h$  attains its extremal values on the boundary of the set of feasible  $(c_1, \hat{c})$ ,

$$\left\{ (c_1, \hat{c}) \mid \frac{3}{2}c_1 + 3\hat{c} = \frac{1}{2}, c_1 + 2\hat{c} = \frac{1}{3} \right\}.$$

Therefore,  $h(c_{\max}, \lambda_{\max}) = -\frac{\ln(3)}{3} \approx -0.366$  and  $h(c_{\min}, \lambda_{\min}) = -\frac{\ln(6)}{2} \approx -0.896$ , where  $c_{\max} = (\frac{1}{3}, 0, 0, 0)$  and  $c_{\min} := (0, \frac{1}{6}, \frac{1}{6}, \frac{1}{6})$  are the extremals of  $h$ . A reasonable parameter range for  $\bar{\alpha}$  is hence  $\bar{\alpha} \in (\frac{\ln 3}{3}, \frac{\ln 6}{2})$ . The final value of  $\bar{\alpha}$  for the numerical computations will be chosen dependent on the initial values. The sign of  $b^2 - b^1$  determines which of the two phases is preferable for small concentrations of  $c_3$ . Here only the positive sign is physical.

At this point the derivation of the model is complete.

Find for  $t \geq 0$  the vector  $c = (c_1, c_2, c_3, c_4)$  and  $\chi$  such that in  $\Omega \subset \mathbb{R}^D$  for  $t > 0$

$$0 = \operatorname{div} \left( \sum_{j=1}^4 L_{1j} \nabla \mu_j \right) + k^{1/b\chi} (c_2^2 - (\kappa)^{1/b\chi} c_1 c_3), \quad (2.29a)$$

$$\partial_t c_i = \operatorname{div} \left( \sum_{j=1}^4 L_{ij} \nabla \mu_j \right) + r_i(c, \chi), \quad i = 2, 3, 4, \quad (2.29b)$$

$$\mu_i = \frac{\partial f}{\partial c_i}(c, \chi), \quad 1 \leq i \leq 4, \quad (2.29c)$$

$$\tau \partial_t \chi = \gamma \Delta \chi - \omega(c, \chi) \quad (2.29d)$$

and for  $t = 0$ ,  $x \in \Omega$

$$c_i(x, 0) = c_{0i}(x), \quad i = 2, 3, 4 \quad (2.29e)$$

$$\chi(x, 0) = \chi_0(x) \quad (2.29f)$$

and for  $t > 0$ ,  $x \in \partial\Omega$

$$\partial_\nu \chi = 0, \quad (2.29g)$$

$$c_i = g_i, \quad 1 \leq i \leq 4, \quad (2.29h)$$

$$\mu_i = h_i, \quad 1 \leq i \leq 4 \quad (2.29i)$$

with given Dirichlet data  $g = (g_1, \dots, g_4)$  and  $h = (h_1, \dots, h_4)$  defined on  $\partial\Omega$ .

As stated before,  $f$  is defined as the integrand of (2.25),  $r_i$  by (2.27) and  $\omega$  by (2.28). Sometimes, in the sequel we will refer to (2.29) as Model I.

Instead of condition (2.29i) we could impose

$$\partial_\nu J_i = 0 \quad \text{on } \partial\Omega, \quad 1 \leq i \leq 4, \quad (2.30)$$

the natural boundary conditions associated to the minimisation problem of the free energy functional, where the fluxes  $J_i$  are defined according to (2.3). Condition (2.29g) may be replaced by a Dirichlet boundary condition.

Relation (2.22) and, as a consequence, the condition  $\frac{3}{2}c_1 + c_2 + c_3 + c_4 = \frac{1}{2}$  allows to drop the equation for  $c_4$  for the numerical treatment of (2.29).

## 2.4 Two further models for simulations relying on data bases of the free energy

In later parts of this work we want to apply extensively the harmonic approximation and to some extent molecular dynamics (MD) simulations to get estimated values for the free energy of the real physical system. Both methods have in common that they can only compute equilibrium states of the free energy and that they will not be able to resolve free lattice electrons and vacancies (but the methods will predict shifts of certain lattice atoms on the atomistic scale). This implies several modifications to Model (2.29) that will be presented now.

Since the electronic potentials cannot be resolved, there will be no reaction term. To remain as compatible with the notations of Model I as possible we suppress the first index  $c_1$  of  $c$  and introduce as variables

$$c_2 \approx \text{Fe}, \quad c_3 \approx \text{Cu}, \quad c_4 \approx \text{Zn}, \quad \chi \approx \text{volume fraction of chalcopyrite phase.}$$

The conservation of mass reads now  $\sum_{i=2}^4 c_i \equiv \frac{1}{2}$  or equivalently

$$c = (c_2, c_3, c_4) \in \Sigma := \left\{ c_2 + c_3 + c_4 \equiv \frac{1}{2} \right\}.$$

We will use the same notations,  $c$  for the concentration vector and  $\Sigma$  for the simplex, as in Model I even though they have now a different meaning. From the context it will always be clear which definition has to be chosen.

For the theoretical free energy density of phase  $l$  we get according to (2.24) with appropriate  $\alpha_i, b^l$

$$f_l(c) = f_l(c_2, c_3, c_4) = b^l \sum_{i=2}^4 c_i \ln c_i + \left( \sum_{i=2}^4 \alpha_i c_i \right)^2, \quad l = 1, 2$$

but typically for this model,  $f$  is not given by a formula but is obtained from ab-initio computations. The results of these computations are stored in huge data bases. To distinguish between a theoretical formula, the free energy density of phase  $l$  gained from the harmonic approximation or MD simulations will be denoted by  $f^l$ .

The existence and uniqueness results of Chapter 3 will be formulated for Model I, but simplifications of the proofs for Model I yield the corresponding existence and uniqueness results for Model II.

The Allen-Cahn equation is replaced by

$$\tau \partial_t \chi = -\partial_\chi(f/T) = \frac{f^2(c) - f^1(c)}{T} + \gamma \Delta \chi + \ln(\chi/(1-\chi)).$$

The logarithmic expression  $\ln(\chi/(1-\chi))$  is needed in order to guarantee  $0 < \chi < 1$  and makes sure that  $\chi$  has physical meaning.

With the above changes we arrive at the following model which we later on refer to as Model II.

Find for  $t \geq 0$  the concentration vector  $c = (c_2, c_3, c_4)$  and  $\chi$  such that in  $\Omega \subset \mathbb{R}^D$  for  $t > 0$

$$\partial_t c_i = \operatorname{div} \left( \sum_{j=2}^4 L_{ij} \nabla \mu_j \right), \quad i = 2, 3, 4, \quad (2.31a)$$

$$\mu_i = \chi \frac{\partial f^1}{\partial c_i}(c) + (1-\chi) \frac{\partial f^2}{\partial c_i}(c), \quad i = 2, 3, 4, \quad (2.31b)$$

$$\tau \partial_t \chi = \gamma \Delta \chi + \frac{f^2(c) - f^1(c)}{T} + \ln(\chi/(1-\chi)), \quad (2.31c)$$

and for  $t = 0$ ,  $x \in \Omega$

$$c_i(x, 0) = c_{0i}(x), \quad i = 2, 3, 4; \quad \chi(x, 0) = \chi_0(x) \quad (2.31d)$$

and for  $t > 0$ ,  $x \in \partial\Omega$

$$\partial_\nu \chi = 0, \quad (2.31e)$$

$$c_i = g_i, \quad 2 \leq i \leq 4, \quad (2.31f)$$

$$\mu_i = h_i, \quad 2 \leq i \leq 4. \quad (2.31g)$$

In Section 4.2, especially with Eq. (4.7), it will be explained how the derivatives  $\frac{\partial f^i}{\partial c_i}(c)$  are computed.

The major theoretical results, in particular the free energy inequality as well as the proof of existence and uniqueness in Chapter 3 will be formulated and proved for Model I, but with very obvious modifications these statements and proofs will also hold for Model II.

Model II still has two disadvantages. Firstly, as a consequence of the Allen-Cahn equation, mushy regions occur. This means there are points in  $\Omega$  that cannot be clearly related to one of the two phases. Secondly, in Eq. (2.31c) any term of the form  $\alpha \ln(\chi/(1-\chi))$  with positive  $\alpha$  may be chosen.

A different formulation that avoids these difficulties is available within the framework of functions of bounded variation  $BV(\Omega)$ , see [76], [34], [68], and consists in replacing (2.31c) by the minimisation ansatz

$$F(c, \chi) = \min_{\tilde{\chi} \in V} F(c, \tilde{\chi}) \quad (2.32)$$

where

$$V := \{\tilde{\chi} \in BV(\Omega) \mid \tilde{\chi}(1-\tilde{\chi}) = 0 \text{ a.e. in } \Omega\} \quad (2.33)$$

and

$$F(c, \tilde{\chi}) := \int_{\Omega} \gamma |\nabla \tilde{\chi}| + \int_{\Omega} (\tilde{\chi} f^1(c) + (1-\tilde{\chi}) f^2(c)). \quad (2.34)$$

The general formalism of this model for a crystal subject to possibly non-linear deformations is introduced in [1]. A restriction of the model in [1] to the special case of linear elasticity is analysed numerically in [17] and the existence theory is treated in [74].

The system (2.31) with (2.31c) replaced by (2.32) and the condition  $\chi \in H^{1,2}(\Omega)$  replaced by  $\chi \in V$  is later on called Model III.

## 2.5 Dimensionality analysis

In this section it is explained how the dimensional physical equations are transformed to a non-dimensional form. This can be done elementary. We carry out this transformation for three space dimensions and Model I, the changes for other dimensions and the other models are straightforward.

One refers a physical parameter (in the sequel marked with a ') to a reference value (marked with a subscript 0) and obtains the dimensionless data. For the space coordinate  $x$  we have for instance

$$x = \frac{x'}{x_0}.$$

The dimensionless value  $x$  refers here to the scale  $x_0$  (which is the reference value in this case), the characteristic length of the geometry.

In particular we set

$$\begin{aligned} x &= \frac{x'}{x_0}, & y &= \frac{y'}{x_0}, & z &= \frac{z'}{x_0}, & t &= \frac{t'}{t_0}, & T &= \frac{T'}{T_0}, \\ c &= \frac{c'}{c_0}, & L &= \frac{L'}{L_0}, & \kappa &= \frac{\kappa'}{\kappa_0}, & k &= \frac{k'}{k_0}, & \gamma &= \frac{\gamma'}{\gamma_0}, \\ E &= \frac{E'}{E_0}, & F &= \frac{F'}{F_0}, & f &= \frac{f'}{f_0}, & e &= \frac{e'}{e_0}, & s &= \frac{s'}{s_0}. \end{aligned}$$

We use SI-units and write the physical dimensions in brackets [...]. We need the relationships

$$F_0 = [kg \cdot m \cdot s^{-2}], \tag{2.35}$$

$$E_0 = [kg \cdot m^2 \cdot s^{-2}]. \tag{2.36}$$

(2.35) follows from Newton's equation  $F = ma$  stating the force needed to apply an acceleration  $a$  to an object with mass  $m$  and (2.36) follows from  $E = Fd$  describing the work done by a force  $F$  acting along a direction  $d$ . Furthermore (2.35) implies for  $f$

$$f_0 = [J] = [kg \cdot m^{-2} \cdot s^{-2}].$$

The chain rule implies  $\partial_{t'}c(t') = \frac{1}{t_0}\partial_t c(t)$  and hence

$$\begin{aligned} \partial_{t'}c'(x', y', z', t') &= \frac{c_0}{t_0} \partial_t c(x, y, z, t), \\ \partial_{x'}c'(x', y', z', t') &= \frac{c_0}{x_0} \partial_x c(x, y, z, t), \end{aligned}$$

where  $c_0 = [kg \cdot m^{-3}]$ . Analogous formulas hold for the first derivatives of the other variables.

For the second derivative one has accordingly

$$\partial_{x'}^2 c'(x', t') = \frac{c_0}{x_0^2} \partial_x^2 c(x, y, t).$$

We insert the found relationships into (2.29). Starting with (2.29b) we find

$$\begin{aligned} \partial_{t'} c'_i + \operatorname{div}' \left( \sum_j L'_{ij} \nabla \frac{\partial f'}{\partial c'_j} \right) &= c_0 t_0^{-1} \partial_t c_i + x_0^{-2} L_0 c_0^{-1} f_0 \operatorname{div} \left( \sum_j L_{ij} \nabla \frac{\partial f}{\partial c_j} \right) \\ &= [s^{-1} \cdot kg \cdot m^{-3}] \partial_t c_i - [m^{-1} \cdot s^{-2}] L_0 \operatorname{div} \left( \sum_j L_{ij} \nabla \frac{\partial f}{\partial c_j} \right) \\ &= [s^{-1} \cdot kg \cdot m^{-3}] \left( \partial_t c_i - \operatorname{div} \left( \sum_j L_{ij} \nabla \frac{\partial f}{\partial c_j} \right) \right) \end{aligned} \quad (2.37b)$$

with  $L_0 := [kg \cdot m^{-2} \cdot s]$ .

$\chi \in [0, 1]$  is a non-dimensional parameter, it can be regarded as the ratio of two densities. Hence,  $\chi_0 = 1$  or  $\chi = \chi'$  and consequently

$$\partial_{t'} \chi = \frac{1}{t_0} \partial_t \chi(x, y, z, t).$$

Now we treat the reaction term in (2.29a). By evident transformations we have

$$(k')^{1/b_x} ((c'_2)^2 - (\kappa')^{1/b_x} (c'_1 c'_3)) = k_0 c_0^2 k_0^{1/b_x - 1} k^{1/b_x} (c_2^2 - \kappa_0^{1/b_x} \kappa^{1/b_x} (c_1 c_3)).$$

With the setting

$$\begin{aligned} k_0 &:= c_0^{-1} t_0^{-1}, \\ \kappa_0 &:= 1 \end{aligned}$$

we obtain for (2.29a)

$$\begin{aligned} \operatorname{div}' \left( \sum_j L'_{ij} \nabla \frac{\partial f'}{\partial c'_j} \right) + (k')^{1/b_x} ((c'_2)^2 - (\kappa')^{1/b_x} c'_1 c'_3) & \quad (2.37a) \\ &= [s^{-1} \cdot kg \cdot m^{-3}] \left( \operatorname{div} \left( \sum_j L_{ij} \nabla \frac{\partial f}{\partial c_j} \right) + k_0^{1/b_x - 1} k^{1/b_x} (c_2^2 - \kappa_0^{1/b_x} \kappa^{1/b_x} c_1 c_3) \right). \end{aligned}$$

Finally we discuss the equation for the phase parameter  $\chi$ . In the modified Allen-Cahn equation the expression  $-\frac{1}{T} \partial_\chi f = \sum_i [s_i - \frac{1}{T} (e_i)]$  and  $W(\chi)$  due to (2.6) have the dimension of an entropy. The same is true for the entropic term

$$k_B (b^2 - b^1) \left( \sum_{i=1}^4 c_i \ln c_i + \bar{\alpha} \right)$$

and these are referred to scale  $s_0$ .

Furthermore

$$\frac{\gamma'}{2} |\nabla' \chi|^2 = \gamma_0 \frac{\gamma}{2} ((\partial_{x'} \chi)^2 + (\partial_{y'} \chi)^2 + (\partial_{z'} \chi)^2) = \left[ \frac{\gamma_0}{x_0^2} \right] \left( \frac{\gamma}{2} |\nabla \chi|^2 \right).$$

Comparing the dimensions, we find with (2.6)  $\frac{\gamma_0}{x_0^2} = s_0$  or

$$\gamma_0 = s_0 x_0^2. \quad (2.38)$$

Using (2.38) this yields:

$$\begin{aligned} \gamma' \Delta' \chi &= \gamma' (\partial_{x'}^2 \chi(x', y', z', t') + \partial_{y'}^2 \chi(x', y', z', t') + \partial_{z'}^2 \chi(x', y', z', t')) \\ &= \frac{\gamma_0}{x_0^2} (\gamma \Delta \chi) = s_0 \gamma \Delta \chi. \end{aligned}$$

As a consequence, (2.29d) is rewritten as

$$\tau t_0^{-1} (\partial_t \chi) = s_0 \left( \gamma \Delta \chi + \omega(c, \chi) \right). \quad (2.37c)$$

Hence we choose

$$\tau := s_0 t_0. \quad (2.39)$$

System (2.29) is transformed to the new formulation (2.37). The diffusion equations are unchanged except the additional term  $k_0^{1/b_\chi - 1}$  that has to be accounted for. This conversion factor becomes part of the numerical routines.

According to the definition of  $\chi$  as the ratio of two concentrations, the modified Allen-Cahn equation is dimensionless. In order to adapt the size of  $\partial_t \chi$ , the scaling parameter  $\tau$  has been introduced.

It is of course well understood that the computed numerical results hold in all cases where the dimensional factors in brackets have identical values.

Finally, we want to briefly discuss how the estimated free energy values that we will gain later by ab-initio computations are used numerically. The value of  $132 \text{ eV} \approx 2.11 \cdot 10^{-17} \text{ J}$  (GULP value) for sphalerite represents the free energy of a homogeneous sphalerite crystal occupying its cubic unit cell with edge length  $a \approx 5.41 \text{ \AA}$  (again GULP data). Setting the volume  $V = (5.41 \text{ \AA})^3 \approx 158.34 \cdot 10^{-30} \text{ m}^3$  of the unit cell of cubic ZnS into a relation with the volume of  $\Omega$  (as chosen for the computations of Sections 5.3, 5.4 and 5.5) we can for instance calculate the free energy of a homogeneous sphalerite crystal contained within one fixed finite element of a given regular triangulation of  $\Omega$  with  $N$  elements to  $\frac{2.66 \cdot 10^9 \text{ J}}{N}$ . Together with the diffusivities that are in the range of  $10^{-4} \text{ ms}^{-1}$  to  $10^{-7} \text{ ms}^{-1}$  and the conversion from seconds to days we obtain reasonable results.

These diffusivity constants for Cu, Zn and Fe were taken from measurements, [55], but it must be pointed out that the physical units  $[\text{m}^2 \text{ s}^{-1}]$  of this data had to be changed to  $[\text{kg m}^2 \text{ s}]$  in order to fit into our formulation.

## 2.6 Free energy inequality for the isothermal system

We will show the thermodynamical correctness of the three presented models under isothermal conditions and with the approximating elliptic equation replaced by the original time-dependent formulation.

We start with System (2.29) and reformulate it:

$$\partial_t c + \text{div}(J) = r, \quad (2.40)$$

$$\tau \partial_t \chi = -\frac{\partial f}{\partial \chi}, \quad (2.41)$$

where

$$J = -L\nabla\mu$$

and  $r$  is defined by (2.27).

An application of the chain rule yields

$$\frac{d}{dt}f(c, \chi) = \sum_{j=1}^4 \frac{\partial f}{\partial c_j} \partial_t c_j + \frac{\partial f}{\partial \chi} \partial_t \chi. \quad (2.42)$$

From this identity we learn that we have to test the equation for  $c_i$  with  $\frac{\partial f}{\partial c_i}$ ,  $1 \leq i \leq 4$  and Eq. (2.41) with  $\frac{\partial f}{\partial \chi}$ . After integrating over  $\Omega$ , one integration by parts and with  $\frac{\partial f}{\partial c_j} = \mu_j$  we obtain:

$$\frac{d}{dt} \int_{\Omega} f(c, \chi) - \int_{\Omega} \left( \sum_{j=1}^4 \mu_j r_j + \sum_{j=1}^4 \nabla \mu_j \cdot J_j + \frac{\partial f}{\partial \chi} \partial_t \chi \right) + \int_{\partial\Omega} \sum_{j=1}^4 \mu_j J_j \cdot \vec{\nu} = 0. \quad (2.43)$$

This is the constitutive equality for the Helmholtz free energy density  $f$ .

To recast (2.43) as an inequality, we notice that as the matrix  $L$  is positive definite,

$$\sum_{j=1}^4 \nabla \mu_j \cdot J_j = -L\nabla\mu : \nabla\mu \leq 0. \quad (2.44)$$

Additionally, by (2.41), we have  $\frac{\partial f}{\partial \chi} \partial_t \chi = -\tau(\partial_t \chi)^2 \leq 0$ .

It remains to show that

$$\int_{\Omega} \sum_{j=1}^4 \mu_j r_j \leq 0. \quad (2.45)$$

We exploit the particular form of  $r$  and  $f$  and Structure (2.17). Let

$$Q(c) := \sum_{i=1}^4 \alpha_i c_i.$$

Since  $r_1 = r_3 = -\frac{1}{2}r_2$ ,  $r_4 = 0$  we have

$$\begin{aligned} \int_{\Omega} \sum_{j=1}^4 \mu_j r_j &= \int_{\Omega} (\mu_1 - 2\mu_2 + \mu_3) r_1 \\ &= \int_{\Omega} \left[ k_B T b_{\chi} \left( \ln \left( \frac{c_1 c_3}{c_2^2} \right) + \frac{E_1 + E_3 - E_S}{k_B T b_{\chi}} - \frac{2E_2 - E_S}{k_B T b_{\chi}} \right) \right. \\ &\quad \left. + 2(\alpha_1 - 2\alpha_2 + \alpha_3) Q(c) \right] r_1 \\ &= \int_{\Omega} \left[ k_B T b_{\chi} \ln \left( \frac{c_1 c_3 (r_+)^{1/b_{\chi}}}{c_2^2 (r_-)^{1/b_{\chi}}} \right) + 2(\alpha_1 - \alpha_2 + \alpha_3) Q(c) \right] r_1. \end{aligned} \quad (2.46)$$

The first term can be estimated analogous to (2.17):

$$\int_{\Omega} k_B T b_{\chi} \ln \left( \frac{c_1 c_3 (r_+)^{1/b_{\chi}}}{c_2^2 (r_-)^{1/b_{\chi}}} \right) r_1 \leq 0 \quad (2.47)$$

but additional considerations are necessary to estimate  $\int_{\Omega} 2(\alpha_1 - 2\alpha_2 + \alpha_3)Q(c)r_1$ . The logarithmic form (2.25) of the free energy guarantees  $c_i > 0$  in  $\Omega_{T_0}$  for  $t > 0$  if this is true for  $t = 0$ . In Chapter 3 a rigorous proof of this statement will be given. From this fact we obtain  $Q(c) > 0$  in  $\Omega_{T_0}$ .

Let

$$\sigma_1 := \sup_{x \in \bar{\Omega}} c_{01}(x, 0), \quad \sigma_2 := \inf_{x \in \bar{\Omega}} c_{20}(x), \quad \sigma_3 := \sup_{x \in \bar{\Omega}} c_{30}(x), \quad (2.48)$$

where  $\sigma_1, \sigma_2, \sigma_3$  are positive constants. By the parabolic maximum principle, [59], as for fixed  $c_2, c_3, \chi$  the mapping  $c_1 \mapsto r_1(c, \chi)$  decreases as  $c_1$  increases, and (now for fixed  $c_1, c_3, \chi$ )  $c_2 \mapsto r_1(c, \chi)$  increases and finally  $c_3 \mapsto r_1(c, \chi)$  decreases, we have  $\sigma_1 = \sup_{\Omega_{T_0}} c_1$ ,  $\sigma_2 = \inf_{\Omega_{T_0}} c_2$  and  $\sigma_3 = \sup_{\Omega_{T_0}} c_3$ .

Now a sufficient condition for  $r_1 > 0$  in  $\Omega_{T_0}$  is

$$\kappa^{1/b_\chi} < \frac{\sigma_2^2}{\sigma_1 \sigma_3}. \quad (2.49)$$

We remark that in the crystallographic measurements, the ratio constant  $\kappa$  never exceeded a value of 0.07 (otherwise the matrix becomes unstable).

Of course, one can replace (2.49) by conditions independent of  $\chi$ . In Chapter 3 we will show that  $0 < \chi < 1$  in  $\Omega_{T_0}$  if this is true for the initial values  $\chi_0$ . If we assume  $\kappa \leq 1$  and  $b^1, b^2 \leq 1$ , a sufficient condition for (2.49) is

$$\kappa^{1/\max(b^1, b^2)} < \frac{\sigma_2^2}{\sigma_1 \sigma_3}.$$

For an estimate of the volume term we require

$$\alpha_1 - 2\alpha_2 + \alpha_3 < 0. \quad (2.50)$$

This is a condition on the ion radii of  $\text{Fe}^{3+}$ ,  $\text{Fe}^{2+}$  and  $\text{Cu}^+$  and fulfilled in nature with  $\alpha_1 - 2\alpha_2 + \alpha_3 = -0.13\text{\AA}$ , see Table 2.1. Together with  $r_1 > 0$  and the above estimate this shows that  $\int_{\Omega} 2(\alpha_1 - 2\alpha_2 + \alpha_3)Q(c)r_1 < 0$ .

Symbol	Species	Ion Radius
$\alpha_1$	$\text{Fe}^{3+}$	0.555 $\text{\AA}$
$\alpha_2$	$\text{Fe}^{2+}$	0.660 $\text{\AA}$
$\alpha_3$	$\text{Cu}^+$	0.635 $\text{\AA}$
$\alpha_4$	$\text{Zn}^{2+}$	0.640 $\text{\AA}$

Table 2.1: Values of sulfide crystal radii taken from [44]

Hence, (2.45) is proved and we have shown the *constitutive free energy inequality*

$$\frac{d}{dt} \int_{\Omega} f(c(t), \chi(t)) + \int_{\partial\Omega} \sum_{j=1}^4 \mu_j J_j \cdot \vec{\nu} \leq 0. \quad (2.51)$$

In a thermodynamically closed system the fluxes on  $\partial\Omega$  disappear. This is in particular fulfilled if we impose that the Dirichlet data does not vary along  $\partial\Omega$ :

$$h_i \equiv \text{const}_i, \quad 1 \leq i \leq 4.$$

A different way to guarantee that the boundary fluxes vanish in (2.51) is to impose

$$\partial_\nu \mu_j = 0 \quad \text{on } \partial\Omega, \quad 1 \leq j \leq 4,$$

the natural boundary conditions associated to the minimum problem of the free energy integral.

To summarise, if the equilibrium constant  $\kappa$  fulfills (2.49) and under the natural condition (2.50) on the ion radii, we obtain  $\sum_{j=1}^4 \mu_j r_j < 0$  in  $\Omega_{T_0}$  and hence

$$\frac{d}{dt} \int_{\Omega} f(c(t), \chi(t)) \leq 0$$

for a thermodynamically closed system.

From now on we shall assume that (2.49) and (2.50) are fulfilled.

The results just shown immediately imply the thermodynamical validity of Model II if the free energy obeys the relationship

$$f(c, \chi) = \chi f^1(c) + (1 - \chi) f^2(c) + \frac{\gamma T}{2} |\nabla \chi|^2 + TW(\chi)$$

(we remind that  $f^l(c)$  denotes the free energy density of phase  $l$ ,  $l = 1, 2$  stored in data bases). This follows from (2.43) with  $r_j = 0$  and the functional derivative  $\mu_j = \frac{\partial f}{\partial c_j}$  is defined by interpolation, see Section 4.2, Eq. (4.7).

For the thermodynamical validation of Model III we observe that  $\frac{\partial f}{\partial \chi} \partial_t \chi = -\tau(\partial_t \chi)^2 \leq 0$  is replaced by  $F(c, \chi) = \min_{\tilde{\chi} \in V} F(c, \tilde{\chi})$  which ensures that  $F$  is non-increasing in  $\chi$  for all times  $t > 0$ .

## 2.7 The non-isothermal case

The justification of the reactive term (2.27) depends on (2.17) and the estimation of the free energy. It is interesting to clarify the question if  $r$  changes for the non-isothermal case. To answer this question we quickly develop the extension to (2.29) if the temperature  $T$  is not a constant but can vary with time. We validate the extended model by an entropy estimate and prove that the second law of thermodynamics holds. Modifications to the other two models are straightforward.

We add to (2.40), (2.41) the energy balance equation

$$\partial_t e + \operatorname{div}(J_5) = 0 \tag{2.52}$$

and assume that there are no heat sources (the second law of thermodynamics holds for a thermodynamically closed system). If we considered a model where the reactions absorb heat, the ansatz (2.52) would have to be modified.

The fluxes in the non-isothermal setting are defined by

$$J_i = \sum_{j=1}^4 L_{ij} \nabla \left( \frac{\mu_j}{T} \right), \quad 1 \leq i \leq 4, \quad J_5 = -\lambda \nabla T.$$

Here,  $\lambda = \lambda(\cdot, T, \nabla T) > 0$  denotes the heat conductivity. The alteration of the fluxes  $J_1, \dots, J_4$  and the new relation (2.52) are all the changes necessary to adjust the model to the non-isothermal setting.

From Gibbs relation  $f = e - Ts$  it follows:

$$\int_{\Omega} \partial_t s = \int_{\Omega} \partial_t \left( \frac{1}{T} e - \frac{1}{T} f \right) = \int_{\Omega} \left[ \frac{1}{T} \partial_t e - \frac{1}{T} \partial_t f - \frac{s}{T} \partial_t T \right]. \quad (2.53)$$

A variation of  $f = f(c, \chi, T)$  similar to (2.42) reveals

$$\int_{\Omega} \frac{1}{T} \partial_t f(c, \chi, T) = \int_{\Omega} \left[ \frac{1}{T} \sum_{j=1}^4 \mu_j \partial_t c_j + \frac{1}{T} \frac{\partial f}{\partial \chi} \partial_t \chi - \frac{s}{T} \partial_t T \right].$$

By inserting this formula in (2.53), the  $\partial_t T$  term drops out and we obtain

$$\int_{\Omega} \partial_t s = \int_{\Omega} \frac{1}{T} \left( \partial_t e - \sum_{j=1}^4 \mu_j \partial_t c_j - \frac{\partial f}{\partial \chi} \partial_t \chi \right).$$

So we test the equations for  $c_i$  with  $\frac{\mu_i}{T}$ , Eq. (2.41) with  $-\frac{1}{T} \frac{\partial f}{\partial \chi}$  and (2.52) with  $\frac{1}{T}$ .

The treatment of the first four equations is done as in the last section. An integration of the last identity (2.52) yields

$$\int_{\Omega} \frac{1}{T} \partial_t e = \int_{\Omega} \frac{\lambda}{T^2} |\nabla T|^2 + \int_{\partial\Omega} \frac{\lambda}{T} \nabla T \cdot \vec{\nu}.$$

So we find

$$\begin{aligned} \frac{d}{dt} \int_{\Omega} s &- \int_{\Omega} \left( \lambda \frac{|\nabla T|^2}{T^2} + L \nabla \left( \frac{\mu}{T} \right) : \nabla \left( \frac{\mu}{T} \right) - \sum_{j=1}^4 \frac{\mu_j}{T} r_j + \frac{1}{T} \frac{(\partial_{\chi} f)^2}{\tau} \right) \\ &+ \int_{\partial\Omega} \left( \sum_{j=1}^4 \frac{\mu_j}{T} J_j - \frac{\lambda \nabla T}{T} \right) \cdot \vec{\nu} = 0. \end{aligned} \quad (2.54)$$

The proof of  $\sum_{j=1}^4 \frac{\mu_j}{T} r_j \leq 0$  is done verbatim as in the last section. In the crucial estimate, the factor  $T$  still present in the isothermal free energy estimate cancels out. This proves that (2.27) defines the reaction terms of the non-isothermal model, too, and that these rates are independent of  $T$ .

From the positive definiteness of  $L$  and from  $\lambda > 0$  we get the *entropy inequality*

$$\frac{d}{dt} \int_{\Omega} s + \int_{\partial\Omega} \left( \frac{1}{T} \sum_{j=1}^4 \mu_j J_j - \lambda \nabla T \right) \cdot \vec{\nu} \geq 0. \quad (2.55)$$

Formally, assuming the boundedness of  $s$  from below and letting  $\lambda$  tend to  $+\infty$ , we recover the constitutive free energy inequality (2.51) (scaled by factor  $\frac{1}{T}$ ). This can be done as explained in [5].

## 2.8 More general forms of the surface energy

The formula  $\int_{\Omega} \frac{\gamma}{2} |\nabla \chi|^2$  in the definition of the free energy (2.25) represents a surface energy depending on  $\chi$  only. In general, different concentration vectors  $c$  will imply different microscale geometries close to the transition layer, hence the interfacial energy will depend on  $c$ .

In this section we will assume that this interfacial energy is a function of  $\nabla c$ . Firstly, we will consider that  $\int_{\Omega} \frac{\gamma}{2} |\nabla \chi|^2$  be replaced by

$$\int_{\Omega} \frac{1}{2} \left( \Lambda \nabla c : \nabla c + \gamma |\nabla \chi|^2 \right) \quad (2.56)$$

where  $\Lambda \in \mathbb{R}^{4 \times D}$  denotes as usual a positive definite symmetric tensor. We will show that this common ansatz leads here to a wrong model. Secondly we will discuss a possible correction of (2.56) with  $\Lambda = \Lambda(c, \chi)$ . The philosophy of this section is to analyse which forms of the surface energy lead to a mathematically consistent model. We will not try at this point to compute the correct physical surface energy by considering sphalerite-chalcopyrite ensembles for different  $c$  vectors.

The additional term  $\frac{1}{2} \Lambda \nabla c : \nabla c$  in (2.56) leads to modified chemical potentials  $\mu_j = \frac{\partial f}{\partial c_j}$ . In order to validate the free energy inequality for the resulting model, it is enough to verify

$$\int_{\Omega} (\mu_1 - 2\mu_2 + \mu_3) r_1 \leq 0, \quad (2.57)$$

as shown in Eq. (2.46) (the same discussion applies with an additional factor  $1/T$  to the non-isothermal case, see (2.54)).

The claim is that such an estimate is not possible for constant  $\Lambda, \gamma$ . To this end it is enough to restrict to the special case

$$(\Lambda_{ik})_{ik} = \text{diag}(\lambda_i)$$

such that  $\Lambda$  has only non-zero entries on the diagonal. Furthermore let  $\chi \equiv \text{const}$  and  $c_4 \equiv \text{const}$  (initial and boundary data chosen appropriately). The free energy estimate must also hold for this special case. Exploiting Estimate (2.47), we then have to ensure that

$$\int_{\Omega} \Delta (-\lambda_1 c_1 + 2\lambda_2 c_2 - \lambda_3 c_3) \tilde{k} (c_2^2 - \tilde{\kappa} c_1 c_3) \leq 0.$$

This inequality does not hold in general. Also, it does not seem possible to find a correction to  $r_1$  such that (2.57) holds. Consequently, (2.56) cannot be justified.

We will now drop the postulate of constant coefficients in the surface energy and will allow  $\Lambda$  to depend on  $c, \chi$ . The gist of the following construction is the simple observation

$$\int_{\Omega} \Delta (k^{1/b_\chi} (c_2^2 - \kappa^{1/b_\chi} c_1 c_3)) (k^{1/b_\chi} (c_2^2 - \kappa^{1/b_\chi} c_1 c_3)) = \int_{\Omega} (\Delta r_1) r_1 = \int_{\Omega} -|\nabla r_1|^2 \leq 0.$$

Here we integrated by parts and assumed  $c_i \equiv \text{const}_i$  at  $\partial\Omega$  or  $\partial_\nu c_i = 0$  and  $\partial_\nu \chi = 0$  at  $\partial\Omega$  which must be fulfilled for a thermodynamically closed system.

For convenience we introduce only for this section the notation  $c_5 := \chi$  and transform  $\Lambda$  to a  $5 \times D$ -tensor  $\tilde{\Lambda}$ . This means for the surface energy

$$\int_{\Omega} \frac{1}{2} \tilde{\Lambda} \nabla c : \nabla c = \int_{\Omega} \frac{1}{2} \sum_{i=1}^5 \sum_{j=1}^3 \sum_{m=1}^3 \tilde{\Lambda}_{im} \frac{\partial c_j}{\partial x_m} \frac{\partial c_i}{\partial x_j}.$$

Following the outline just explained we construct a tensor  $\tilde{\Lambda} = \tilde{\Lambda}_{ij}(c, \chi)$  such that

$$- \int_{\Omega} (\Delta r_1) r_1 = \int_{\Omega} \left( \frac{\partial}{\partial c_1} - 2 \frac{\partial}{\partial c_2} + \frac{\partial}{\partial c_3} \right) \left( \frac{1}{2} \tilde{\Lambda} \nabla c : \nabla c \right) r_1.$$

By simple (but quite lengthy) computations we find

$$\begin{aligned} \nabla r_1 &= k^{1/b_\chi} \ln(k) \frac{b^2 - b^1}{(b_\chi)^2} (c_2^2 - \kappa^{1/b_\chi} c_1 c_3 \ln(\kappa)) \nabla \chi \\ &\quad + 2k^{1/b_\chi} c_2 \nabla c_2 - (\kappa k)^{1/b_\chi} (c_1 \nabla c_3 + c_3 \nabla c_1) \end{aligned}$$

and similarly

$$\begin{aligned} \Delta r_1 &= \ln(k) \kappa^{1/b_\chi} \frac{(b^2 - b^1)^2}{b_\chi^4} \left[ (\ln(\kappa) + 2)(c_2^2 - c_1 c_3 \kappa^{1/b_\chi}) + (\ln(\kappa))^2 \kappa^{1/b_\chi} c_1 c_3 \right] |\nabla \chi|^2 \\ &\quad - 2(\kappa k)^{1/b_\chi} \nabla c_1 \cdot \nabla c_3 - (\kappa k)^{1/b_\chi} \ln(\kappa) \ln(k) \frac{b^2 - b^1}{b_\chi^2} (c_1 \nabla c_3 \cdot \nabla \chi + c_3 \nabla c_1 \cdot \nabla \chi) \\ &\quad + 2k^{1/b_\chi} c_2 \Delta c_2 - (\kappa k)^{1/b_\chi} c_1 \Delta c_3 + 4 \ln(k) k^{1/b_\chi} \frac{b^2 - b^1}{b_\chi^2} c_2 \nabla c_2 \cdot \nabla \chi + 2k^{1/b_\chi} |\nabla c_2|^2 \\ &\quad + \ln(k) \kappa^{1/b_\chi} \frac{b^2 - b^1}{b_\chi^2} (c_2^2 - \kappa^{1/b_\chi} c_1 c_3 \kappa) \Delta \chi - (\kappa k)^{1/b_\chi} c_3 \Delta c_1. \end{aligned} \quad (2.58)$$

Now we compute for  $l = 1, 2, 3$

$$\begin{aligned} &\frac{\partial}{\partial x_l} \int_{\Omega} \frac{1}{2} \tilde{\Lambda} \nabla c : \nabla c \\ &= -\frac{1}{2} \int_{\Omega} \left[ \sum_{j=1}^3 \sum_{m=1}^3 \frac{\partial}{\partial x_j} \left( \tilde{\Lambda}_{lm} \frac{\partial c_j}{\partial c_j} \partial x_m \right) + \sum_{i=1}^5 \sum_{m=1}^3 \frac{\partial}{\partial x_m} \left( \tilde{\Lambda}_{im} \frac{\partial c_i}{\partial x_l} \right) \right] \end{aligned}$$

and obtain

$$\begin{aligned} \int_{\Omega} \left( \frac{\partial}{\partial c_1} - 2 \frac{\partial}{\partial c_2} + \frac{\partial}{\partial c_3} \right) \left( \frac{1}{2} \tilde{\Lambda} \nabla c : \nabla c \right) &= -\frac{1}{2} \int_{\Omega} \left\{ \sum_{i=1}^5 \sum_{m=1}^3 \tilde{\Lambda}_{im} \left( \frac{\partial c_i}{\partial x_1} - 2 \frac{\partial c_i}{\partial x_2} + \frac{\partial c_i}{\partial x_3} \right) \right\} \\ &\quad \sum_{j=1}^3 \sum_{m=1}^3 \frac{\partial}{\partial x_j} \left[ \left( \tilde{\Lambda}_{1m} - 2 \tilde{\Lambda}_{2m} + \tilde{\Lambda}_{3m} \right) \frac{\partial c_j}{\partial x_m} \right]. \end{aligned} \quad (2.59)$$

When comparing (2.58) with (2.59) we can read off expressions for  $\tilde{\Lambda}_{im}$  which are not unique and will depend on  $c_1, c_2, c_3, \chi, k$  and  $\kappa$ . Except the fact that they have the right sign after integrating by parts, there seems no justification for these complicated terms.

## Chapter 3

# Existence and Uniqueness Results for the derived Models

This chapter is devoted to the proof of global existence and uniqueness of a solution to the formulation (2.29) with classical Dirichlet boundary conditions, i.e.  $g = h = 0$ , and Neumann boundary condition  $\partial_\nu \chi = 0$  at  $\partial\Omega$  for  $\chi$ , and with the elliptic equation (2.29a) being replaced by the original parabolic equation. If the general Dirichlet condition  $c = \bar{c}$  on  $\partial\Omega$  is imposed for a given function  $\bar{c} \in H^{1,2}(\bar{\Omega}; \mathbb{R}^4)$ , one can formally set  $\tilde{c} := c - \bar{c}$  and gain from the results for  $\tilde{c}$  which are provided in this chapter directly the corresponding statements for  $c$ .

The results stated in this chapter are also valid for Model II, provided we assume that the free energy  $f$  is smooth. This is made precise in Remark 3.2. Remark 3.3 at the end of this chapter lists the necessary steps to extend the main existence result to Model III.

The proof of existence is done in three steps. An additional (and artificial) surface energy term

$$\int_{\Omega} \frac{\lambda}{2} |\nabla c|^2$$

for a small constant  $\lambda > 0$  is added to the free energy functional. This term is necessary to guarantee the existence of a minimiser (Lemma 3.1). The first part, found in Sections 3.1 to 3.7, discusses the case of polynomial free energies for the resulting model. The growth conditions in Section 3.4 are set up accordingly.

The second step, carried out in Sections 3.9 to 3.12, generalises to the same model with logarithmic free energies. For the proof, a regularised functional is introduced and the results for the polynomial free energy are exploited.

In the last step, the limit  $\lambda \searrow 0$  is discussed and an existence result is established for the original model (2.29).

The structure of this chapter follows the argumentation in [38] but several modifications arise from the presence of a reaction term, from the additional Allen-Cahn equation and from the free energy functional that requires different growth conditions, approximations and estimates than the Cahn-Hilliard model.

In [38] several older results are used among which the articles [29] and [31] should be particularly mentioned; the general outline of the approach in [38] is related to the earlier paper [5]. The principle of showing compactness results for a discrete

model that allow to pass to the limit of a continuum model is by now classical and goes back to [50].

### 3.1 Preliminaries

In this chapter,  $f = f(c, \chi)$  denotes the free energy density without the surface energy terms  $\frac{\gamma}{2}|\nabla\chi|^2 + \frac{\lambda}{2}|\nabla c|^2$ , see also Definition (3.12) below.  $C$  will denote generic constants that can change from estimate to estimate.

For the purpose of this chapter the formulation (2.29) in  $c$  variables is more practical than a formulation in  $d$  variables (introduced on page 10). With the additional surface term we will consider the formulation (where  $0 < T_0 < \infty$  is a given stop time)

Find for  $t \geq 0$  the vector  $(c, \mu, \chi)$  with  $c = (c_1, c_2, c_3, c_4)$  such that in  $\Omega_{T_0} := \Omega \times (0, T_0)$

$$\partial_t c = \operatorname{div}(L\nabla\mu) + r(c, \chi), \quad (3.1a)$$

$$\mu(c, \chi) = \frac{\partial f}{\partial c}(c, \chi) - \lambda\Delta c, \quad (3.1b)$$

$$\tau\partial_t\chi = \gamma\Delta\chi - \omega(c, \chi) \quad (3.1c)$$

and for  $t = 0$  in  $\Omega$

$$c(\cdot, 0) = c_0(\cdot), \quad \chi(\cdot, 0) = \chi_0(\cdot) \quad (3.1d)$$

and for  $t > 0$  in  $\partial\Omega$

$$c_i = \mu_i = \partial_\nu\chi = 0, \quad 1 \leq i \leq 4. \quad (3.1e)$$

The matrix  $L$  in (3.1) is positive definite,  $T_0 > 0$  denotes the stop time,  $\omega = \partial_\chi(f/T)$ , and the reaction term is

$$r_1 = r_1(c, \chi) = k^{1/b_\chi}(c_2^2 - \kappa^{1/b_\chi}c_1c_3), \quad r(c, \chi) = (r_1, -\frac{1}{2}r_1, r_1, 0). \quad (3.2)$$

Now, let us collect general properties of the model and some necessary tools that will be needed in the sequel.

As a consequence of the assumed relation (2.22) and the sulphur concentration  $c_S$  that is kept constant, the concentration vector  $c$  lies inside the simplex  $\Sigma$ ,

$$c \in \Sigma := \left\{ d = (d_1, \dots, d_4) \in \mathbb{R}^4 \mid \frac{3}{2}d_1 + d_2 + d_3 + d_4 = \frac{1}{2} \right\}. \quad (3.3)$$

We do not propose  $0 \leq c_i \leq 1$  in  $\Omega$  because for the polynomial free energies considered here this is simply not true. This is one of the reasons why logarithmic free energies are introduced later on. Let

$$\begin{aligned} X_1 &:= \left\{ c \in H_0^{1,2}(\Omega; \mathbb{R}^4) \mid c \in \Sigma \text{ almost everywhere} \right\}, \\ X_2 &:= H_E^{1,2}(\Omega; \mathbb{R}) := \{ \tilde{\chi} \in H^{1,2}(\Omega; \mathbb{R}) \mid \partial_\nu\tilde{\chi} = 0 \text{ at } \partial\Omega \}. \end{aligned}$$

Since we have (classical) Dirichlet boundary conditions for the equations of conservation of mass, we consider the space of test functions

$$Y := H_0^{1,2}(\Omega; \mathbb{R}^4)$$

and its dual

$$\mathcal{D} := (H_0^{1,2}(\Omega; \mathbb{R}^4))' = H^{-1,2}(\Omega; \mathbb{R}^4).$$

Now we consider the mapping  $\mathcal{L}(\mu) : Y \rightarrow \mathcal{D}$  corresponding to  $\mu \mapsto -\operatorname{div}(L\nabla\mu)$  with Dirichlet boundary conditions, defined by

$$\mathcal{L}(\mu)(\zeta) := \int_{\Omega} L\nabla\mu : \nabla\zeta.$$

Instead of Dirichlet data one could also consider Neumann boundary conditions. Due to the presence of  $r$ , this will not imply conservation of mass for the components  $c_i$  of  $c$ .

By definition of  $Y$  it is clear that  $\mathcal{L}(\mu) \in \mathcal{D}$ . To simplify the argumentation later we will need the inverse  $\mathcal{G}$  of  $\mathcal{L}$ . The existence of  $\mathcal{G}$  is derived from the Poincaré inequality and the Lax-Milgram theorem, since  $L$  is positive definite. From this we find that  $\mathcal{G}$  is positive definite, self-adjoint, injective and compact.

Hence we have

$$(L\nabla\mathcal{G}v, \nabla\zeta)_{L^2} = (\zeta, v) \quad \text{for all } \zeta \in Y \text{ and } v \in \mathcal{D}.$$

We define for  $v_1, v_2 \in \mathcal{D}$  the  $L$  scalar product by

$$(v_1, v_2)_L := (L\nabla\mathcal{G}v_1, \nabla\mathcal{G}v_2)_{L^2}$$

with the corresponding norm

$$\|v\|_L := \sqrt{(v, v)_L}.$$

Functions  $v \in Y$  canonically define an element in  $\mathcal{D}$  and consequently,  $(\cdot, \cdot)_L$  and  $\|\cdot\|_L$  are as well defined for functions in  $Y$ .

With the help of Young's inequality we find for  $\delta > 0$  and all  $d \in Y$  the estimate

$$\begin{aligned} \|d\|_{L^2} &= (L\nabla\mathcal{G}d, \nabla d)_{L^2} \\ &\leq \|L^{\frac{1}{2}}\nabla\mathcal{G}d\|_{L^2} \|L^{\frac{1}{2}}\nabla d\|_{L^2} \\ &\leq \frac{C_L}{\delta} \|d\|_L^2 + \delta \|\nabla d\|_{L^2}^2, \end{aligned} \tag{3.4}$$

where  $C_L$  is a positive constant depending on  $L$ .

The Green's function  $\mathcal{G}$  allows to rewrite the conservation of mass equations as

$$\mathcal{G}(\partial_t c - r(c, \chi)) = \mu := \left( \frac{\partial f}{\partial c_j} \right)_{1 \leq j \leq 4}. \tag{3.5}$$

### 3.2 The weak formulation of the problem

$(c, \mu, \chi) \in L^2(0, T_0; H_0^{1,2}(\Omega; \mathbb{R}^4)) \times L^2(0, T_0; H_0^{1,2}(\Omega; \mathbb{R}^4)) \times L^2(0, T_0; H^1(\Omega; \mathbb{R}))$  with  $r(c, \chi), \omega(c, \chi) \in L^1(\Omega_{T_0})$  is called a *weak solution* of (3.1) if

$$-\int_{\Omega_{T_0}} \partial_t \xi \cdot (c - c_0) + \int_{\Omega_{T_0}} L\nabla\mu : \nabla\xi - \int_{\Omega_{T_0}} r(c, \chi)\xi = 0 \tag{3.6a}$$

for all  $\xi \in L^2(0, T_0; H_0^1(\Omega; \mathbb{R}^4))$  with  $\partial_t \xi \in L^2(\Omega_{T_0})$ ,  $\xi(T_0) = 0$ , and

$$\int_{\Omega_{T_0}} \mu \cdot \eta = \int_{\Omega_{T_0}} \left( \frac{\partial f}{\partial c}(c) \cdot \eta + \lambda \nabla c \cdot \nabla \eta \right) \quad (3.6b)$$

for all  $\eta \in L^2(0, T_0; H_0^1(\Omega; \mathbb{R}^4)) \cap L^\infty(\Omega_{T_0}; \mathbb{R}^4)$ , and

$$- \int_{\Omega_{T_0}} \tau \partial_t \zeta (\chi - \chi_0) + \int_{\Omega_{T_0}} \gamma \nabla \chi \cdot \nabla \zeta - \int_{\Omega_{T_0}} \omega(c, \chi) \zeta = 0 \quad (3.6c)$$

for all  $\zeta \in L^2(0, T_0; H^1(\Omega; \mathbb{R}))$  with  $\partial_t \zeta \in L^2(\Omega_{T_0})$ ,  $\zeta(T_0) = 0$ . Here we set  $\omega(c, \chi) := \partial_\chi(f(c, \chi)/T)$ .

In (3.6b) we demand  $\eta \in L^\infty(\Omega_{T_0}; \mathbb{R}^4)$  in order to be able to generalise to a model with elasticity. More about this is found in Section 5.4.

### 3.3 A semi-implicit time discretisation

We fix an  $M \in \mathbb{N}$  and set  $h := \frac{T_0}{M}$ . For  $m \geq 1$  and given  $(c^{m-1}, \mu^{m-1}, \chi^{m-1})$ , consider

$$\frac{c^m - c^{m-1}}{h} = \operatorname{div}(L \nabla \mu^m) + r(c^{m-1}, \chi^{m-1}), \quad (3.7a)$$

$$\mu^m = \frac{\partial f}{\partial c}(c^m, \chi^m) - \lambda \Delta c^m, \quad (3.7b)$$

$$\tau \frac{\chi^m - \chi^{m-1}}{h} = \gamma \Delta \chi^m + \omega(c^m, \chi^m). \quad (3.7c)$$

For the subsequent sections we introduce as abbreviation  $r^{m-1} := r(c^{m-1}, \chi^{m-1})$ .

(3.7) is apparently the implicit time discretisation of System (3.1) except for the reaction term  $r$  that has been treated explicitly. Therefore, we call the resulting scheme semi-implicit.

### 3.4 Structural Assumptions

In order to be able to establish the existence of weak solutions in the sense of Section 3.2, the following assumptions are made:

(A1)  $\Omega \subset \mathbb{R}^D$  is a bounded domain with Lipschitz boundary.

(A2) The free energy density  $f$  can be written as

$$f(c, \chi) = f^1(c, \chi) + f^2(c, \chi) \quad \text{for all } c \in \mathbb{R}^4, \chi \in \mathbb{R} \quad (3.8)$$

with  $f^1, f^2 \in C^2(\mathbb{R}^4 \times \mathbb{R}; \mathbb{R})$  and  $f^1(\cdot, \chi)$  convex for every  $\chi \in \mathbb{R}$ ,  $f^1(c, \cdot)$  convex for every  $c \in \mathbb{R}^4$ . Furthermore,

(A2.1)  $f^1 \geq 0$ .

(A2.2) There exists a constant  $C_1 > 0$  such that

$$\begin{aligned} |\partial_c f^2(c, \chi)| &\leq C_1(|c| + 1) \quad \text{for all } c \in \Sigma, \chi \in \mathbb{R}, \\ |\partial_\chi f^2(c, \chi)| &\leq C_1(|\chi| + 1) \quad \text{for all } c \in \Sigma, \chi \in \mathbb{R}. \end{aligned} \quad (3.9)$$

(A2.3) For all  $\delta > 0$  there exists a constant  $C_\delta > 0$  such that

$$|\partial_c f^1(c, \chi)| + |\partial_\chi f^1(c, \chi)| \leq \delta f^1(c, \chi) + C_\delta \quad \text{for all } c \in \Sigma, \chi \in \mathbb{R}.$$

(A3) The initial data  $(c_0, \chi_0)$  fulfill

$$f(c_0, \chi_0) < \infty, \omega(c_0, \chi_0) < \infty.$$

(A4.1) The diffusion tensor  $L$  is symmetric and positive definite.

(A4.2)  $\gamma > 0$  is a constant;  $0 < \lambda < \lambda_0$  where  $\lambda_0$  is a small constant such that the estimate  $\partial_t F \leq 0$  is valid.

(A5)  $r(c, \chi)$  is a continuous function in both variables. Additionally, the reaction term  $r$  is chosen in accordance to  $f$  such that

$$\int_{\Omega} \mu \cdot r \leq 0. \quad (3.10)$$

(A6) The coefficients  $\alpha_i > 0$  satisfy Condition (2.50). Furthermore  $0 < \kappa < 1$ ,  $k > 0$  and  $0 < b^1, b^2 \leq 1$ . The initial values  $c_0$  of  $c$  and  $\kappa, b^1, b^2$  fulfill (2.49)

$$\kappa^{1/\max(b^1, b^2)} < \frac{\sigma_2^2}{\sigma_1 \sigma_3}. \quad (3.11)$$

By Assumption (A2.3) any polynomial growth is allowed for  $f^1$ , whereas exponential growth is not. For the non-convex part, sublinear growth of  $\partial_c f^2$  in  $c$  and  $\partial_\chi f^2$  in  $\chi$  is prescribed. (A6) will guarantee  $r_1 > 0$ .

If we approximate a logarithmic free energy function  $f$  by a polynomial function, we also have to replace the reaction term by a suitable approximation. This is the gist of (A5). (A5) is needed only for the a-priori estimate in Lemma 3.3. In Section 3.9 it is shown how a suitable  $r$  can be constructed for approximations  $f^\delta$  of  $f$ .

If one chooses  $\lambda > 0$  small enough, one can guarantee  $\partial_t F(c(t), \chi(t)) \leq 0$  because in this case the term with the possibly 'wrong' sign  $\lambda \Delta c r_1$  can be compensated by  $(\alpha_1 - 2\alpha_2 + \alpha_3)Q(c)r_1(c) < 0$ . Condition (A4.2) is needed only at one point, namely in Eq. (3.20) in the proof of Lemma 3.3 where the free energy estimate is exploited to derive a-priori bounds.

From now on we assume without further stating that the assumptions (A1)-(A6) hold.

### 3.5 Existence of solutions to the time discrete scheme

For the treatment of Formulation 3.1 it is suitable to introduce the free energy functional

$$F(c, \chi) := \int_{\Omega} \left( f(c, \chi) + \frac{\lambda}{2} |\nabla c|^2 + \frac{\gamma}{2} |\nabla \chi|^2 \right). \quad (3.12)$$

Additionally, for each time step  $m$  in the semi-implicit time discretisation (3.7), given step size  $h > 0$  and given  $(c^{m-1}, \chi^{m-1})$  we define the discrete energy functional

$$F^{m,h}(c, \chi) := F(c, \chi) + \frac{1}{2h} \|c - c^{m-1} - hr^{m-1}\|_L^2 + \frac{\tau}{2h} \|\chi - \chi^{m-1}\|_{L^2}^2. \quad (3.13)$$

**Lemma 3.1:** (*Existence of a minimiser*)

Let  $(c^{m-1}, \chi^{m-1}) \in X_1 \times X_2$  be given. Then for  $0 < h < \min\{\frac{\tau}{2C_1}, \frac{\lambda}{8C_1^2C_L}\}$  the functional  $F^{m,h}$  possesses a minimiser in  $X_1 \times X_2$ .

**Proof:** We will show that  $F^{m,h}$  is coercive and weakly lower semicontinuous. Using Assumptions (A2.1) and (A2.2) we find

$$\begin{aligned} F^{m,h}(c, \chi) &\geq \frac{\lambda}{2} \|\nabla c\|_{L^2}^2 + \frac{\gamma}{2} \|\nabla \chi\|_{L^2}^2 - C_1(\|c\|_{L^2}^2 + \|\chi\|_{L^2}^2) \\ &\quad + \frac{1}{2h} \left( \|c - c^{m-1} - hr^{m-1}\|_L^2 + \tau \|\chi - \chi^{m-1}\|_{L^2}^2 \right) - C \\ &\geq \left( \frac{\lambda}{2} - \delta C_1 \right) \|\nabla c\|_{L^2}^2 + \frac{\gamma}{2} \|\nabla \chi\|_{L^2}^2 + \left( \frac{\tau}{2h} - C_1 \right) \|\chi - \chi^{m-1}\|_{L^2}^2 \\ &\quad + \left( \frac{1}{2h} - \frac{C_1 C_L}{\delta} \right) \|c - c^{m-1} - hr^{m-1}\|_L^2 - C, \end{aligned}$$

where in the second estimate (3.4) was used and  $C = C(c^{m-1}, \chi^{m-1}, r)$ . Now, for  $0 < h < \min\{\frac{\tau}{2C_1}, \frac{\lambda}{8C_1^2C_L}\}$  by choosing  $\delta = \frac{\lambda}{4C_1}$ , we conclude with the help of the Poincaré inequality that  $F^{m,h}$  is coercive on  $X_1 \times X_2$ . Let

$$d := \inf\{F^{m,h}(c, \chi) \mid c \in X_1, \chi \in X_2\}, \quad d > -\infty.$$

If we consider a minimising sequence  $(c_l, \chi_l)_{l \in \mathbb{N}} \subset X_1 \times X_2$  with  $F^{m,h}(c_l, \chi_l) \rightarrow d$ , the coercivity of  $F^{m,h}$  implies the boundedness of  $(c_l, \chi_l)$  uniformly in  $l$ . Passing to a subsequence if necessary, by the reflexivity of  $X_1 \times X_2$  we may assume

$$(c_l, \chi_l) \rightharpoonup (c, \chi) \in X_1 \times X_2 \quad \text{for } l \rightarrow \infty$$

and by Rellich's theorem or Sobolev's embedding theorem,

$$(c_l, \chi_l) \rightarrow (c, \chi) \in L^2(\Omega, \mathbb{R}^4) \times L^2(\Omega, \mathbb{R}) \text{ for } l \rightarrow \infty$$

and  $(c_l, \chi_l) \rightarrow (c, \chi)$  a.e. in  $\Omega$ .

To verify the weak lower semicontinuity of  $F^{m,h}$  in  $X_1 \times X_2$  we first remark that this is true for all convex terms. For  $\int_{\Omega} f^1(c, \chi)$  this follows from Assumption (A2) and for  $\int_{\Omega} f^2(c, \chi)$  from (A2.2) and the dominated convergence theorem of Lebesgue. This implies

$$F^{m,h}(c, \chi) \leq \liminf_{l \rightarrow \infty} F^{m,h}(c_l, \chi_l). \quad \square$$

**Lemma 3.2:** (*Euler-Lagrange equations*)

The minimiser  $(c^m, \chi^m)$  of  $F^{m,h}$  fulfills

$$\int_{\Omega} \frac{c^m - c^{m-1}}{h} \cdot \xi + \int_{\Omega} L \nabla \mu^m : \nabla \xi = \int_{\Omega} r^{m-1} \xi \quad \text{for all } \xi \in Y, \quad (3.14a)$$

$$\int_{\Omega} \left( \lambda \nabla c^m \cdot \nabla \eta + \partial_c f(c^m, \chi^m) \cdot \eta \right) = \int_{\Omega} \mu^m \cdot \eta \quad \text{for } \eta \in Y \cap L^\infty(\Omega; \mathbb{R}^4), \quad (3.14b)$$

$$\int_{\Omega} \left[ \tau \frac{\chi^m - \chi^{m-1}}{h} + \omega(c^m, \chi^m) \right] \zeta + \int_{\Omega} \gamma \nabla \chi^m \cdot \nabla \zeta = 0 \quad \text{for } \zeta \in H^1(\Omega). \quad (3.14c)$$

Here,  $\mu^m = \mathcal{G}\left(\frac{c^m - c^{m-1}}{h} - r^{m-1}\right)$ .

**Proof:** We choose directions  $\xi \in Y \cap L^\infty(\Omega; \mathbb{R}^4)$ ,  $\zeta \in X_2 \cap L^\infty(\Omega; \mathbb{R})$  and determine the variations of  $F^{m,h}(c, \chi)$  with respect to  $c$  and  $\chi$  for  $\xi, \zeta$ . We start with the variation w.r.t.  $c$ , i.e.

$$\lim_{s \rightarrow 0} \left( (F^{m,h}(c^m + s\xi, \chi^m) - F^{m,h}(c^m, \chi^m))s^{-1} \right). \quad (3.15)$$

Since  $f^1$  is convex in  $c$ , we have

$$f^1(c^m, \chi^m) \geq f^1(c^m + s\xi, \chi^m) - s \partial_c f^1(c^m + s\xi, \chi^m) \cdot \xi.$$

This implies

$$\begin{aligned} f^1(c^m + s\xi, \chi^m) &\leq f^1(c^m, \chi^m) + |s \partial_c f^1(c^m + s\xi, \chi^m)| \|\xi\|_{L^\infty} \\ &\leq f^1(c^m, \chi^m) + |s| f^1(c^m + s\xi, \chi^m) \|\xi\|_{L^\infty} + C|s|. \end{aligned}$$

The last is by Assumption (A2.3) with  $\delta = 1$ . Hence, for  $s$  small enough, we find

$$\left| \frac{f^1(c^m + s\xi, \chi^m) - f^1(c^m, \chi^m)}{s} \right| \leq C(f^1(c^m, \chi^m) + 1).$$

Assumption (A2.2) and Lebesgue's dominated convergence theorem imply

$$\lim_{s \rightarrow 0} \frac{1}{s} \left( \int_{\Omega} f(c^m + s\xi, \chi^m) - f(c^m, \chi^m) \right) = \int_{\Omega} \partial_c f(c^m, \chi^m) \cdot \xi.$$

The variation of the quadratic form  $c \mapsto \frac{1}{2h} \|c^m - c^{m-1} - hr^{m-1}\|_L^2$  yields

$$\begin{aligned} &\lim_{s \rightarrow 0} \left( s^{-1} (2h)^{-1} (\|c^m + s\xi - c^{m-1} - hr^{m-1}\|_L^2 - \|c^m - c^{m-1} - hr^{m-1}\|_L^2) \right) \\ &= \left( \frac{c^m - c^{m-1} - hr^{m-1}}{h}, \xi \right)_L = \left( \mathcal{G} \left( \frac{c^m - c^{m-1}}{h} - r^{m-1} \right), \xi \right)_{L^2} = \left( \mu^m, \xi \right)_{L^2} \end{aligned}$$

and finally

$$\frac{\lambda}{2} \lim_{s \rightarrow 0} \left\{ s^{-1} \left[ (\nabla(c+s\xi), \nabla(c+s\xi))_{L^2} - (\nabla c, \nabla c)_{L^2} \right] \right\} = \lambda (\nabla c, \nabla \xi)_{L^2} = -\lambda (\Delta c, \xi)_{L^2}.$$

Because  $(c^m, \chi^m)$  is a minimiser, the variation in (3.15) is 0. Hence we obtain (3.14a) and (3.14b).

To derive (3.14c), we consider the variation of  $F^{m,h}(c^m, \chi^m)$  w.r.t.  $\chi$ . As before,

$$\lim_{s \rightarrow 0} \left( \tau s^{-1} (2h)^{-1} (\|\chi^m + s\zeta - \chi^{m-1}\|_{L^2}^2 - \|\chi^m - \chi^{m-1}\|_{L^2}^2) \right) = \left( \tau \frac{\chi^m - \chi^{m-1}}{h}, \zeta \right)_{L^2}.$$

It remains to prove

$$\lim_{s \rightarrow 0} \int_{\Omega} \left( f(c^m, \chi^m + s\zeta) - f(c^m, \chi^m) \right) = \int_{\Omega} \partial_\chi f(c^m, \chi^m) \zeta.$$

Since this limit can be justified in the same way as (3.15), Identity (3.14c) follows.  $\square$

### 3.6 Uniform estimates

In the preceding sections we showed for  $1 \leq m \leq M$  and arbitrary  $M \in \mathbb{N}$  the existence of a discrete solution  $(c^m, \mu^m, \chi^m)$ . We define the piecewise constant extension  $(c_M, \mu_M, \chi_M)$  of  $(c^m, \mu^m, \chi^m)_{1 \leq m \leq M}$  by

$$(c_M(t), \mu_M(t), \chi_M(t)) := (c_M^m, \mu_M^m, \chi_M^m) := (c^m, \mu^m, \chi^m) \quad \text{for } t \in ((m-1)h, mh]$$

and  $c_M(0) = c_0$ ,  $\chi_M(0) = \chi_0$ ,  $\mu_M(0)$  obtained from Eq. (3.14b).

The piecewise linear extension  $(\bar{c}_M, \bar{\mu}_M, \bar{\chi}_M)$  for  $t = (\beta m + (1-\beta)(m-1))h$  with appropriate  $\beta \in [0, 1]$  is given by the interpolation

$$(\bar{c}_M, \bar{\mu}_M, \bar{\chi}_M)(t) := \beta(c_M^m, \mu_M^m, \chi_M^m) + (1-\beta)(c_M^{m-1}, \mu_M^{m-1}, \chi_M^{m-1}).$$

**Lemma 3.3:** (*A-priori estimates*)

For sufficiently small  $h$  the following a-priori estimates are valid.

(a) For all  $M \in \mathbb{N}$  and all  $t \in [0, T_0]$  we have the dissipation inequality

$$F(c_M, \chi_M)(t) + \frac{1}{2} \int_{\Omega_t} (L \nabla \mu_M : \nabla \mu_M + |\partial_t \bar{\chi}_M|^2) \leq F(c_0, \chi_0). \quad (3.16)$$

(b) There exists a constant  $C > 0$  such that

$$\sup_{0 \leq t \leq T_0} \left\{ \|c_M(t)\|_{H^1} + \|\chi_M(t)\|_{H^1} \right\} \leq C, \quad (3.17)$$

$$\sup_{0 \leq t \leq T_0} \int_{\Omega} f^1(c_M(t), \chi_M(t)) + \|\nabla \mu_M\|_{L^2(\Omega_{T_0})} + \|\partial_t \bar{\chi}_M\|_{L^2(\Omega_{T_0})} \leq C. \quad (3.18)$$

**Proof:** The idea of the proof is to use the decay of  $t \mapsto F(c(t), \chi(t))$ . The original proof in [31] could be reused in all later works on the subject, and it is instructive to understand in which way for our reactive system, corresponding to Inequality (2.45), a modification of this proof becomes necessary. Simultaneously this modification reveals that the explicit treatment of the reaction term in (3.7a) is the natural formulation.

As  $(c^m, \chi^m)$  is a minimiser of  $F^{m,h}$ ,

$$\begin{aligned} F(c^m, \chi^m) + \frac{1}{2h} \|c^m - c^{m-1} - hr^{m-1}\|_L^2 + \frac{\tau}{2h} \|\chi^m - \chi^{m-1}\|_{L^2}^2 \\ \leq F(c^{m-1} + hr^{m-1}, \chi^{m-1}). \end{aligned} \quad (3.19)$$

A direct calculation yields

$$\frac{1}{2h} \|c^m - c^{m-1} - hr^{m-1}\|_L^2 = \frac{h}{2} (\nabla \mu^m, L \nabla \mu^m)_{L^2}.$$

To bring the right hand side of (3.19) in a form suitable for recursion, we remark that for sufficiently small  $h$

$$F(c^{m-1} + hr^{m-1}, \chi^{m-1}) \leq F(c^{m-1}, \chi^{m-1}).$$

This is a consequence of (A5), i.e.

$$\int_{\Omega} \mu^{m-1} \cdot r^{m-1} \leq 0. \quad (3.20)$$

( $\sigma(c^{m-1} + hr^{m-1}) = \sigma(c^{m-1}) + hD\sigma(c^{m-1})r^{m-1} + O(h^2)$  with  $\sigma(z) := F(z, \chi^{m-1})$ .)

Estimate (3.20) holds for sufficiently small  $\lambda$  due to Assumption (A4.2) and (A6).

By iterating (3.19) with estimated right hand side, we find

$$F(c_M^m, \chi_M^m) + \frac{1}{2} \int_0^{mh} \left( (\nabla \mu_M^m, L \nabla \mu_M^m)_{L^2} + (\partial_t^h \chi_M^m, \partial_t^h \chi_M^m)_{L^2} \right) dt \leq F(c_0, \chi_0).$$

Using the assumptions and with the help of the Poincaré inequality this proves the lemma.  $\square$

We extend  $c_M, \chi_M$  by the initial values  $c_0, \chi_0$  of  $c, \chi$  for  $t \in (-h, 0]$ . Now, for the linear interpolation  $\bar{c}_M$  of  $c_M^m$ , the Euler-Lagrange equation (3.14a) can be rewritten as

$$\int_{\Omega} \partial_t \bar{c}_M(t) \cdot \xi + \int_{\Omega} L \nabla \mu_M(t) : \nabla \xi = \int_{\Omega} r(c_M(t-h), \chi_M(t-h)) \cdot \xi \quad \text{for all } \xi \in Y \quad (3.21)$$

which holds for almost all  $t \in (0, T_0)$ . Together with the uniform estimates of Lemma 3.3, (3.21) allows to show compactness in time.

**Lemma 3.4:** (*Compactness for  $c_M$  and  $\mu_M$* )

There exists a constant  $C > 0$  such that for all  $t_1, t_2 \in [0, T_0]$

$$\|\bar{c}_M(t_2) - \bar{c}_M(t_1)\|_{L^2} \leq C|t_2 - t_1|^{\frac{1}{4}}.$$

Furthermore, there is a subsequence  $(c_M)_{M \in \mathcal{N}}$  and a subsequence  $(\mu_M)_{M \in \mathcal{N}}$  with  $\mathcal{N} \subset \mathbb{N}$  and there are  $c \in L^\infty(0, T_0; Y)$ ,  $\mu \in L^2(0, T_0; Y)$  such that

$$\begin{aligned} (i) \quad \bar{c}_M &\rightarrow c \text{ in } C^{0,\alpha}([0, T_0]; L^2(\Omega; \mathbb{R}^4)) \text{ for all } \alpha \in (0, \frac{1}{4}), \\ (ii) \quad c_M &\rightarrow c \text{ in } L^\infty(0, T_0; L^2(\Omega; \mathbb{R}^4)), \\ (iii) \quad c_M &\rightarrow c \text{ almost everywhere in } \Omega_{T_0}, \\ (iv) \quad c_M &\xrightarrow{*} c \text{ in } L^\infty(0, T_0; H_0^1(\Omega; \mathbb{R}^4)), \\ (v) \quad \mu_M &\rightharpoonup \mu \text{ in } L^2(0, T_0; H_0^1(\Omega; \mathbb{R}^4)) \end{aligned}$$

as  $M \in \mathcal{N}$  tends to infinity.

**Proof:** We test Eq. (3.21) with  $\xi := \bar{c}_M(t_2) - \bar{c}_M(t_1)$ , where  $t_1, t_2 \in [0, T_0]$  with  $t_1 < t_2$ . After integration in time from  $t_1$  to  $t_2$ , we obtain

$$\begin{aligned} \|\bar{c}_M(t_2) - \bar{c}_M(t_1)\|_{L^2}^2 &+ \int_{t_1}^{t_2} \int_{\Omega} L \nabla \mu_M(t) : \nabla (\bar{c}_M(t_2) - \bar{c}_M(t_1)) dt \\ &= \int_{t_1}^{t_2} \int_{\Omega} r(c_M(t-h), \chi_M(t-h)) (\bar{c}_M(t_2) - \bar{c}_M(t_1)) dt. \end{aligned}$$

The  $c_M^m$  are uniformly bounded in  $Y$ , therefore the linear interpolants  $\bar{c}_M$  are uniformly bounded in  $L^\infty(0, T_0; Y)$ . Thus we obtain with the continuity of  $r$

$$\begin{aligned} & \|\bar{c}_M(t_2) - \bar{c}_M(t_1)\|_{L^2}^2 \\ & \leq C \|\bar{c}_M\|_{L^\infty(H^1)} \int_{t_1}^{t_2} \left( \|\nabla \mu_M(t)\|_{L^2} + \|r(c_M(t-h), \chi_M(t-h))\|_{L^2} \right) dt \\ & \leq C \|\bar{c}_M\|_{L^\infty(H^1)} \left[ (t_2 - t_1)^{\frac{1}{2}} \|\nabla \mu\|_{L^2(\Omega_{T_0})} + (t_2 - t_1) \|r(c_M, \chi_M)\|_{L^\infty(L^2)} \right]. \end{aligned}$$

Employing the a-priori estimates (3.17) and (3.18) we have shown

$$\|\bar{c}_M(t_2) - \bar{c}_M(t_1)\|_{L^2} \leq C |t_2 - t_1|^{\frac{1}{4}} \quad \text{for all } t_1, t_2 \in [0, T_0]$$

for a positive constant  $C$ . This is the equicontinuity of  $(\bar{c}_M)_{M \in \mathbb{N}}$ .

The boundedness of  $(\bar{c}_M)$  in  $L^\infty(0, T_0; H_0^{1,2}(\Omega))$  and the fact that  $H^1$  is compactly embedded in  $L^2$  yields as a consequence of the Arzelà-Ascoli theorem part (i).

The claims (ii), (iii) and (iv) follow exactly as in [38]. We choose for  $t \in [0, T_0]$  values  $m \in \{1, \dots, M\}$  and  $\beta \in [0, 1]$  such that  $t = (\beta m + (1 - \beta)(m - 1))h$ . From the definition of  $\bar{c}$  we get at once

$$\begin{aligned} \|\bar{c}_M(t) - c_M(t)\|_{L^2} &= \|\beta c_M^m + (1 - \beta)c_M^{m-1} - c_M^m\|_{L^2} \\ &= (1 - \beta) \|c_M^m - c_M^{m-1}\|_{L^2} \\ &\leq Ch^{\frac{1}{4}}. \end{aligned}$$

This tends to zero as  $M$  becomes infinite. With the help of (i), this proves (ii). Since for a subsequence we have convergence almost everywhere, (iii) is proved, too. Claim (iv) is a direct consequence of Estimate (3.17) which gives the boundedness of  $c_M$  in  $L^\infty(0, T_0; Y)$ .

For the proof of (v) we notice that due to Estimate (3.18), the  $(\nabla \mu_M)$  are uniformly bounded in  $L^2(\Omega_{T_0})$ . By the Poincaré inequality the  $(\mu_M)$  are in fact uniformly bounded in  $L^2(0, T_0; H_0^1(\Omega))$ . With the Banach-Alaoglu theorem (v) follows.  $\square$

**Lemma 3.5:** (*Compactness for  $\chi_M$* )

For a suitable subsequence  $\mathcal{N} \subset \mathbb{N}$  we have

$$\begin{aligned} (i) \quad \bar{\chi}_M &\rightarrow \chi \text{ in } C^{0,\alpha}([0, T_0]; L^2(\Omega)) \text{ for all } \alpha \in (0, \frac{1}{2}), \\ (ii) \quad \chi_M &\rightarrow \chi \text{ in } L^\infty(0, T_0; L^2(\Omega)), \\ (iii) \quad \chi_M &\rightarrow \chi \text{ almost everywhere in } \Omega_{T_0}, \\ (iv) \quad \chi_M &\overset{*}{\rightharpoonup} \chi \text{ in } L^\infty(0, T_0; H^1(\Omega)), \\ (v) \quad \partial_c f(c_M, \chi_M) &\rightarrow \partial_c f(c, \chi) \text{ in } L^1(\Omega_{T_0}), \\ (vi) \quad \partial_\chi f(c_M, \chi_M) &\rightarrow \partial_\chi f(c, \chi) \text{ in } L^1(\Omega_{T_0}) \end{aligned}$$

as  $M \in \mathcal{N}$  tends to infinity.

**Proof:** Similar to Eq. (3.21) we can reformulate Identity (3.14c) to

$$\tau \int_{\Omega} \partial_t \bar{\chi}_M(t) \zeta + \int_{\Omega} \gamma \nabla \chi_M(t) \cdot \nabla \zeta + \int_{\Omega} \omega(c_M(t), \chi_M(t)) \zeta = 0 \quad \text{for all } \zeta \in H^1(\Omega) \quad (3.22)$$

which holds for almost all  $t \in [0, T_0]$ .

We test (3.22) with  $\zeta := \bar{\chi}_M(t_2) - \bar{\chi}_M(t_1)$ , where  $t_1, t_2 \in [0, T_0]$ ,  $t_2 > t_1$ . After integration in time from  $t_1$  to  $t_2$  we get

$$\begin{aligned} \tau \|\bar{\chi}_M(t_2) - \bar{\chi}_M(t_1)\|_{L^2}^2 + \int_{t_1}^{t_2} \int_{\Omega} \gamma \nabla \chi_M(t) \cdot \nabla (\bar{\chi}_M(t_2) - \bar{\chi}_M(t_1)) dt \\ + \int_{t_1}^{t_2} \omega(c_M(t), \chi_M(t)) (\bar{\chi}_M(t_2) - \bar{\chi}_M(t_1)) dt = 0. \end{aligned}$$

From the uniform boundedness of  $\bar{\chi}_M$  in  $L^\infty(0, T_0; H^1(\Omega))$  and in  $L^\infty(\Omega_{T_0})$  we obtain:

$$\begin{aligned} \int_{t_1}^{t_2} \int_{\Omega} \gamma \nabla \chi_M(t) \cdot \nabla (\bar{\chi}_M(t_2) - \bar{\chi}_M(t_1)) dt &\leq C \|\bar{\chi}_M\|_{L^\infty(H^1)} \int_{t_1}^{t_2} \|\nabla \chi_M(t)\|_{L^2} dt, \\ \int_{t_1}^{t_2} \omega(c_M(t), \chi_M(t)) (\bar{\chi}_M(t_2) - \bar{\chi}_M(t_1)) dt &\leq C \|\bar{\chi}_M\|_{L^\infty(\Omega_{T_0})} \int_{t_1}^{t_2} \omega(c_M(t), \chi_M(t)) dt. \end{aligned}$$

With the continuity of  $\omega$ , these estimates imply

$$\|\bar{\chi}_M(t_2) - \bar{\chi}_M(t_1)\|_{L^2} \leq C |t_2 - t_1|^{\frac{1}{2}} \quad \text{for all } t_1, t_2 \in [0, T_0]$$

and exactly as in Lemma 3.4 this yields statements (i)-(iv).

In order to prove (v) and (vi), we first notice that by Assumption (A2),  $\partial_c f$  and  $\partial_\chi f$  are continuous functions. Hence, by (iii) and Lemma 3.4(iii),

$$\begin{aligned} \partial_c f(c_M, \chi_M) &\rightarrow \partial_c f(c, \chi) \quad \text{almost everywhere in } \Omega_{T_0}, \\ \partial_\chi f(c_M, \chi_M) &\rightarrow \partial_\chi f(c, \chi) \quad \text{almost everywhere in } \Omega_{T_0}. \end{aligned}$$

The growth condition of Assumption (A2.3) on  $f^1$  now yields that for arbitrary  $\delta > 0$  and all measurable  $E \subset \Omega$

$$\int_E |\partial_c f^1(c_M, \chi_M)| \leq \delta \int_E f^1(c_M, \chi_M) + C_\delta |E| \leq \delta C + C_\delta |E|.$$

Therefore,  $\int_E |\partial_c f^1(c_M, \chi_M)| \rightarrow 0$  as  $|E| \rightarrow 0$  uniformly in  $M$  and by Vitali's theorem,  $f^1(c_M, \chi_M) \rightarrow f^1(c, \chi)$  in  $L^1(\Omega_{T_0})$  as  $M \in \mathcal{N}$  tends to infinity. The identical result for  $f^2$  follows directly from (A2.2) and the dominated convergence theorem of Lebesgue.

The proof of  $\partial_\chi f(c_M, \chi_M) \rightarrow \partial_\chi f(c, \chi)$  exploiting (A2.3) and (A2.2) is similar.  $\square$

### 3.7 Global existence of solutions for polynomial free energy

We are now in the position to state one of the main results.

**Theorem 3.1:** *(Global existence for System (3.1) with polynomial free energy)*  
Let the assumptions of Section 3.4 hold. Then, there exists a weak solution  $(c, \mu, \chi)$  of Formulation (3.1) in the sense of (3.6) such that

- (i)  $c \in C^{0, \frac{1}{4}}([0, T_0]; L^2(\Omega; \mathbb{R}^4))$ ,
- (ii)  $\partial_t c \in L^2(0, T_0; (H_0^1(\Omega; \mathbb{R}^4))')$ ,
- (iii)  $\chi \in C^{0, \frac{1}{2}}([0, T_0]; L^2(\Omega))$ ,
- (iv)  $\partial_t \chi \in L^2(0, T_0; (H_0^1(\Omega))')$ .

**Proof:** We are going to prove that  $(c, \mu, \chi)$  introduced in Lemmata 3.4 and 3.5 is the desired weak solution in the sense of (3.6).

First we show (3.6b). From (3.14b) we deduce

$$\int_{\Omega} \lambda \nabla c_M \cdot \nabla \eta + \partial_c f(c_M, \chi_M) \cdot \eta = \int_{\Omega} \mu_M \cdot \eta \quad \text{for all } \eta \in Y \cap L^\infty(\Omega; \mathbb{R}^4).$$

The convergence of

$$\int_{\Omega} \lambda c_M \cdot \nabla \eta \rightarrow \int_{\Omega} \lambda c \cdot \nabla \eta$$

as  $M \rightarrow \infty$  is clear by linearity and the convergence

$$\int_{\Omega} \partial_c f(c_M, \chi_M) \cdot \eta \rightarrow \int_{\Omega} \partial_c f(c, \chi) \cdot \eta \quad (3.23)$$

is again evident by Vitali's theorem similar to the proof of Lemma 3.5 by using the almost everywhere convergence of  $c_M$  and  $\chi_M$ , the growth condition (A2.3), Estimate (3.18) on  $f^1$  and the boundedness of  $\eta$ .

In the same way, we obtain (3.6c) from (3.22).

From Eq. (3.21) we learn

$$- \int_{\Omega_{T_0}} \partial_t \xi (\bar{c}_M - c_0) + \int_{\Omega_{T_0}} L \nabla \mu_M : \nabla \xi - \int_{\Omega_{T_0}} r(c_M(t-h), \chi_M(t-h)) \cdot \xi = 0$$

for all  $\xi \in L^2(0, T_0; Y)$  with  $\partial_t \xi \in L^2(\Omega_{T_0})$  and  $\xi(T_0) = 0$ . Passing to the limit  $M \rightarrow \infty$  together with Lemma 3.4 and after applying Vitali's theorem to the reaction term similar to (3.23) this implies (3.6a).  $\square$

### 3.8 Uniqueness of the solution

To show uniqueness of problem (3.1), we use an integration in time method. The proof requires the validity of the free energy inequality and the validity of (A6).

**Theorem 3.2:** *(Uniqueness of the solution to Formulation (3.1))*

*The solution  $(c, \mu, \chi)$  obtained in Theorem 3.1 is unique in the spaces stated in this theorem.*

**Proof:** Assume that  $(c^i, \chi^i, \mu^i)$ ,  $i = 1, 2$  are two solutions of System (3.1). Now, let  $c := c^2 - c^1$ ,  $\chi := \chi^2 - \chi^1$ ,  $\mu := \mu^2 - \mu^1$ ,  $r := r(c^2, \chi^2) - r(c^1, \chi^1)$  and  $\omega := (\partial_\chi f(c^2, \chi^2) - \partial_\chi f(c^1, \chi^1))/T$ .

The difference  $(c, \chi, \mu)$  solves the weak formulation

$$-\int_{\Omega_{T_0}} \partial_t \xi \cdot c + \int_{\Omega_{T_0}} L \nabla \mu : \nabla \xi - \int_{\Omega_{T_0}} r \cdot \xi = 0, \quad (3.24a)$$

$$\int_{\Omega_{T_0}} [(\partial_c f(c^2, \chi^2) - \partial_c f(c^1, \chi^1)) \cdot \eta + \lambda \nabla c \cdot \nabla \eta] = \int_{\Omega_{T_0}} \mu \cdot \eta, \quad (3.24b)$$

$$-\int_{\Omega_{T_0}} \tau \partial_t \zeta \chi + \int_{\Omega_{T_0}} \gamma \nabla \chi \cdot \nabla \zeta - \int_{\Omega_{T_0}} \omega \cdot \zeta = 0. \quad (3.24c)$$

For given  $\eta \in L^2(0, T_0; H_0^1(\Omega, \mathbb{R}^4))$  and  $t_0 \in (0, T_0)$  we define

$$\xi(\cdot, t) := \begin{cases} \int_t^{t_0} \eta(\cdot, s) ds & \text{if } t \leq t_0, \\ 0 & \text{if } t > t_0. \end{cases} \quad (3.25)$$

We use this as a test function in (3.24a) and obtain after integration by parts in time

$$\begin{aligned} 0 &= \int_{\Omega_{t_0}} c \cdot \eta + \int_{\Omega_{t_0}} L \nabla \mu : \nabla \left( \int_t^{t_0} \eta(\cdot, s) ds \right) - \int_{\Omega_{t_0}} r \cdot \left( \int_t^{t_0} \eta(\cdot, s) ds \right) \\ &= \int_{\Omega_{t_0}} c \cdot \eta + \int_{\Omega_{t_0}} L \nabla \left( \int_0^t \mu(s) ds \right) : \nabla \eta - \int_{\Omega_{t_0}} \left( \int_0^t r(s) ds \right) \cdot \eta. \end{aligned} \quad (3.26)$$

This implies

$$\mathcal{G} \left( c(t) - \int_0^t r(s) ds \right) = - \int_0^t \mu(s) ds \quad \text{and} \quad \partial_t \mathcal{G} \left( c(t) - \int_0^t r(s) ds \right) = -\mu(t).$$

By choosing  $\eta := \mu$  in (3.26) we obtain

$$0 = \int_{\Omega_{t_0}} c \cdot \mu + \int_{\Omega_{t_0}} L \nabla \left( \mathcal{G} \left( \int_0^t r(s) ds - c \right) \right) : \nabla \left( \partial_t \mathcal{G} \left( \int_0^t r(s) ds - c \right) \right) - \int_{\Omega_{t_0}} \left( \int_0^t r(s) ds \right) \cdot \mu$$

and consequently

$$0 = \int_{\Omega_{t_0}} c \cdot \mu + \int_{\Omega} L \nabla \mathcal{G} \left( \int_0^{t_0} r(s) ds - c(t_0) \right) : \nabla \mathcal{G} \left( \int_0^{t_0} r(s) ds - c(t_0) \right) - \int_{\Omega_{t_0}} \left( \int_0^t r(s) ds \right) \cdot \mu. \quad (3.27)$$

In Eq. (3.24b) we test with  $\eta := \mathcal{X}_{[0, t_0]} c$ . Hence we have

$$\int_{\Omega_{t_0}} c \cdot \mu = \int_{\Omega_{t_0}} \left[ \lambda |\nabla c|^2 + (\partial_c f(c^2, \chi^2) - \partial_c f(c^1, \chi^1)) \cdot c \right]. \quad (3.28)$$

From (3.27) and (3.28) we deduce

$$\left\| \left( \int_0^{t_0} r \right) - c(t_0) \right\|_L^2 + \int_{\Omega_{t_0}} \lambda |\nabla c|^2 - \int_{\Omega_{t_0}} \left( \int_0^t r(s) ds \right) \cdot \mu = - \int_{\Omega_{t_0}} (\partial_c f(c^2, \chi^2) - \partial_c f(c^1, \chi^1)) \cdot c. \quad (3.29)$$

From the free energy estimate we infer that if conditions (2.50), (3.11) and (A4.2) hold (i.e. if  $\lambda < \lambda_0$ ), then

$$\int_{\Omega_{t_0}} \left( \int_0^t r(s) ds \right) \cdot \mu \leq 0. \quad (3.30)$$

Therefore we obtain as a consequence of (3.29)

$$\lambda \int_{\Omega_{t_0}} |\nabla c|^2 \leq - \int_{\Omega_{t_0}} (\partial_c f(c^2, \chi^2) - \partial_c f(c^1, \chi^1)) \cdot c. \quad (3.31)$$

In (3.24c) we choose a test function  $\zeta$  analogous to (3.25). This leads to

$$\frac{\tau}{\gamma} \int_{\Omega_{t_0}} \chi \eta + \int_{\Omega_{t_0}} \nabla \left( \int_0^t \chi(s) ds \right) : \nabla \eta(t) - \frac{1}{\gamma} \int_{\Omega_{t_0}} \eta(t) \int_0^t \omega(s) ds = 0. \quad (3.32)$$

This implies because of  $\chi(0) = 0$

$$(-\Delta)^{-1} \left( \frac{\tau}{\gamma} \chi(t) - \frac{1}{\gamma} \int_0^t \omega(s) ds \right) = - \int_0^t \chi(s) ds$$

and

$$\partial_t (-\Delta)^{-1} \left( \frac{\tau}{\gamma} \chi(t) - \frac{1}{\gamma} \int_0^t \omega(s) ds \right) = -\chi(t).$$

We set  $\eta := \chi$  in (3.32). As in the treatment of Eq. (3.24a) this yields

$$0 = \gamma \tau \int_{\Omega_{t_0}} |\chi|^2 + \left\| \tau \chi(t_0) - \left( \int_0^{t_0} \omega(s) ds \right) \right\|_{L^2}^2 - \gamma \int_{\Omega_{t_0}} \chi(t) \int_0^t \omega(s) ds$$

and consequently with Young's inequality

$$\tau \int_{\Omega_{t_0}} |\chi|^2 \leq \delta \int_{\Omega_{t_0}} |\chi|^2 + \frac{C}{\delta} \int_{\Omega_{t_0}} \left( \int_0^t \omega(s) ds \right)^2. \quad (3.33)$$

Now we add (3.31) and (3.33) to find

$$\begin{aligned} \lambda \int_{\Omega_{t_0}} |\nabla c|^2 + \tau \int_{\Omega_{t_0}} |\chi|^2 \leq \\ \delta \int_{\Omega_{t_0}} |\chi|^2 + \frac{C}{\delta} \int_{\Omega_{t_0}} \left[ \left( \int_0^t \omega(s) ds \right)^2 + |\partial_c f(c^2, \chi^2) - \partial_c f(c^1, \chi^1)|^2 \right]. \end{aligned}$$

For small  $\delta$  the first integral on the right hand side can be absorbed on the left.  $\partial_c f$  and  $\omega$  are Lipschitz continuous due to Assumption (A2), therefore

$$\left( \int_0^t \omega(s) ds \right)^2 + |\partial_c f(c^2, \chi^2) - \partial_c f(c^1, \chi^1)|^2 \leq C_0 (|c|^2 + |\chi|^2)$$

with a suitable constant  $C_0$ . By exploiting the Poincaré inequality we find at last

$$\int_{\Omega_{t_0}} (|\nabla c|^2 + |\chi|^2) \leq C \int_{\Omega_{t_0}} (|\nabla c|^2 + |\chi|^2) + \int_0^t \int_{\Omega_{t_0}} (|\nabla c|^2 + |\chi|^2).$$

With Gronwall's inequality this finally yields  $c = \chi = 0$  in  $\Omega_{t_0}$  and with (3.24b)  $\mu = 0$  in  $\Omega_{t_0}$ . By repeating the argument, since  $t_0 > 0$ , this holds in the whole of  $\Omega_{T_0}$ .  $\square$

### 3.9 Logarithmic free energy

In the following four sections we are going to extend Theorem 3.1 to logarithmic free energies. The results will in particular be tailor made for the free energy functional considered in Chapter 2,

$$f(c, \chi) = \chi b^1 \sum_{j=1}^4 c_j \ln c_j + (1 - \chi) b^2 \sum_{j=1}^4 c_j \ln c_j + \sum_{i=1}^3 c_i E_i + \left( \sum_{j=1}^4 \alpha_j c_j \right)^2 + TW(\chi) \quad (3.34)$$

(in accordance with Definition (2.8) if we agree with the convention of this chapter that  $f$  denotes the free energy density without surface energy terms). Of course it would be possible to modify the statements to hold for other energy functionals.

It is well known that the logarithmic shape of  $f$  has its origin in the system entropy and a rigorous derivation from statistical thermodynamics is possible if random pairwise interactions are permitted. We will use the statements in the first part of this chapter concerning polynomial free energies that can be regarded as a Taylor expansion.

The well known main difficulty in the mathematical discussion is that  $f$  becomes singular as one of the  $c_j$  approaches 0. Instead of the very natural idea of differentiating the equations with the possibly singular terms with respect to time, see [29], we use the method presented in [38], because it can be generalised to an extended model with elasticity, see Section 5.4.

For the proof of  $0 < c_j < 1$ ,  $1 \leq j \leq 4$  we approximate  $f$  for  $\delta > 0$  by some  $f^\delta$  that fulfills the requirements of Section 3.4 and find suitable a-priori estimates that put us in the position to pass to the limit  $\delta \rightarrow 0$ .

The logarithmic form of the free energy guarantees that the concentration vector  $c$  lies inside the transformed Gibbs simplex

$$G := \Sigma \cap \{c \in \mathbb{R}^4 \mid c_j \geq 0 \text{ for } 1 \leq j \leq 4\}$$

and that  $\chi \in (0, 1)$ . Therefore  $(c, \chi)$  has physical meaning.

The assumptions (A2) and (A3) of Section 3.4 are replaced by the following ones:

(A2')  $f$  is of the form (3.34) with constants  $\alpha_j > 0$ ,  $b^1 > 0$ ,  $b^2 > 0$ ,  $T > 0$ .

(A3') The initial values  $c_0 \in X_1$ ,  $\chi_0 \in X_2$  fulfill  $c_0 \in G$ ,  $\chi \in [0, 1]$  almost everywhere and

$$\int_{\Omega} c_{0l} > 0 \quad \text{for } 1 \leq l \leq 4, \quad \int_{\Omega} \chi > 0, \quad \int_{\Omega} (1 - \chi) > 0.$$

(A6') Additional to the conditions in (A6) we demand

$$\kappa^{1/\max(b^1, b^2)} \leq \frac{1}{e^2}. \quad (3.35)$$

The assumptions (A1) and (A4) remain unchanged and continue to hold.

To proceed, we define for  $d > 0$  the convex function

$$\psi(d) := d \ln d$$

and for  $\delta > 0$  its regularisation (defined for  $d \in \mathbb{R}$ )

$$\psi^\delta(d) := \begin{cases} d \ln d & \text{for } d \geq \delta, \\ d \ln \delta - \frac{\delta}{2} + \frac{d^2}{2\delta} & \text{for } d < \delta. \end{cases}$$

The regularised free energy functional is defined in such a way that  $\psi^\delta \in C^2$  and the derivative  $(\psi^\delta)'$  is monotone increasing. This ansatz goes back to [29].

The free energy of the regularised  $\delta$ -problem is found by replacing  $\sum_i c_i \ln c_i$  by  $\sum_i \psi^\delta(c_i)$  in (2.25).

Since the convex combination

$$\bar{f}(c, \chi) := \chi f_1(c) + (1 - \chi) f_2(c)$$

would define a non-convex functional in  $c$  if  $\chi \notin [0, 1]$ , we consider the following penalisation ( $f^\delta = f^{1,\delta} + f^2$ , see Assumption (A2))

$$f^{1,\delta}(c, \chi) := \begin{cases} \chi b^1 \sum_j \psi^\delta(c_j) + (1 - \chi) b^2 \sum_j \psi^\delta(c_j) + T[\psi^\delta(\chi) + \psi^\delta(1 - \chi)] & \text{if } \chi \in (0, 1), \\ +\infty & \text{else} \end{cases}$$

$$f^2(c, \chi) := \left( \sum_{j=1}^4 \alpha_j c_j \right)^2.$$

Due to the expression  $\psi^\delta(\chi) + \psi^\delta(1 - \chi)$  in the definition of  $f^\delta$  it is obvious that every minimiser  $\chi$  fulfills  $0 < \chi < 1$  in  $\Omega_{T_0}$ . This is proved rigorously in Lemma 3.8 below.

It can be easily checked that the functional  $F^{m,h}$  of Section 3.1 still has a minimiser  $(c^m, \chi^m)$  for every  $m$  and sufficiently small  $h$ . For  $\chi \in (0, 1)$ ,  $f^{1,\delta}$  is still continuously differentiable. Since  $f^{1,\delta}$ ,  $f^2$  fulfill the assumptions of Section 3.4, the earlier existence results can be carried over.

The regularisation  $f^\delta$  of  $f$  also implies that  $\omega(c^\delta, \chi^\delta) = \partial_\chi(f^\delta(c^\delta, \chi^\delta)/T)$  depends on  $\delta$  and therefore we will replace  $\omega(c^m, \chi^m)$  in the implicit time discretisation (3.7c) by  $\omega^\delta(c^m, \chi^m)$  and the weak formulation (3.6c) by

$$- \int_{\Omega_{T_0}} \tau \partial_t \zeta (\chi^\delta - \chi_0) + \int_{\Omega_{T_0}} \gamma \nabla \chi^\delta \cdot \nabla \zeta - \int_{\Omega_{T_0}} \omega^\delta(c^\delta, \chi^\delta) \zeta = 0 \quad (3.36)$$

for all  $\zeta \in L^2(0, T_0; H^1(\Omega; \mathbb{R}))$  with  $\partial_t \zeta \in L^2(\Omega_{T_0})$ ,  $\zeta(T_0) = 0$ .

Later we will show that  $\omega^\delta(c^\delta, \chi^\delta) \rightarrow \omega(c, \chi)$  in  $L^1(\Omega_{T_0})$  as  $\delta \searrow 0$ .

The only assumption that needs further clarification is (A5). In order to verify Condition (3.10), we have to construct an approximation  $r^\delta = (r_1^\delta, -r_1^\delta, r_1^\delta, 0)$  of  $r$  and have to check that

$$\int_{\Omega} k_B T b_\chi \left[ (\psi^\delta)'(c_1) - 2(\psi^\delta)'(c_2) + (\psi^\delta)'(c_3) + \frac{E_1 - 2E_2 + E_3}{k_B T b_\chi} \right] r_1^\delta \leq 0. \quad (3.37)$$

We claim that a good choice for  $r_1^\delta$  is

$$r_1^\delta(c, \chi) := k^{1/b_\chi} \left( \max(c_2, \delta)^2 - \kappa^{1/b_\chi} \max(c_1, \delta) \max(c_3, \delta) \right).$$

$r_1^\delta$  is a continuous function and we will see below that  $r_1^\delta > 0$  is fulfilled. In order to verify (3.37), we want to consider three characteristic cases:

Case 1:  $c_1 \geq \delta$ ,  $c_2 \geq \delta$ ,  $c_3 \geq \delta$ :

Apparently  $r^\delta = r$ , and (3.10) follows verbatim as in the proof of the free energy inequality in Section 2.6.

Case 2:  $c_1 < \delta$ ,  $c_2 \geq \delta$ ,  $c_3 \geq \delta$ :

From the definition of  $\psi^\delta$  we find that we have to estimate

$$\begin{aligned} & \int_{\Omega} k_B T b_\chi \left[ \ln \delta + \frac{c_1}{\delta} - 2 \ln c_2 - 2 + \ln c_3 + 1 + \frac{E_1 + E_3 - 2E_2}{k_B T b_\chi} \right] r_1^\delta \\ &= \int_{\Omega} k_B T b_\chi \left[ \ln \left( \frac{\delta c_3 \kappa^{1/b_\chi}}{c_2^2} \right) + \frac{c_1}{\delta} - 1 \right] r_1^\delta. \end{aligned}$$

Estimate (3.37) follows now from  $(\ln(\delta c_3 \kappa^{1/b_\chi}) - \ln(c_2^2)) r_1^\delta < 0$  and because of  $\frac{c_1}{\delta} - 1 < 0$  and  $r_1^\delta = k^{1/b_\chi} (c_2^2 - \kappa^{1/b_\chi} \delta c_3) > 0$  due to (3.11). We emphasise that we really need  $r_1^\delta > 0$  in order to have  $\int_{\Omega} (\alpha_1 - 2\alpha_2 + \alpha_3) Q(c^\delta) r_1^\delta < 0$  which allows to compensate the surface energy term for sufficiently small  $\lambda$ .

Case 3:  $c_1 < \delta$ ,  $c_2 < \delta$ ,  $c_3 < \delta$ :

Here we have to estimate

$$\int_{\Omega} k_B T b_\chi \left[ \ln \left( \frac{\delta^2}{\delta^2} \right) + \frac{c_1}{\delta} - 2 \frac{c_2}{\delta} + \frac{c_3}{\delta} + \frac{E_1 - 2E_2 + E_3}{k_B T b_\chi} \right] r_1^\delta.$$

We observe  $r_1^\delta = k^{1/b_\chi} \delta^2 (1 - \kappa^{1/b_\chi}) > 0$  because  $\kappa < 1$  by assumption. Finally

$$\int_{\Omega} \left( \frac{E_1 - 2E_2 + E_3}{k_B T b_\chi} + \frac{c_1 - 2c_2 + c_3}{\delta} \right) < \int_{\Omega} (\ln(\kappa^{1/b_\chi}) + 2) \leq 0$$

if  $\kappa$  satisfies (3.35).

The remaining cases can be treated similar to Case 2. The case  $c_2 < \delta$  is only possible as long as  $\delta \geq \sigma_2$ .

### 3.10 Uniform estimates

The following lemma was first stated and proved by Elliott and Luckhaus [29] for logarithmic free energies typical for the Cahn-Hilliard system.

**Lemma 3.6:** *(Uniform bound from below on  $f^\delta$ )*

For  $\delta_0 = \frac{1}{e}$  there exists a  $K > 0$  such that for all  $\delta \in (0, \delta_0)$

$$f^\delta(c, \chi) \geq -K \quad \text{for all } c \in \Sigma, \chi \in [0, 1].$$

**Proof:** For  $\delta_0 < \frac{1}{e}$  one has  $\psi^\delta(d) \geq -\frac{1}{e}$  for all  $\delta < \delta_0$ . As  $b^l, T > 0$ , the proof is complete.  $\square$

The following lemma summarises the results for the regularised problem proved in Sections 3.1 to 3.7.

**Lemma 3.7:** *(A-priori and compactness results for the regularised problem)*

(a) For  $\delta \in (0, \delta_0)$  there exists a weak solution  $(c^\delta, \mu^\delta, \chi^\delta)$  of (3.1) with a logarithmic free energy that satisfies (A2')-(A6') in the sense of (3.6) with (3.6c) replaced by (3.36).

(b) There exists a constant  $C > 0$  independent of  $\delta$  such that for all  $\delta \in (0, \delta_1)$  with some constant  $\delta_1 \leq \delta_0$

$$\begin{aligned} \sup_{t \in [0, T_0]} \left\{ \|c^\delta(t)\|_{H^1} + \|\chi^\delta(t)\|_{H^1} \right\} &\leq C, \\ \sup_{t \in [0, T_0]} \int_{\Omega} f^{1, \delta}(c^\delta(t), \chi^\delta(t)) + \|\nabla \mu^\delta\|_{L^2(\Omega_{T_0})} &\leq C \end{aligned} \quad (3.38)$$

and

$$\begin{aligned} \|c^\delta(t_2) - c^\delta(t_1)\|_{L^2} &\leq C|t_2 - t_1|^{\frac{1}{4}}, \\ \|\chi^\delta(t_2) - \chi^\delta(t_1)\|_{L^2} &\leq C|t_2 - t_1|^{\frac{1}{2}} \end{aligned}$$

for all  $t_1, t_2 \in [0, T_0]$ .

(c) One can extract subsequences  $(c^\delta)_{\delta \in \mathcal{R}}$ ,  $(\mu^\delta)_{\delta \in \mathcal{R}}$  and  $(\chi^\delta)_{\delta \in \mathcal{R}}$  where  $\mathcal{R} \subset (0, \delta_1)$  is a countable set with zero as the only accumulation point such that

- (i)  $c^\delta \rightharpoonup c$  in  $C^{0, \alpha}([0, T_0]; L^2(\Omega; \mathbb{R}^4))$  for all  $\alpha \in (0, \frac{1}{4})$ ,
- (ii)  $c^\delta \rightarrow c$  almost everywhere in  $\Omega_{T_0}$ ,
- (iii)  $c^\delta \overset{*}{\rightharpoonup} c$  in  $L^\infty(0, T_0; H_0^1(\Omega; \mathbb{R}^4))$ ,
- (iv)  $\chi^\delta \rightarrow \chi$  in  $C^{0, \alpha}([0, T_0]; L^2(\Omega))$  for all  $\alpha \in (0, \frac{1}{2})$ ,
- (v)  $\chi^\delta \rightarrow \chi$  almost everywhere in  $\Omega_{T_0}$  and  $0 \leq \chi^\delta, \chi \leq 1$  a.e. in  $\Omega_{T_0}$ ,
- (vi)  $\chi^\delta \overset{*}{\rightharpoonup} \chi$  in  $L^\infty(0, T_0; H^1(\Omega))$ ,
- (vii)  $\mu^\delta \rightharpoonup \mu$  in  $L^2(0, T_0; H_0^1(\Omega; \mathbb{R}^4))$

as  $\delta \in \mathcal{R}$  tends to zero.

**Proof:** Using Lemma 3.6, the regularised problem satisfies the assumptions of Section 3.4 and by Theorem 3.1, a weak solution for fixed  $\delta \in (0, \delta_0)$  exists. This proves (a). The estimates in (b) are a direct consequence of Lemma 3.3 and Lemma 3.4, where due to Assumption (A4.2) we have to choose  $\delta$  small enough for Lemma 3.3 to hold. From Lemma 3.3, it follows that  $F^\delta(c_0, \chi_0)$  does not depend on  $\delta$ , hence the constant on the right hand side does not depend on  $\delta$ .

(c) is proved by Lemmata 3.4 and 3.5.  $\square$

### 3.11 Higher integrability for the logarithmic free energy

Since  $\varphi^\delta := (\psi^\delta)'$  will be singular as  $\delta \rightarrow 0$  we introduce for  $r > 0$

$$\varphi_r^\delta(d) := \begin{cases} \varphi^\delta(d) |\varphi^\delta(d)|^{r-1} & \text{if } \varphi^\delta(d) \neq 0, \\ 0 & \text{if } \varphi^\delta(d) = 0. \end{cases}$$

By definition,  $\varphi_r^\delta \in C^0(\mathbb{R})$ .

For  $0 < r < 1$ ,  $\varphi_r^\delta$  is not differentiable at the zero point of  $\varphi^\delta$ . To overcome this difficulty, for  $\varrho > 0$  we introduce the function  $\varphi_r^{\delta, \varrho}$  with  $\varphi_r^{\delta, \varrho} = \varphi_r^\delta$  in  $\mathbb{R} \setminus [0, 1]$  and define  $\varphi_r^{\delta, \varrho}$  in  $[0, 1]$  such that  $\varphi_r^{\delta, \varrho}$  is a  $C^1$  function, monotone increasing and  $\varphi_r^{\delta, \varrho} \rightarrow \varphi_r^\delta$  in  $C^0(\mathbb{R})$  as  $\varrho \searrow 0$ .

For the approximation of  $\varphi^\delta(\chi^\delta)$  in the modified Allen-Cahn equation it is more suitable to introduce the Dirac sequence

$$\varphi^{\delta, \varepsilon}(x) := (\varphi^\delta * J_\varepsilon)(x) := \varepsilon^{-D} \int_{\mathbb{R}^D} \varphi^\delta(x) J((x-y)/\varepsilon) dy$$

where the kernel  $J \in C^\infty(B^1(0))$  is a positive smooth polynomial (motivated by Assumption (A2)). As is well known,  $\varphi^{\delta, \varepsilon} \in C^\infty$  and  $\varphi^{\delta, \varepsilon} \rightarrow \varphi^\delta$  in  $L^p(\Omega)$  as  $\varepsilon \searrow 0$  for any  $p \geq 1$ , see for instance [4], [19].

Even though by construction  $0 < \chi^\delta < 1$  almost everywhere, it might still happen that for the limit the sets  $\{x \in \Omega \mid \chi(x) = 0\}$  and  $\{x \in \Omega \mid \chi(x) = 1\}$  have non-zero Lebesgue measure and that the entropic terms in the free energy density become singular. To show that this is not the case we need the following

**Lemma 3.8:** (*Integrability of the regularised free energy*)

*There exists a constant  $C > 0$  such that for all  $\delta \in (0, \delta_0)$*

- (i)  $\|\varphi^\delta(c_l^\delta)\|_{L^q(\Omega_{T_0})} \leq C$  for a suitable  $q > 1$  and all  $1 \leq l \leq 4$ ,
- (ii)  $\|\varphi^\delta(\chi^\delta) + \varphi^\delta(1 - \chi^\delta)\|_{L^2(\Omega_{T_0})} \leq C$ .

**Proof:** The weak formulation (3.6b) for the generalised chemical potential reads

$$\begin{aligned} \int_{\Omega_{T_0}} \mu^\delta \cdot \eta &= \int_{\Omega_{T_0}} \left\{ \lambda \sum_{l=1}^4 \nabla c_l^\delta \cdot \nabla \eta_l + 2 \left[ \alpha_l \sum_{j=1}^4 \alpha_j c_j^\delta \right]_{1 \leq l \leq 4} \cdot \eta + \sum_{l=1}^3 E_l \eta_l \right\} \\ &+ \int_{\Omega_{T_0}} (\chi^\delta b^1 + (1 - \chi^\delta) b^2) [\varphi^\delta(c_l^\delta)]_{1 \leq l \leq 4} \cdot \eta \end{aligned} \quad (3.39)$$

for all  $\eta \in L^2(0, T_0; H^1(\Omega; \mathbb{R}^4)) \cap L^\infty(\Omega_{T_0}, \mathbb{R}^4)$ . We choose  $\eta := [\varphi_r^{\delta, \varrho}(c_l^\delta)]_{1 \leq l \leq 4}$  in (3.39) which is an admissible test function because of the Sobolev embedding theorem and because of  $\varphi_r^{\delta, \varrho} \in C^1$ . We obtain

$$\begin{aligned} \int_{\Omega_{T_0}} \sum_{l=1}^4 \mu_l^\delta \varphi_r^{\delta, \varrho}(c_l^\delta) &= \int_{\Omega_{T_0}} \lambda \sum_{l=1}^4 \nabla c_l^\delta \cdot \nabla \varphi_r^{\delta, \varrho}(c_l^\delta) + \int_{\Omega_{T_0}} \sum_{l=1}^4 \varphi_r^{\delta, \varrho}(c_l^\delta) \left( 2\alpha_l \sum_{j=1}^4 \alpha_j c_j^\delta + E_l \right) \\ &\quad + \int_{\Omega_{T_0}} \sum_{l=1}^4 (\chi^\delta b^1 + (1 - \chi^\delta) b^2) \varphi^\delta(c_l^\delta) \varphi_r^{\delta, \varrho}(c_l^\delta). \end{aligned}$$

In the above formula, we set for simplicity  $E_4 := 0$ . Due to  $(\varphi_r^{\delta, \varrho})' \geq 0$  we find

$$\int_{\Omega_{T_0}} \lambda \sum_{l=1}^4 \nabla c_l^\delta \cdot \nabla \varphi_r^{\delta, \varrho}(c_l^\delta) \geq 0.$$

This implies

$$\begin{aligned} &\int_{\Omega_{T_0}} \sum_{l=1}^4 (\chi^\delta b^1 + (1 - \chi^\delta) b^2) \varphi^\delta(c_l^\delta) \varphi_r^{\delta, \varrho}(c_l^\delta) \\ &\leq \int_{\Omega_{T_0}} \sum_{l=1}^4 \mu_l^\delta \varphi_r^{\delta, \varrho}(c_l^\delta) - \int_{\Omega_{T_0}} \sum_{l=1}^4 \varphi_r^{\delta, \varrho}(c_l^\delta) \left( 2\alpha_l \sum_{j=1}^4 \alpha_j c_j^\delta + E_l \right) \\ &\leq C \max_{1 \leq l \leq 4} \|\varphi_r^{\delta, \varrho}(c_l^\delta)\|_{L^2(\Omega_{T_0})} \left( \|\mu^\delta\|_{L^2(\Omega_{T_0})} + \|c^\delta\|_{L^2(\Omega_{T_0})} \right) \end{aligned}$$

where the constant  $C$  in the last line depends on  $\alpha_1, \dots, \alpha_4$  and on  $E_1, \dots, E_3$ .

For  $\varrho \searrow 0$  employing Lemma 3.6 and Lemma 3.7 this proves

$$\int_{\Omega_{T_0}} \sum_{l=1}^4 (\chi^\delta b^1 + (1 - \chi^\delta) b^2) \varphi^\delta(c_l^\delta) \varphi_r^{\delta, \varrho}(c_l^\delta) \leq C. \quad (3.40)$$

A direct computation finally yields

$$\begin{aligned} \int_{\Omega_{T_0}} \sum_{l=1}^4 (\chi^\delta b^1 + (1 - \chi^\delta) b^2) \varphi^\delta(c_l^\delta) \varphi_r^{\delta, \varrho}(c_l^\delta) &\geq \int_{\Omega_{T_0}} \max_{1 \leq l \leq 4} (\chi^\delta b^1 + (1 - \chi^\delta) b^2) |\varphi^\delta(c_l^\delta)|^{r+1} \\ &\geq \int_{\Omega_{T_0}} C \max_{1 \leq l \leq 4} |\varphi^\delta(c_l^\delta)|^{r+1} \end{aligned}$$

for a constant  $C = C(b^1, b^2)$ . In the last estimate we used  $\chi^\delta b^1 + (1 - \chi^\delta) b^2 > 0$  almost everywhere in  $\Omega_{T_0}$ . Together with (3.40) this proves (i).

Next we consider the weak formulation (3.36)

$$\begin{aligned} &-\int_{\Omega_{T_0}} \tau \partial_t \zeta (\chi^\delta - \chi_0) + \int_{\Omega_{T_0}} \gamma \nabla \chi^\delta \cdot \nabla \zeta - \int_{\Omega_{T_0}} (b^2 - b^1) \sum_{j=1}^4 \psi^\delta(c_j^\delta) \zeta \\ &+ \int_{\Omega_{T_0}} T(\varphi^\delta(\chi^\delta) + \varphi^\delta(1 - \chi^\delta)) \zeta = 0 \end{aligned} \quad (3.41)$$

of the Allen-Cahn equation. We test Eq. (3.41) with  $\zeta := \varphi^{\delta,\varepsilon}(\chi) + \varphi^{\delta,\varepsilon}(1 - \chi)$ . Since by Theorem 3.1  $\chi^\delta \in C^{0,\frac{1}{2}}(0, T_0; L^2(\Omega_{T_0}))$ , we can use Fourier theory to formally shift a half time derivative from  $\zeta$  to  $\chi^\delta - \chi_0$ . After this procedure we find with Lemma 3.7

$$\int_{\Omega_{T_0}} \tau \partial_t^{\frac{1}{2}} (\varphi^{\delta,\varepsilon}(\chi^\delta) + \varphi^{\delta,\varepsilon}(1 - \chi^\delta)) \partial_t^{\frac{1}{2}} (\chi^\delta - \chi_0) \leq C.$$

To estimate the second integral in (3.41), we notice

$$\int_{\Omega_{T_0}} \gamma \nabla \chi^\delta \cdot \nabla (\varphi^{\delta,\varepsilon}(\chi^\delta) + \varphi^{\delta,\varepsilon}(1 - \chi^\delta)) = \int_{\Omega_{T_0}} \gamma |\nabla \chi^\delta|^2 [(\varphi^{\delta,\varepsilon})'(\chi^\delta) - (\varphi^{\delta,\varepsilon})'(1 - \chi^\delta)].$$

By Lemma 3.7,  $\chi^\delta$  is bounded in  $L^\infty(0, T_0; H^1(\Omega))$  which implies the boundedness of the integral.

When choosing  $\delta$  sufficiently small in (i) we find  $c_j \in (0, 1)$  for  $1 \leq j \leq 4$ , see also the proof of Theorem 3.3. This guarantees that  $\psi^\delta(c_j)$  does not become singular and thus proves the boundedness of the third integral in (3.41) independently of  $\delta$ . Finally, we have

$$\begin{aligned} 0 &\leq \int_{\Omega_{T_0}} (\varphi^\delta(\chi^\delta) + \varphi^\delta(1 - \chi^\delta)) (\varphi^{\delta,\varepsilon}(\chi^\delta) + \varphi^{\delta,\varepsilon}(1 - \chi^\delta)) \\ &\rightarrow \|\varphi^\delta(\chi^\delta) + \varphi^\delta(1 - \chi^\delta)\|_{L^2(\Omega_{T_0})} \quad \text{as } \varepsilon \searrow 0. \end{aligned}$$

By combining these results, (ii) follows.  $\square$

## 3.12 Global existence of solutions for logarithmic free energies

**Theorem 3.3:** *(Global existence of solutions of System (3.1))*

*Let the assumptions of Section 3.9 hold. Then, there exists a weak solution  $(c, \mu, \chi)$  in the sense of (3.6) of Formulation (3.1) with logarithmic free energy such that*

- (i)  $c \in C^{0,\frac{1}{4}}([0, T_0]; L^2(\Omega; \mathbb{R}^4))$ ,
- (ii)  $\partial_t c \in L^2(0, T_0; (H_0^1(\Omega; \mathbb{R}^4))')$ ,
- (iii)  $\chi \in C^{0,\frac{1}{2}}([0, T_0]; L^2(\Omega))$ ,
- (iv)  $\partial_t \chi \in L^2(0, T_0; (H_0^1(\Omega))')$ ,
- (v) *there exists a  $q > 1$  such that  $\ln c_j \in L^q(\Omega_{T_0})$  for  $1 \leq j \leq 4$ ,  $\ln \chi, \ln(1 - \chi) \in L^2(\Omega_{T_0})$  and in particular  $0 < c_j, \chi < 1$  a.e.*

**Proof:** We pass to the limit  $\delta \searrow 0$  in the weak formulation (3.6) with  $f$  defined by (3.34) and have to show that  $(c, \mu, \chi)$  found in Lemma 3.7 is a solution.

For the limit in (3.6b), we must take care of the term

$$\chi^\delta b^1 \sum_{j=1}^4 \varphi^\delta(c_j^\delta) + (1 - \chi^\delta) b^2 \sum_{j=1}^4 \varphi^\delta(c_j^\delta). \quad (3.42)$$

From the almost everywhere convergence of  $c_l^\delta$  to  $c_l$ , Lemma 3.8 (i) and the Lemma of Fatou we find

$$\int_{\Omega_{T_0}} \liminf_{\delta \searrow 0} |\varphi^\delta(c_l^\delta)|^q \leq \liminf_{\delta \searrow 0} \int_{\Omega_{T_0}} |\varphi^\delta(c_l^\delta)|^q \leq C.$$

Next we will show that

$$\lim_{\delta \searrow 0} \varphi^\delta(c_l^\delta) = \begin{cases} \varphi(c_l) & \text{if } \lim_{\delta \searrow 0} c_l^\delta = c_l > 0, \\ \infty & \text{if } \lim_{\delta \searrow 0} c_l^\delta = c_l \leq 0 \end{cases} \quad (3.43)$$

almost everywhere in  $\Omega_{T_0}$ . For each  $(x, t) \in \Omega_{T_0}$  with  $\lim_{\delta \searrow 0} c_l^\delta(x, t) = c_l(x, t) > 0$ , we obtain from  $\varphi^\delta(d) = \varphi(d)$  for  $d \geq \delta$  that  $\varphi^\delta(c_l^\delta(x, t)) \rightarrow \varphi(c_l(x, t))$ . In the second case of a point  $(x, t) \in \Omega_{T_0}$  with  $\lim_{\delta \searrow 0} c_l^\delta(x, t) = c_l(x, t) \leq 0$ , we have for  $\delta$  small enough

$$|\varphi^\delta(c_l^\delta(x, t))| \geq \varphi(\max\{\delta, c_l^\delta(x, t)\}) \rightarrow \infty \quad \text{for } \delta \searrow 0.$$

This proves (3.43). A similar statement holds for  $\psi^\delta(\chi^\delta)$ .

From Eq. (3.43) and Lemma 3.8 (i) we deduce  $0 < c_l < 1$  almost everywhere,  $\int_{\Omega_{T_0}} |\varphi(c_l)|^q \leq C$  and  $\varphi^\delta(c_l^\delta) \rightarrow \varphi(c_l)$  almost everywhere. With Vitali's theorem we find

$$\varphi^\delta(c_l^\delta) \rightarrow \varphi(c_l) \quad \text{in } L^1(\Omega_{T_0}).$$

This allows to pass to the limit in (3.6b).

Now we want to consider the limit in (3.36). The relation  $0 < c_j < 1$  almost everywhere implies  $b^l \sum_{j=1}^4 \psi^\delta(c_j^\delta) \rightarrow b^l \sum_{j=1}^4 \psi(c_j)$ ,  $l = 1, 2$  almost everywhere in  $\Omega_{T_0}$  as in the first case of (3.43). From  $\varphi^\delta(c_j^\delta) \in L^q(\Omega_{T_0})$ , the uniform boundedness of  $\chi^\delta$  and Vitali's theorem we recover for  $\delta \searrow 0$

$$\begin{aligned} \chi^\delta b^1 \sum_{j=1}^4 \psi^\delta(c_j^\delta) &\rightarrow \chi b^1 \sum_{j=1}^4 \psi(c_j) \quad \text{in } L^1(\Omega_{T_0}), \\ (1 - \chi^\delta) b^2 \sum_{j=1}^4 \psi^\delta(c_j^\delta) &\rightarrow (1 - \chi) b^2 \sum_{j=1}^4 \psi(c_j) \quad \text{in } L^1(\Omega_{T_0}) \end{aligned}$$

such that

$$\omega^\delta(c^\delta, \chi^\delta) \rightarrow \omega(c, \chi) \quad \text{in } L^1(\Omega_{T_0}) \quad \text{for } \delta \searrow 0.$$

By repeating the argumentation from above for  $\varphi^\delta(\chi^\delta) + \varphi^\delta(1 - \chi^\delta)$  we deduce  $0 < \chi < 1$  almost everywhere in  $\Omega_{T_0}$  which again with the help of Vitali's theorem and Lemma 3.8 (ii) yields

$$\varphi^\delta(\chi^\delta) + \varphi^\delta(1 - \chi^\delta) \rightarrow \varphi(\chi) + \varphi(1 - \chi) \quad \text{in } L^1(\Omega_{T_0}). \quad (3.44)$$

So we can also pass to the limit in (3.36).

The limit for (3.6a) can be justified in the same way as in the proof of Theorem 3.1 if we additionally show

$$r^\delta(c^\delta, \chi^\delta) \rightarrow r(c, \chi) \quad \text{in } L^1(\Omega_{T_0}). \quad (3.45)$$

From the almost everywhere convergence of  $c_l^\delta$  to  $c_l$  and  $c_l > 0$  almost everywhere in  $\Omega_{T_0}$  we obtain

$$\max(c_l^\delta, \delta) \rightarrow c_l \quad \text{almost everywhere in } \Omega_{T_0}, \quad \delta \searrow 0, \quad 1 \leq l \leq 3.$$

Since the functions  $\chi \mapsto k^{1/b_\chi}$  and  $\chi \mapsto \kappa^{1/b_\chi}$  are in  $C^1$ , we find

$$k^{1/b_{\chi^\delta}} \left( \max(c_2^\delta, \delta)^2 - \kappa^{1/b_{\chi^\delta}} \max(c_1, \delta) \max(c_3, \delta) \right) \rightarrow k^{1/b_\chi} \left( c_2^2 - \kappa^{1/b_\chi} c_1 c_3 \right)$$

almost everywhere in  $\Omega_{T_0}$  as  $\delta \searrow 0$ .

By Lebesgue's dominated convergence theorem we find (3.45), because  $k^{1/b_{\chi^\delta}} \leq k^{1/\min(b^1, b^2)}$  almost everywhere in  $\Omega_{T_0}$  if  $k \geq 1$  respectively  $k^{1/b_{\chi^\delta}} \leq k^{1/\max(b^1, b^2)}$  almost everywhere if  $k < 1$  and the analogous estimate for the  $\kappa$ -term, hence

$$\int_{\Omega_{T_0}} |r_1^\delta| \leq C \int_{\Omega_{T_0}} \left( |c_2^2| + |c_1 c_3| \right)$$

for a constant  $C$  that depends on  $\kappa$  and  $k$ .  $\square$

**Remark 3.1** *Uniqueness of the solution to Theorem 3.3 can be obtained in exactly the same way as in Theorem 3.2 if we replace (A6) by (A6').*

### 3.13 The limit equations

The last step is the limit  $\lambda \rightarrow 0$ . This limit can be carried out in much the same way as before by showing a-priori estimates and compactness results.

**Lemma 3.9:** *(A-priori and compactness results for the  $\lambda$ -problem)*

(a) *For  $\lambda \in (0, \lambda_0)$  there exists a weak solution  $(c^\lambda, \mu^\lambda, \chi^\lambda)$  of (3.1) with a logarithmic free energy that satisfies (A2')-(A6').*

(b) *There exists a constant  $C > 0$  independent of  $\lambda$  such that for all  $\lambda \in (0, \lambda_0)$*

$$\sup_{t \in [0, T_0]} \left\{ \|c^\lambda(t)\|_{H^1} + \|\chi^\lambda(t)\|_{H^1} \right\} \leq C,$$

$$\sup_{t \in [0, T_0]} \int_{\Omega} f^1(c^\lambda(t), \chi^\lambda(t)) + \|\nabla \mu^\lambda\|_{L^2(\Omega_{T_0})} \leq C$$

and

$$\|c^\lambda(t_2) - c^\lambda(t_1)\|_{L^2} \leq C|t_2 - t_1|^{\frac{1}{4}},$$

$$\|\chi^\lambda(t_2) - \chi^\lambda(t_1)\|_{L^2} \leq C|t_2 - t_1|^{\frac{1}{2}}$$

for all  $t_1, t_2 \in [0, T_0]$ .

(c) *One can extract subsequences  $(c^\lambda)_{\lambda \in \mathcal{R}}$ ,  $(\mu^\lambda)_{\lambda \in \mathcal{R}}$  and  $(\chi^\lambda)_{\lambda \in \mathcal{R}}$  where  $\mathcal{R} \subset (0, \lambda_0)$  is a countable set with zero as the only accumulation point such that*

- (i)  $c^\lambda \rightarrow c$  in  $C^{0,\alpha}([0, T_0]; L^2(\Omega; \mathbb{R}^4))$  for all  $\alpha \in (0, \frac{1}{4})$ ,
- (ii)  $c^\lambda \rightarrow c$  almost everywhere in  $\Omega_{T_0}$ ,
- (iii)  $c^\lambda \overset{*}{\rightharpoonup} c$  in  $L^\infty(0, T_0; H_0^1(\Omega; \mathbb{R}^4))$ ,
- (iv)  $\chi^\lambda \rightarrow \chi$  in  $C^{0,\alpha}([0, T_0]; L^2(\Omega))$  for all  $\alpha \in (0, \frac{1}{2})$ ,
- (v)  $\chi^\lambda \rightarrow \chi$  almost everywhere in  $\Omega_{T_0}$  and  $0 \leq \chi^\lambda, \chi \leq 1$  a.e. in  $\Omega_{T_0}$ ,
- (vi)  $\chi^\lambda \overset{*}{\rightharpoonup} \chi$  in  $L^\infty(0, T_0; H^1(\Omega))$ ,
- (vii)  $\mu^\lambda \rightarrow \mu$  in  $L^2(0, T_0; H_0^1(\Omega; \mathbb{R}^4))$

as  $\lambda \in \mathcal{R}$  tends to zero.

**Proof:**

By Theorem 3.3, a weak solution for fixed  $\lambda \in (0, \lambda_0)$  exists. This proves (a).

The estimates in (b) are a direct consequence of Lemma 3.7, where due to Assumption (A4.2) we have to choose  $\lambda < \lambda_0$  for Lemma 3.3 to hold. Since  $F^\lambda(c_0, \chi_0)$  can be estimated independently of  $\lambda$ , the constant  $C$  on the right hand side does not depend on  $\lambda$ .

(c) is proved by Lemma 3.7.  $\square$

We make precise what we mean by a weak solution to Model I.

$(c, \mu, \chi) \in L^2(0, T_0; H_0^{1,2}(\Omega; \mathbb{R}^4)) \times L^2(0, T_0; H_0^{1,2}(\Omega; \mathbb{R}^4)) \times L^2(0, T_0; H^{1,2}(\Omega; \mathbb{R}))$  with  $r(c, \chi), \omega(c, \chi) \in L^1(\Omega_{T_0})$  is called a *weak solution* of Formulation (2.29) if

$$- \int_{\Omega_{T_0}} \partial_t \xi \cdot (c - c_0) + \int_{\Omega_{T_0}} L \nabla \mu : \nabla \xi - \int_{\Omega_{T_0}} r(c, \chi) \xi = 0 \quad (3.46a)$$

for all  $\xi \in L^2(0, T_0; H_0^1(\Omega; \mathbb{R}^4))$  with  $\partial_t \xi \in L^2(\Omega_{T_0})$ ,  $\xi(T_0) = 0$ , and

$$\int_{\Omega_{T_0}} \mu \cdot \eta = \int_{\Omega_{T_0}} \frac{\partial f}{\partial c}(c) \cdot \eta \quad (3.46b)$$

for all  $\eta \in L^2(0, T_0; H_0^1(\Omega; \mathbb{R}^4)) \cap L^\infty(\Omega_{T_0}; \mathbb{R}^4)$ , and

$$- \int_{\Omega_{T_0}} \tau \partial_t \zeta (\chi - \chi_0) + \int_{\Omega_{T_0}} \gamma \nabla \chi \cdot \nabla \zeta - \int_{\Omega_{T_0}} \omega(c, \chi) \zeta = 0 \quad (3.46c)$$

for all  $\zeta \in L^2(0, T_0; H^1(\Omega; \mathbb{R}))$  with  $\partial_t \zeta \in L^2(\Omega_{T_0})$ ,  $\zeta(T_0) = 0$ .

**Theorem 3.4:** (Global existence of solutions for Model I with logarithmic  $f$ )

Let the assumptions of Section 3.9 hold. Then, there exists a weak solution  $(c, \mu, \chi)$  in the sense of (3.46) of Formulation (2.29) with a logarithmic free energy that satisfies (A2')-(A6') such that

- (i)  $c \in C^{0, \frac{1}{4}}([0, T_0]; L^2(\Omega; \mathbb{R}^4))$ ,
- (ii)  $\partial_t c \in L^2(0, T_0; (H_0^1(\Omega; \mathbb{R}^4))')$ ,
- (iii)  $\chi \in C^{0, \frac{1}{2}}([0, T_0]; L^2(\Omega))$ ,
- (iv)  $\partial_t \chi \in L^2(0, T_0; (H_0^1(\Omega))')$ ,
- (v) there exists a  $q > 1$  such that  $\ln c_j \in L^q(\Omega_{T_0})$  for  $1 \leq j \leq 4$ ,  
 $\ln \chi, \ln(1 - \chi) \in L^2(\Omega_{T_0})$  and in particular  $0 < \chi, c_j < 1$  a.e. in  $\Omega$ .

**Proof:** We pass to the limit  $\lambda \searrow 0$  in the weak formulation (3.6). In order to show that the limit  $(c, \mu, \chi)$  found in Lemma 3.9 is a solution we only have to observe that in (3.6b)  $\lambda \Delta \mu \rightarrow 0$  in  $H_0^{1,2}(\Omega)$  as  $\lambda \searrow 0$ .  $\square$

**Theorem 3.5:** (*Uniqueness of solutions for Model I*)

If  $\partial_c f, \partial_\chi f$  are Lipschitz continuous, the solution  $(c, \mu, \chi)$  of the Model I obtained in Theorem 3.4 is unique in the spaces stated in this theorem.

**Proof:** The proof of Theorem 3.2 can be reused after sharpening Estimate (3.30). We have according to (A4.2)

$$-\int_{\Omega_{t_0}} \left( \int_0^t r(s) ds \right) \cdot \mu \geq \int_{\Omega_{t_0}} r_1(t)(2\mu_2(t) - \mu_1(t) - \mu_3(t)) \geq \lambda \int_{\Omega_{t_0}} |\nabla c|^2$$

for an arbitrary constant  $\lambda < \lambda_0$ . Then one can proceed with the proof.  $\square$

**Remark 3.2** *The statements of Theorem 3.4 and Theorem 3.5 hold as well for Model II, provided we assume that  $f(c, \chi) := \chi f^1(c) + (1-\chi)f^2(c)$  is continuously differentiable and  $c \mapsto f^1(c), c \mapsto f^2(c)$  are convex functions. Here,  $f^i(c)$  do not refer to the decomposition (3.8) in (A2), but rather to (2.31). Due to Eq. (2.31c) we define*

$$\omega(c, \chi) := \frac{f^2(c) - f^1(c)}{T} + \ln \chi - \ln(1 - \chi).$$

*In Chapter 4,  $f^1(c)$  and  $f^2(c)$  will be computed by ab-initio methods and stored in huge data bases. Consequently, the resulting functions will be piecewise constant. The data bases represent approximations of the smooth physical functions. The proof of existence of solutions to Model II is in many regards simpler as the existence proof to Model I, as there is no reaction term. Therefore, the assumption (A5), (A6) and later (A6') and the construction of  $r^\delta$  are not needed.*

### 3.14 Proof of existence of solutions to Model III

The structure of the existence proof of Theorems 3.1, 3.3 can be maintained for the proof of existence of solutions to Model III provided several changes are made. These modifications are discussed in this section.

- There are no reaction terms in Model III. Therefore in the above proofs one formally sets  $r^m = r^{m-1} := 0$ .
- The space  $X_2$  is replaced by  $V$ , defined in (2.33), the weak formulation (3.6c) is replaced by Eq. (2.32). Instead of (3.7c) we have

$$F(c^m, \chi^m) = \min_{\tilde{\chi} \in V} F(c^m, \tilde{\chi}).$$

- The structural assumptions of Section 3.4 are changed as follows. In (A2) it is assumed now that  $f^1(\cdot, \chi)$  is convex for every  $\chi \in \{0, 1\}$ . Estimate (3.9)

is dropped (notice that  $W(\chi)$  is no component of the free energy). The estimate in Assumption (A2.3) is altered to

$$|\partial_c f^1(c, \chi)| \leq \delta f^1(c, \chi) + C_\delta \quad \text{for all } c \in \Sigma, \chi \in [0, 1].$$

The assumptions (A5) and (A6) are discarded.

- Definition (3.13) is replaced by

$$F^{m,h}(c, \chi) := F(c, \chi) + \frac{1}{2h} \|c - c^{m-1}\|_L^2.$$

The term  $\int_\Omega \delta |\nabla \chi|$  guarantees the coercivity of  $F$  w.r.t.  $\chi \in V$ . The lower semicontinuity of  $F^{m,h}$  w.r.t.  $\chi$  follows from (2.32) and consequently Lemma 3.1 holds as before if  $0 < h < \frac{\lambda}{8C_L^2}$ .

- There is no Euler-Lagrange equation for  $\chi$ , this means Eq. (3.14c) no longer appears. The other parts of Lemma 3.2 remain unchanged.
- The dissipation inequality (3.16) is replaced by

$$F(c_M, \chi_M)(t) + \frac{1}{2} \int_{\Omega_t} (L \nabla \mu_M : \nabla \mu_M) \leq F(c_0, \chi_0).$$

The a-priori estimates (3.17) and (3.18) read now

$$\begin{aligned} \sup_{0 \leq t \leq T_0} \left\{ \|c_M(t)\|_{H^1} + \|\chi_M(t)\|_{BV} \right\} &\leq C, \\ \sup_{0 \leq t \leq T_0} \int_{\Omega} f^1(c_M(t), \chi_M(t)) + \|\nabla \mu_M\|_{L^2(\Omega_{T_0})} &\leq C \end{aligned}$$

and as there are no reaction terms present, the original proof of [31] can be re-used for the revised version of Lemma 3.3.

- The statements (i), (iv) and (vi) of Lemma 3.5 no longer hold. (vi) is not needed any more as there is no term  $\omega = \partial_\chi(f/T)$  in the equations of Model III. Statements (iii), (v) are valid as before ((v) is proved as before), (ii) is replaced by

$$\chi_M \rightarrow \chi \quad \text{in } L^\infty(0, T_0; BV(\Omega)) \quad \text{with } \chi(1 - \chi) = 0 \text{ a.e. in } \Omega$$

as  $M \in \mathcal{N}$  tends to infinity.

In order to prove Lemma 3.5 (iii), fix  $t \in [0, T_0]$ . The sequence  $\chi_M(\cdot, t) \subset BV(\Omega)$  is uniformly bounded in  $BV(\Omega)$  and from the compact embedding  $BV(\Omega) \hookrightarrow L^1(\Omega)$  we infer the existence of a subsequence  $\mathcal{N}$  with  $\chi_{\mathcal{N}}(\cdot, t) \rightarrow \chi(\cdot, t)$  in  $L^1(\Omega)$ . If  $\varphi \in C_0^\infty(\Omega)$ , then for  $1 \leq i \leq n$

$$\lim_{\mathcal{N} \rightarrow \infty} \int_{\Omega} \varphi D_i \chi_{\mathcal{N}}(\cdot, t) = - \lim_{\mathcal{N} \rightarrow \infty} \int_{\Omega} \chi_{\mathcal{N}}(\cdot, t) D_i \varphi = \int_{\Omega} \chi(\cdot, t) D_i \varphi$$

and furthermore

$$\left| \int_{\Omega} \chi(\cdot, t) D_i \varphi \right| \leq \sup_{x \in \Omega} |\varphi(x)| \liminf_{\mathcal{N} \rightarrow \infty} \int_{\Omega} |\nabla \chi_{\mathcal{N}}(\cdot, t)| < \infty.$$

Hence,  $\chi(\cdot, t) \in BV(\Omega)$  and  $\chi_{\mathcal{N}} \rightarrow \chi$  in  $L^\infty(0, T_0; BV(\Omega))$ . Since in particular  $\chi_{\mathcal{N}} \rightarrow \chi$  in  $L^1(\Omega_{T_0})$ , we conclude  $\chi_{\mathcal{N}} \rightarrow \chi$  almost everywhere in  $\Omega_{T_0}$  for a subsequence  $\mathcal{N}$ . This proves (iii). From the pointwise limit we get  $\chi(1 - \chi) = 0$  almost everywhere in  $\Omega$ , hence Lemma 3.5 (ii).

- **Theorem 3.6:** (*Global existence for Model III with polynomial free energy*)  
There exists a weak solution  $(c, \mu, \chi)$  of Formulation (2.31) with polynomial free energy such that

- (i)  $c \in C^{0, \frac{1}{4}}([0, T_0]; L^2(\Omega; \mathbb{R}^4))$ ,
- (ii)  $\partial_t c \in L^2(0, T_0; (H_0^1(\Omega; \mathbb{R}^4))')$ ,
- (iii)  $\chi \in L^\infty(0, T_0; BV(\Omega))$  with  $\chi(1 - \chi) = 0$  a.e. in  $\Omega$ .

- The term  $TW(\chi)$  is removed from (3.34). (A6') is dropped. (A3') reads:  
The initial values  $c_{0i} \in X_1$  fulfill  $\int_{\Omega} c_{0l} > 0$  for  $1 \leq l \leq 4$ .
- The expression  $T[\psi^\delta(\chi) + \psi^\delta(1 - \chi)]$  does no longer occur in the definition of  $f^{1, \delta}$ .
- In Lemma 3.7, Estimate (3.38) reads now

$$\sup_{t \in [0, T_0]} \left\{ \|c^\delta(t)\|_{H^1} + \|\chi^\delta(t)\|_{BV} \right\} \leq C.$$

The statements (c) (iv), (vi) of Lemma 3.7 no longer hold. (v) reads

$$\chi^\delta \rightarrow \chi \quad \text{almost everywhere in } \Omega_{T_0} \text{ and } \chi(1 - \chi) = 0 \quad \text{a.e. in } \Omega_{T_0}.$$

- Lemma 3.8 (ii) is no longer valid.
- **Theorem 3.7:** (*Global existence of solutions of Model III*)  
There exists a weak solution  $(c, \mu, \chi)$  of Formulation (2.31) with logarithmic free energy such that

- (i)  $c \in C^{0, \frac{1}{4}}([0, T_0]; L^2(\Omega; \mathbb{R}^4))$ ,
- (ii)  $\partial_t c \in L^2(0, T_0; (H_0^1(\Omega; \mathbb{R}^4))')$ ,
- (iii)  $\chi \in L^\infty(0, T_0; V)$ ,
- (v) there exists a  $q > 1$  such that  $\ln c_j \in L^q(\Omega_{T_0})$  for  $1 \leq j \leq 4$ ,  
in particular  $0 < c_j < 1$  a.e.

The proof of this theorem is a simplification of Theorem 3.3 by removing Eq. (3.44) and Eq. (3.45) together with the proofs of these statements.

**Remark 3.3** *Simple examples show that uniqueness to Model II cannot be expected in general due to a possible ambiguity in  $\chi$ .*



## Chapter 4

# Computational Methods

This chapter contains all important aspects concerning the numerical implementation to model diffusion induced segregation. It contains the description of the solution method to System (2.29) and discusses three ways to find estimates for the free energy of the sphalerite-chalcopryrite system. As different approximations and models are used, consequently a collection of very different parts is contained. Where it seems necessary for the understanding, the theoretical background for the applied techniques is provided as well.

The first part, enclosed in Section 4.1, describes the general approach to solve (2.29) with a finite element method. Simultaneously it builds the foundations for the more advanced simulations in the later part of this chapter when the free energy functional (2.25) is replaced by computer based calculations of the free energy of the real physical system. This goes along with a modification of the Allen-Cahn equation. Section 4.2 explains the main ideas of this ansatz.

Three different methods for computing the Helmholtz free energy have been used. The most elementary method consists in finding solutions of the harmonic approximation. These solutions were obtained with the program package GULP. A description of this ansatz is given in Sections 4.3 and 4.4.

The second method employed are molecular dynamics (MD) computations which are found in Section 4.5. The two methods represent two different ways to approximate the entropic part of  $F$ : MD computations represent the order-disorder entropy well, the harmonic approximation the harmonic part of the entropy. Even though the MD simulations are too time consuming to be used on a large scale, they may serve to compare with the harmonic approximation for selected concentration values. In Chapter 5 we will analyse this further and will find that the difference of the two predicted free energies is not always negligible.

Additionally, some quantum mechanical computations have been carried out to allow a comparison with data of higher quality serving as reference. Mainly, quantum mechanical computations are desperately needed to obtain a reasonable estimate of the elastic parameters  $C_{ij}$  of chalcopryrite. Without this data, no fitting to the chalcopryrite structure with GULP would be possible. Free energy, lattice constants and elastic parameters are also computed quantum mechanically for sphalerite and show very good agreement with the measurements.

The quantum mechanical computations were made in the framework of the well-known density function theory and use Troullier-Martins pseudopotentials. The

relevant steps are explained in Section 4.6. It should be pointed out that the quantum mechanical computations have a very high quality and often differ less than 5% from measured data, but are too time consuming to be used systematically to fill a data base for the finite element approach.

The results of numerical computations corresponding to the methods and models presented in this chapter are collected in Chapter 5.

One computational technique is not contained in this chapter, which is the minimisation process associated to Eq. (2.32). The implementation details to this minimisation are found in Section 5.6.

## 4.1 General numerical solution technique

The experience has shown that the numerical computation of reaction-diffusion equations is frequently a difficult task due to the possible occurrence of boundary layers and stability problems. Several different methods are applicable for solving System (2.29). The probably simplest ansatz is the use of a predictor-corrector method, see [69] for a general presentation and a comparison of the different variants. But because of the ellipticity of Eq. (2.29a), a fixed point for the iterated solutions (as the proof relies on the contraction principle) of this scheme cannot be guaranteed and in practice the algorithm is observed to converge rather slowly.

A class of much more efficient algorithms is available with the variety of Newton's methods. Since later on we are also going to use operators defined by huge data bases, the explicit computation of the derivatives needed for the classical Newton method would have to use interpolation schemes and is not very practical. Therefore in the following we make use of a Newton-Krylov method. The method is for instance discussed in [21], and a less technical presentation is available in the textbook [45]. In comparison to the formentioned predictor-corrector iteration the Newton-Krylov ansatz made the computations in average about 80 times faster.

To explain the approach, consider we want to solve a nonlinear equation  $f(x) = 0$  for a known differentiable function  $f : \mathbb{R}^p \rightarrow \mathbb{R}^q$ . The classical and well known *Newton's method* for solving this equation is:

Given  $x_0 \in \mathbb{R}^p$ , solve iteratively for  $j = 1, 2, \dots$

$$x_j := x_{j-1} - (Df(x_{j-1}))^{-1} f(x_j), \quad (4.1)$$

which is a linearisation of the original problem inasmuch as in practice one solves

$$A_j d_j = -f(x_{j-1}), \quad (4.2)$$

together with the update  $x_j := d_j + x_{j-1}$ . The disadvantage of (4.2) is that the matrix  $A_j = Df(x_{j-1})$  has to be kept in computer memory and must be updated in every step of the iteration. These draw backs can be partly overcome by using a Quasi-Newton method that replaces  $A_j$  by an approximation of  $Df(x_{j-1})$ . The heart of the Newton-Krylov method is the use of a forward difference, e.g.

$$A_j z := \frac{f(x_{j-1} + \eta z) - f(x_{j-1})}{\eta} \quad (4.3)$$

for a fixed small constant  $\eta > 0$  and persuing the solution of the linear system (4.2) with the generalised minimal residual method, GMRES, see [61] for details. For the practical implementation, only a multiplication routine  $z \mapsto Az$  must be present and  $A$  need not be stored explicitly.

Apparently, this variant is very versatile and is easy to implement. It combines the fast convergence of Newton's method with the excellent damping properties of GMRES. An extensive analysis of the method is present in [21]. In [21] it is shown that for  $x_0$  close to the solution and mild additional assumptions (in particular  $f \in C^{1,1}$ ), the iteration of the Newton-Krylov method converges to the desired solution. The proof relies on the fact that the Newton-Krylov algorithm is essentially the same as applying the regular GMRES method to the perturbed problem  $(A + \text{Id})x = b$  with  $A = Df(z)$  and  $b = -f(z)$ .

We use the algorithm just presented to solve the weak formulation of (2.29) in the Sobolev space  $H^{1,2}(\Omega)$  together with linear finite elements. Since this is fairly standard, we keep the presentation short.

Let  $\mathcal{T}^h$  be a triangulation of  $\Omega$ , where  $h := \max_{T \in \mathcal{T}^h} \text{diam}T$ . In the Galerkin approximation,  $H^{1,2}(\Omega)$  is replaced by

$$S^h := \{\varphi \in C^0(\bar{\Omega}) \mid \varphi|_T \text{ is linear for all } T \in \mathcal{T}^h\} \subset H^{1,2}(\Omega)$$

with basis  $(\varphi_i)_{1 \leq i \leq N}$ , where  $N$  denotes the number of nodes  $(x_i)_{1 \leq i \leq N}$ . We use lumped masses, i.e. approximate the inner product  $(u, v) := \int_{\Omega} uv$  in  $L^2(\Omega)$  by

$$(u, v)^h := \sum_{i=1}^N M_{ii} u(x_i) v(x_i).$$

Here  $M_{ii} := \sum_{j=1}^N \int_{\Omega} \varphi_i \varphi_j$ . Hence,  $M_{ij} = \delta_{ij} \sum_{k=1}^N \tilde{M}_{ik}$  with the 'full' mass matrix  $\tilde{M}$  and  $\delta_{ij}$  is the Kronecker delta.

We find the semi-discrete scheme

$$(\partial_t c^h, \xi)^h + (L \nabla \mu^h, \nabla \xi) - (r(c^h, \chi^h), \xi)^h = 0 \quad \forall \xi \in (S^h)^4, \quad (4.4a)$$

$$(L \nabla \mu^h, \nabla \xi) = (L \nabla \frac{\partial f}{\partial c}(c^h, \chi^h), \nabla \xi) \quad \forall \xi \in (S^h)^4, \quad (4.4b)$$

$$(\partial_t \chi^h, \zeta)^h + \gamma (\nabla \chi^h, \nabla \zeta) - (\omega(c^h, \chi^h), \zeta)^h = 0 \quad \forall \zeta \in S^h, \quad (4.4c)$$

$$c^h(\cdot, 0) = c_0^h \in (S^h)^4, \quad (4.4d)$$

$$\chi^h(\cdot, 0) = \chi_0^h \in S^h. \quad (4.4e)$$

Finally, an implicit time discretisation is used to resolve  $\partial_t c$  and  $\partial_t \chi$ .

It is evident that this approach is not particularly fast and optimisations and speedups are at hand in many ways. One basic improvement consists in a splitting of the time discretisation that was originally invented for the Navier-Stokes equations known as  $\theta$ -scheme, see [20], [73]. More sophisticated improvements are regarding a parallelisation of the code by multi-grid methods or domain decomposition.

## 4.2 A table lookup principle for the free energy

One main criticism concerning Model (2.29) is that the fundamental mechanism to govern the phase parameter  $\chi$  depends on (2.25) which is a theoretical formula for  $F$  that has no regard to the sphalerite-chalcopyrite-system.

To incorporate free energy expressions more closely related to reality, we are going to replace the continuum approach of Section 4.1 in the following way. Let  $c$  be a given concentration vector. In a first independent computation step two approximations  $f^1(c)$  and  $f^2(c)$  are computed that simulate the actual free energy density of the material in the bulk phases, hence represent two local minima of  $f$ . How these approximations can be found is the topic of a later part of this chapter. For instance in the *harmonic approximation* with GULP, introduced in Section 4.3, the values  $f^1(c)$ ,  $f^2(c)$  are obtained from modified chalcopyrite and sphalerite configurations. Generally,  $f^1(c)$  and  $f^2(c)$  are stored beforehand in huge data bases. Each entry in these data bases references to a small range of concentration vectors  $c$  (approximation of  $f$  by a piecewise constant function).

As before there is a surface energy

$$f_S(\chi) := \int_{\Omega} \gamma |\nabla \chi|^2$$

contributing to the free energy density. We use the tangent to the minima  $f^1$  and  $f^2$  to substitute into the Allen-Cahn equation:

$$\tau \partial_t \chi = -\partial_{\chi} \left( \frac{f}{T} \right) \approx \frac{f^2(c) - f^1(c)}{T} + \gamma \Delta \chi + \ln(\chi/(1 - \chi)). \quad (4.5)$$

As in the former ansatz the logarithm  $\ln(\chi/(1 - \chi))$  guarantees  $0 < \chi < 1$  in  $\Omega_{T_0}$  and as long as an evolution equation for  $\chi$  is used it is not possible to avoid this term. There is freedom in this ansatz as any expression  $\alpha \ln(\chi/(1 - \chi))$  with  $\alpha > 0$  is possible.

For known  $\chi$  and given tabular values  $f^1(c)$  and  $f^2(c)$  the chemical potentials compute to

$$\mu_j(c) = \chi \frac{\partial f^1}{\partial c_j}(c) + (1 - \chi) \frac{\partial f^2}{\partial c_j}(c), \quad 1 \leq j \leq 4. \quad (4.6)$$

It remains to find approximations for  $\frac{\partial f^m}{\partial c_j}$ . This is done by central differencing of the tabular entries where possible and by one sided differences at the beginning and end of the data base. To make this precise, let  $M_j \in \mathbb{N}$  be the dimension of that data base w.r.t.  $c_j$ , that is  $f^m(c_1, \dots, c_j, \dots, c_4)$  is constant for  $c_j \in [c_j^l, c_j^{l+1})$  ( $c_j^l$  is a monotone sequence in  $l$ ) and  $1 \leq l \leq M_j - 1$ . Set for  $c_j \in (c_j^l, c_j^{l+1})$  (where we suppress the frozen components  $c_n$  for  $n \neq j$ )

$$\frac{\partial f^m}{\partial c_j}(c_j) = \begin{cases} \frac{f^m(c_j^{l+1}) - f^m(c_j^{l-1})}{c_j^{l+1} - c_j^{l-1}} & \text{if } 2 \leq l \leq M_j - 1, \\ \frac{f^m(c_j^1) - f^m(c_j^2)}{c_j^1 - c_j^2} & \text{if } l = 1, \\ \frac{f^m(c_j^{M_j}) - f^m(c_j^{M_j-1})}{c_j^{M_j} - c_j^{M_j-1}} & \text{if } l = M_j. \end{cases} \quad (4.7)$$

For the harmonic approximation and the MD-simulations presented later in this chapter it is assumed that the lattice is in electric equilibrium. The effect of

the electric potential cannot be resolved by the method and will be ignored. Furthermore the  $c_1$  variable is dropped leading to Formulation (2.31), with the chemical potentials defined by (4.6), (4.7).

To estimate the necessary size of the data base, numerical experiments were done where the data base was filled with data of the theoretical free energy (2.24). Finally, the parameters  $M_2 = M_4 = 30$ ,  $M_3 = 40$  were chosen. Larger values of  $M_j$  are desirable because they lead to smaller approximation errors, but the numerical effort grows enormously, as every entry has to be computed by a costly averaging process. The theoretical error between the tabular value and the correct function value for  $\mu \in C^3$  is  $O(N_j^{-2})$  w.r.t.  $c_j$  except for the first and the last entry of the tabular (it is well known that  $c \mapsto f_i(c)$  is a smooth function for phase  $i = 1, 2$ , hence  $\mu \in C^3$  is no severe assumption).

Instead of Eq. (4.5) it is preferable to use the minimum formulation (2.32).

### 4.3 The harmonic free energy approximation

This section presents the most elementary method to simulate the free energies of the sphalerite and chalcopyrite structure for given concentration vector  $c$ . We will take advantage of well known methods from lattice dynamics and solid state physics. As general reference and introduction the two text books [27] and [8] are recommended.

Let us have a look at the so-called *harmonic approximation*. This notion corresponds to the splitting

$$E = E_{\text{perf}} + E_{\text{vib}} = E_{\text{perf}} + E_{\text{harm}} + E_{\text{anharm}}$$

of the internal energy. Here,  $E_{\text{perf}}$  denotes the internal energy connected to the rigid perfect crystal when all atoms are fixed at their perfect lattice positions and  $E_{\text{vib}}$  is the energy associated to lattice vibrations.  $E_{\text{vib}}$  in turn can be split into the harmonic vibrational energy  $E_{\text{harm}}$  and into the anharmonic contributions  $E_{\text{anharm}}$ . The concept of the harmonic approximation is to neglect  $E_{\text{anharm}}$ .

The fundamental (and somewhat naive) idea of lattice dynamics to estimate  $E$  is to compute the contributions between all atoms (and shells and atom units) and summing up. This implies that we neglect quantum mechanical effects and assume that the lattice has a periodic structure. In the computations the lattice symmetry is used, theoretically the unit cell being replicated infinitely many times. As this is of course practically impossible, a cutoff is introduced.

Let  $u_i = (u_{i1}, u_{i2}, u_{i3})$  be the displacement vector of the  $i$ -th atom. The relationship between  $E_{\text{vib}}$  and  $E_{\text{anharm}}$  is the Taylor expansion

$$\begin{aligned} E &= E_{\text{perf}} + \frac{1}{2!} \sum_{p=1}^3 \sum_{i,j} \frac{\partial^2 E}{\partial u_{i,p} \partial u_{j,p}} u_{i,p} u_{j,p} \\ &\quad + \frac{1}{3!} \sum_{p=1}^3 \sum_{i,j,k} \frac{\partial^3 E}{\partial u_{i,p} \partial u_{j,p} \partial u_{k,p}} u_{i,p} u_{j,p} u_{k,p} + \dots \end{aligned} \quad (4.8)$$

The terms with derivatives of order 3 or higher define the anharmonic contributions  $E_{\text{anharm}}$ . In (4.8) there are no first order terms because the lattice is assumed to be in equilibrium.

Even though some effects as heat conductivity and thermal expansion can only be conclusively explained when considering anharmonic effects, as long as the atomic displacements remain small, we have  $E \approx E_{\text{perf}} + E_{\text{harm}}$ . The energy  $E_{\text{harm}}$  is always bounded from below and solving the harmonic approximation is relatively simple.

$E_{\text{perf}}$  and  $E_{\text{harm}}$  will be computed on the basis of short-range interatomic potentials and long-range electrostatic approximations. For these computations, the program package GULP, see [37], has been used.

The main advantage of GULP is the low computational effort that allows to gain results quickly. Hence it is well suited to get an overview and ideal for the large-scale computations to generate the free energy table. The anharmonicity could be added later and in simple cases a renormalisation of the frequencies, see [18] is possible. In more complicated situations (in particular when the displacement  $u$  becomes large, i.e. when the crystal is subject to huge temperatures and pressures) more sophisticated approaches as thermodynamic integration between carefully chosen reference states, see [3], or even quantum corrections may become necessary.

The lattice energy  $E_{\text{perf}}$  is computed by the formula

$$E_{\text{perf}} = \frac{1}{2} \sum_{i,j} \varphi_{ij}(r_{ij}). \quad (4.9)$$

Here,  $r_{ij}$  is the distance between atoms  $i$  and  $j$  and  $\varphi_{ij}$  is the energy between the species  $i$  and  $j$ . The factor  $\frac{1}{2}$  in (4.9) accounts for the fact that every pair  $(i, j)$  is counted twice.

As has already been mentioned, for the computation of the short-range interactions, i.e. for the computation of  $E_{\text{perf}}$ , interatomic potentials are being used. Best known are the *Lennard-Jones potential*

$$\varphi(r) := -4\varepsilon \left[ \left( \frac{\sigma}{r} \right)^6 - \left( \frac{\sigma}{r} \right)^{12} \right] \quad (4.10)$$

and the *Buckingham potential*

$$\varphi(r) := -4\varepsilon \left( \frac{\sigma}{r} \right)^6 + B \exp \left( - \frac{r}{\rho} \right), \quad (4.11)$$

but there are many others. In this work, the latter (4.11) will be favored because the practical experience has shown it to yield more reliable predictions. In (4.10) and (4.11),  $r$  is the distance between the atoms,  $\sigma$  that particular interatomic distance where the energy vanishes and  $\varepsilon$  is the potential energy at equilibrium separation. The  $\left(\frac{\sigma}{r}\right)^6$  term describes the van-der Waals induced dipole moments whereas  $\left(\frac{\sigma}{r}\right)^{12}$  stands for the repulsive forces. In (4.11) the repulsive term has been replaced by an exponential expression. The two parameters,  $B$  originally standing for the intensity of the interaction and  $\rho$  for the relative size of the atoms considered, are in practice merely constants to be fitted against experimental data.

It is assumed that for the long-range potential the electrostatic or Coulomb interactions

$$E_C := \frac{1}{2} \sum_l \sum_{i,j} \frac{q_i q_j}{4\pi\varepsilon_0 r_{ij}(l)}$$

are dominant, where  $q_i$  is the charge on the  $i$ -th atom,  $\varepsilon_0$  the dielectric permittivity constant and  $r_{ij}(l)$  denotes the distance between the  $i$ -th atom in the unit cell (referred to  $l = 0$ ) and the  $j$ -th atom in the  $l$ -th unit cell.  $E_C$  represents the binding energy in solids and is the counterpart to the short-range repulsive interactions.

Due to the  $r^{-1}$  term the convergence of  $E_C$  is critical. A well known and by now classical way to efficiently compute  $E_C$  is by means of an Ewald sum technique, [33], where the Coulomb sum is decomposed in one part in real space and one in reciprocal space, by virtue of

$$\frac{1}{r} = \int_0^\eta \exp(-r^2 \varrho^2) d\varrho + \frac{\sqrt{\pi}}{2} \frac{\operatorname{erfc}(\eta r)}{r},$$

where  $\eta$  is a free parameter (that could be adjusted within GULP) and

$$\operatorname{erfc}(x) := \frac{2}{\sqrt{\pi}} \int_x^\infty e^{-y^2} dy$$

is called the *complementary error function*. Using the fast decay of  $\operatorname{erfc}(x)$  for large  $x$  and a theta function transformation, one ends up with

$$E_C = \frac{1}{8\pi\varepsilon_0} \left\{ \sum_l \sum_{i,j} \frac{q_i q_j \operatorname{erfc}(\eta r_{ij}(l))}{r_{ij}(l)} + \sum_{i,j} \frac{4q_i q_j \pi}{V} \sum_G \frac{\exp(-G^2/4\eta^2)}{G^2} \exp(iG \cdot (r_j - r_i)) \right\}. \quad (4.12)$$

$V$  denotes here the volume of the unit cell and the sum is taken over all reciprocal lattice vectors  $G$ . The decomposition just described exploits the fact that a slowly decaying function will drop quickly to zero after the transformation.

The Ewald decomposition is found to be a very effective way to compute  $E_C$ . Currently it is discussed if multipole methods can be an alternative.

With  $E_C$  and Formula (4.12) we have computed the first component of  $E_{\text{harm}}$ . It remains to calculate the energy of the harmonic oscillators, the phonons. A phonon can be considered as a particle-like vibrational quantum. We assume that we are in thermodynamical equilibrium and that the number of harmonic oscillators with energy level  $E_l$  follows Boltzmann's rule and is proportional to  $\exp(-E_l/(k_B T))$ . The energy levels  $E_l$  obey the formula

$$E_{jq} = \hbar\omega_j(q) \left( \frac{1}{2} + n_{jq} \right), \quad n_{jq} = 0, 1, 2, \dots \quad (4.13)$$

where  $\hbar$  is Planck's constant and  $q$  denotes the wave vector,  $j$  the dispersion branch. We suppress the dependence on  $q$  and  $j$  and write (4.13) in the form

$$E_l = \hbar\omega \left( \frac{1}{2} + l \right). \quad (4.14)$$

With the above mentioned relation of the harmonic oscillators due to Boltzmann's law the mean energy for frozen  $(q, j)$  is computed to

$$\bar{E} = \frac{\sum_{l=0}^{\infty} E_l \exp\left(-\frac{E_l}{k_B T}\right)}{\sum_{l=0}^{\infty} \exp\left(-\frac{E_l}{k_B T}\right)} = -\frac{d}{d\beta} \ln \left( \sum_{l=0}^{\infty} \exp(-\beta E_l) \right) \quad (4.15)$$

with the abbreviation  $\beta := (k_B T)^{-1}$ . With the help of (4.14) we obtain

$$\begin{aligned} \sum_{l=0}^{\infty} \exp(-\beta E_l) &= \exp\left(-\frac{\hbar\omega}{2}\beta\right) \sum_{l=0}^{\infty} \exp(-\hbar\beta\omega l) \\ &= \frac{\exp\left(-\frac{\hbar\omega}{2}\beta\right)}{1 - \exp(-\hbar\omega\beta)}. \end{aligned}$$

For the mean energy this yields

$$\begin{aligned} \bar{E} &= -\frac{d}{d\beta} \ln \exp\left(-\frac{\hbar\omega}{2}\beta\right) + \frac{d}{d\beta} \ln(1 - \exp(-\hbar\omega\beta)) \\ &= \frac{\hbar\omega}{2} + \frac{\hbar\omega \exp(-\hbar\omega\beta)}{1 - \exp(-\hbar\omega\beta)} = \hbar\omega \left(\frac{1}{2} + \frac{1}{\exp(\frac{\hbar\omega}{\beta}) - 1}\right) \\ &=: \hbar\omega \left(\frac{1}{2} + \bar{n}\right). \end{aligned}$$

This last identity holds for every  $(q, j)$ . After relabeling ( $\bar{E}_{jq} \rightarrow E_m$ ,  $\bar{n}_{jq} \rightarrow n_m$ ) and with (4.14) we therefore arrive at the *Bose-Einstein relation*

$$n_m = \frac{1}{\exp(\hbar\omega_m/(k_B T)) - 1}$$

which is known to hold for all spinless particles.

We define the *partition function* by

$$Z := \sum_{m=0}^{\infty} \exp\left(\frac{-E_m}{k_B T}\right).$$

Using well known results from statistical mechanics by Gibbs and by di Marzio, we get at once

$$\begin{aligned} S &= k_B T \left(\frac{\partial \ln Z}{\partial T}\right)_V + k_B \ln Z, \\ F &= E - TS. \end{aligned} \tag{4.16}$$

In Eq. (4.16), the internal energy is given by

$$E = E_{\text{perf}} - \frac{1}{Z} \frac{\partial Z}{\partial \beta},$$

where the term  $-\frac{1}{Z} \frac{\partial Z}{\partial \beta}$  is explained by Identity (4.15); and (4.16) together with (4.9) completely define the free energy.

For the constrained minimisation of the free energy within GULP, the Broyden, Fletcher, Goldfarb and Shanno (BFGS) variant of the Newton-Raphson method were used, see [11]. As is well understood, in general only local minima in the energy landscape are found by this method.

## 4.4 Free energy computation with GULP

After the general introduction of the last section we now discuss the details.

## I Fitting of heuristic potentials

We begin with the fitting to ZnS. We use a shell model, first introduced in [26]. In this model, the rigid atom is split into an inner part comprising of the nucleus with the tightly bound inner electrons and into an outer part with the loosely bound shell electrons. This allows to take into account dipole moments caused by the interactions with neighboring ions. Additionally, a harmonic three body potential is used to account for the directionality on the  $S-Zn-S$  bond according to the Taylor expansion

$$W_{3b}(\theta) := \frac{1}{2}k_2(\theta - \theta_0)^2 + \frac{1}{6}k_3(\theta - \theta_0)^3 + \frac{1}{12}k_4(\theta - \theta_0)^4,$$

where  $\theta_0$  is the angle of the unstressed three-body system and  $k_2$ ,  $k_3$  and  $k_4$  determine the sensibility w.r.t. angular changes. Three body potentials are extensively discussed in [65].

With GULP it is possible to set up interactions of potentials between shells and other atoms/shells and these potentials can and should be fitted to give reasonable results. For sphalerite and chalcopyrite this is a tricky business, probably because the bondings in sulphides are not purely ionic but may range from ionic to covalent through to metallic. The fitting is done in the spirit of the work by Wright and Jackson, [75], in such a way that the calculated numerical data fits best to the physical constants gained by experiments. Table 4.1 shows this ( $a$  denotes the lattice parameter of the cubic lattice,  $V$  the volume of the unit cell and  $C_{il}$  specify the elastic constants). To find the potential parameters, one starts with a simple model without shells where for instance the charges of S and Zn are fixed to  $-2$  and  $+2$ . By a least squares optimisation run the parameters for the spring constant and in case of sphalerite for the  $S-Zn-S$  interactions are fitted. The parameters thus obtained are then used in an extended model that includes shells and three body terms.

	EXP1	EXP2	P1	P2	P3
$a/\text{\AA}$	5.41	5.41	5.403	5.403	5.402
$V/\text{\AA}^3$	158.29	158.29	157.77	157.77	157.69
$C_{11}/GPa$	9.42	9.76	8.6	9.37	9.18
$C_{12}/GPa$	5.68	5.9	6.54	6.16	5.83
$C_{44}/GPa$	4.36	4.51	3.8	4.03	4.41
$\varepsilon_{\text{stat}}$	7.9	-	8.565	7.21	7.33
$\varepsilon_{\text{hf}}$	5.8	-	4.815	4.56	3.64

Table 4.1: Comparison of experimental and calculated data for ZnS

For P1, a Buckingham potential is fitted and a shell is only used for the  $S$  ions. In P2, a three body potential for  $S-Zn-S$  is added. In particular this results in better values for  $C_{44}$ ,  $\varepsilon_{\text{hf}}$  and  $\varepsilon_{\text{st}}$ . Finally, in P3 a shell to the Zn is included as well. The necessary parameters for a complete definition of the potentials are maintained in Table 4.2 below. For all the Buckingham potentials, the cutoff level was set to  $12\text{\AA}$ .

The potentials P1 and P3 correspond to PS1 and PS3 in [75]. Some of the values in Table 4.1 vary slightly from the figures reported there because all computations were redone with the newer version GULP 1.3. The data set EXP1 refers to the experimental results in [54], EXP2 to the recently made measurements in [14] (in these experiments no measurements of  $\varepsilon_{\text{stat}}$  and  $\varepsilon_{\text{hf}}$  were made).

	P1	P2	P3
POTENTIAL PARAMETERS:			
<u><math>S - S</math></u>			
$A/eV$	1200.0	1200.0	1200.0
$\varrho/\text{\AA}$	0.149	0.149	0.149
$C/eV\text{\AA}^6$	120.0	120.0	120.0
<u><math>Zn - S</math></u>			
$A/eV$	613.36	613.36	528.9
$\varrho/\text{\AA}$	0.399	0.399	0.411
$C/eV\text{\AA}^6$	0.0	0.0	0.0
SHELL MODEL:			
$SK_S/eV\text{\AA}^{-2}$	12.7	12.7	16.86
$ZnK_S/eV\text{\AA}^{-2}$	0.0	0.0	2.181
THREE BODY TERMS:			
$S - Zn - S$ force constant/ $eV\text{rad}^{-2}$		0.713	0.713
$S - Zn - S$ bond angle /degrees		109.47	109.47
$k_2/eV\text{rad}^{-2}$		3.0	3.0
$k_3/eV\text{rad}^{-3}$		3.0	3.0
$k_4/eV\text{rad}^{-4}$		5.0	5.0

Table 4.2: Potential parameters for P1, P2 and P3 used for ZnS

As can be seen, the agreement documented in Table 4.1 is suitably well with an error in the size of uncertainty of the measured parameters. This proves that GULP can be used to compute fundamental material properties of sulphides. P2 and P3 seem both be very well suited to represent the structure of ZnS.

The fitting procedure to chalcopyrite is similar. For P4, Cu and Fe cores replace Zn. The S shell is fitted to yield good values for the lattice constants and the volume of the primitive cell. But there is one bottleneck: up to now it has not been possible to measure the elastic parameters  $C_{il}$  for chalcopyrite in experiment. The slanted parameters in Table 4.3 are the result of the quantum mechanical computations in Section 4.6 and the GULP potential is fitted to these parameters. To further improve the quality of the results, three body potentials for  $S - Cu - S$  and  $S - Fe - S$  are added. Table 4.3 provides the results of the fitting, Table 4.4 the fitting parameters.

The elastic constants  $C_{15}$ ,  $C_{43}$  and  $C_{56}$  should vanish for tetragonal lattice geometries, but GULP computes these parameters to be in the range of  $10^{-5}$  to

$2.7 \cdot 10^{-4}$  either due to rounding errors or because the relaxed geometry is not completely optimal. These values are not listed in Table 4.3.

	Exp2/QM	P4	P5
$a/\text{\AA}$	5.2864	5.601	5.59
$b/\text{\AA}$	5.2864	5.601	5.59
$c/\text{\AA}$	10.4102	10.71	10.70
$V/\text{\AA}^3$	145.46	168.08	167.73
$C_{11}/GPa$	<i>17.83</i>	18.02	18.12
$C_{12}/GPa$	<i>5.81</i>	5.67	5.64
$C_{13}/GPa$	<i>6.27</i>	6.59	6.59
$C_{33}/GPa$	<i>13.15</i>	14.23	14.25
$C_{44}/GPa$	<i>13.19</i>	18.86	18.93
$C_{66}/GPa$	<i>4.93</i>	8.68	8.70

Table 4.3: Comparison of experimental/quantum mechanical and calculated data for chalcopyrite

We see that there is almost no improvement when using the three body potentials. The agreement to the quantum mechanical parameters is quite good, except for the elastic constants  $C_{44}$  and  $C_{66}$ .

	P4	P5
POTENTIAL PARAMETERS:		
<u>S – S</u>		
$A/eV$	1200.0	1200.0
$\varrho/\text{\AA}$	0.508	0.508
$C/eV\text{\AA}^6$	120.0	120.0
<u>Fe – S</u>		
$A/eV$	5694.68	5694.68
$\varrho/\text{\AA}$	0.2748	0.2748
$C/eV\text{\AA}^6$	0.0	0.0
<u>Cu – S</u>		
$A/eV$	110.62	100.619
$\varrho/\text{\AA}$	0.327	0.327
$C/eV\text{\AA}^6$	0.0	0.0
SHELL MODEL:		
$SK_S/eV\text{\AA}^{-2}$	12.70	12.70
THREE BODY TERMS:		
$S - Cu - S$ force constant/ $eV\text{rad}^{-2}$		0.01164
$S - Cu - S$ bond angle /degrees		109.47
$k_2/eV\text{rad}^{-2}$		2.5
$k_3/eV\text{rad}^{-3}$		2.5
$k_4/eV\text{rad}^{-4}$		4.0
$S - Fe - S$ force constant/ $eV\text{rad}^{-2}$		0.01169
$S - Fe - S$ bond angle /degrees		109.47
$k_2/eV\text{rad}^{-2}$		2.5
$k_3/eV\text{rad}^{-3}$		2.5
$k_4/eV\text{rad}^{-4}$		4.0

Table 4.4: Potential parameters for P4 and P5 used for chalcopyrite

## II Computation of the free energy as a function of $c$

A concentration vector  $c$  only determines the concentrations of  $\text{Cu}^+$ ,  $\text{Zn}^{2+}$  and Fe, but not the position of the atoms within the lattice. Hence, there is a large number of different configurations representing the same vector  $c$ . In order to account for that issue, a supercell approach has been pursued in which all atoms are placed manually and no lattice symmetry is used a-priori. Consequently, the lattice unit cell is copied many times and randomly certain atoms are replaced in order to fulfill the prescribed concentration percentage. The replacement mechanism is described in more detail below.

The following picture displays the three-dimensional lattice structure of cubic ZnS (space group  $F\bar{4}3m$ ) and of tetragonal chalcopyrite (space group  $I\bar{4}2d$ ). In older work by Groß, the space group of chalcopyrite had wrongly been identified as  $P42m$  but recent articles, [14] and [48], have it right.

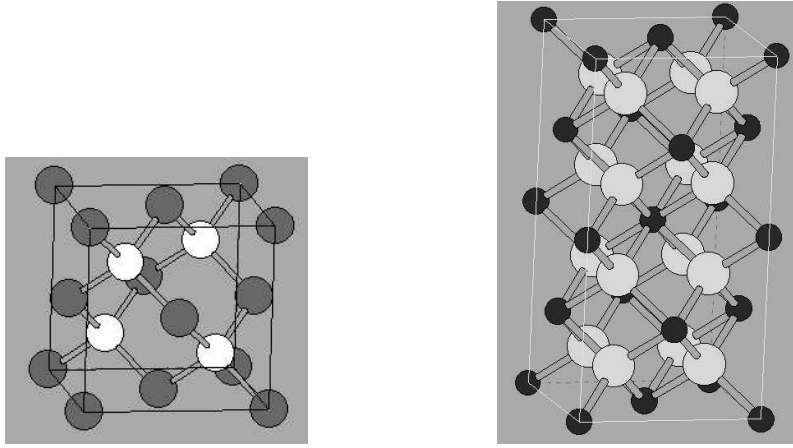


Figure 4.1: The unit cells of sphalerite and chalcopyrite

The fundamental mechanism that determines the predominant lattice structure is well understood. Decisive is the ratio  $r_+/r_-$ , where  $r_+$  denotes the ion radius of the positive ion (e.g.  $\text{Zn}^{2+}$  for ZnS) and  $r_-$  the radius of the negative ion (e.g.  $\text{S}^{2-}$  for ZnS). As long as  $r_+/r_- < \sqrt{2} - 1 \approx 0.414$ , the larger ions can still touch leading to a closest cubic packing as in NaCl with coordination number 6. In other cases, the ZnS structure is preferable where any ion of one kind is surrounded by 4 ions of the other kind. The four anions form the corners of a tetrahedron that is centered by a cation and vice versa. If we place the corners of such a tetrahedron in the cubic unit cell with edge length  $a$  and assume that the anion-balls still touch, we find from simple geometric considerations

$$a\sqrt{2} = 2r_- \quad (4.17)$$

and for the space diagonal

$$a\sqrt{3} = r_- + 2r_+ + r_-$$

and hence for the ratio

$$\frac{r_+}{r_-} = \sqrt{\frac{3}{2}} - 1 \approx 0.225. \quad (4.18)$$

With the measured  $r_+ = 0.64\text{\AA}$  from Table 2.1 and  $r_-$  from Eq. (4.17) we find  $r_+/r_- \approx 0.167$  indicating that the anion balls don't touch in reality. For  $r_+/r_- > \sqrt{3}-1 \approx 0.732$ , the CsCl structure with coordination number 8 becomes favorable.

From Fig. 4.1 we can read off the lattice transformation from sphalerite to chalcopyrite. The Zn atoms at the corners of the unit cell are replaced by Cu, the six Zn atoms at the centers of every face are replaced by four Fe atoms and two Cu atoms, where due to symmetry opposing faces are occupied by the same atom type (Fe or Cu). As the bonding energies change, some S atoms slightly shift their positions resulting in an overall change of the space group. In direction of the lattice vector  $c$  of the unit cell, this corresponds to an almost doubling of the lattice constant.

From these considerations we can derive a natural replacement mechanism for the transformation from sphalerite to chalcopyrite (and vice versa). The positions where Cu atoms and Fe atoms are found in chalcopyrite determine those lattice points where Cu and Fe must be placed when altering the structure of sphalerite. The positions of the sulphur atoms are automatically adjusted during the minimisation run of GULP.

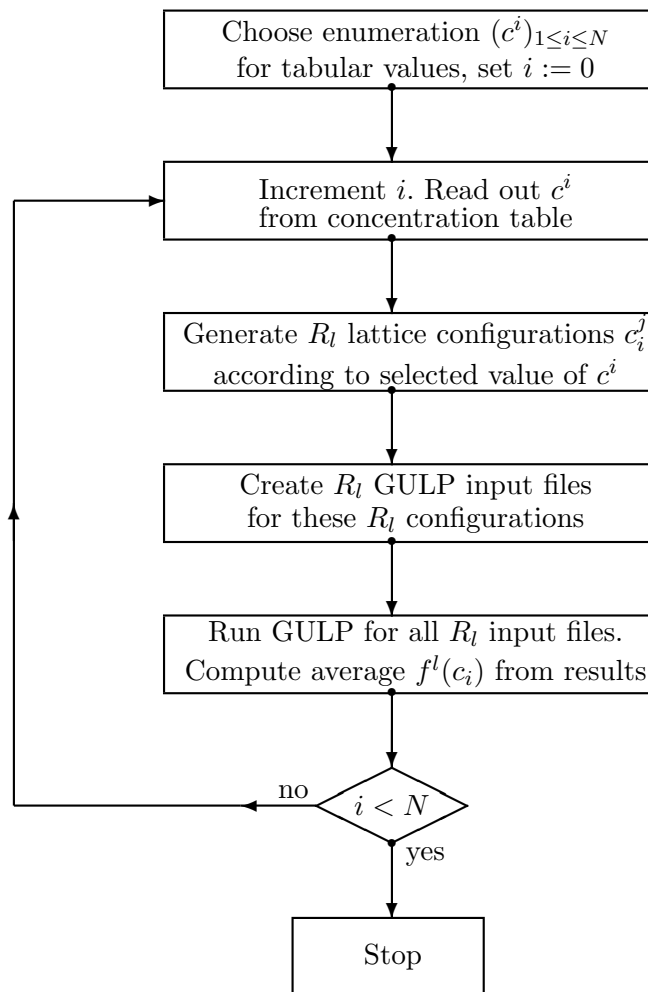


Figure 4.2: Flow chart of the file builder for geometry  $l$ ,  $l = 1, 2$

As many atomistic states represent the same concentration vector and as beforehand it is not clear which of them are preferable, a file builder generates a certain number  $R_l$  of different GULP input files ( $R_l$  is chosen dynamically, see Section 5.2, with  $20 \leq R_l \leq 50$ , where  $(f^l(c_i^j))_{1 \leq j \leq 20}$  are always computed to sample the distribution) each with an atomistic configuration  $c_i^\alpha$ ,  $1 \leq \alpha \leq R_l$  corresponding to the selected concentration vector  $c_i$ . For each input file, GULP is invoked and the free energies  $f^l(c_i^\alpha)$  are computed. Finally, the entry in the table is defined by the arithmetic mean

$$f^l(c_i) := \frac{\sum_{\alpha=1}^{R_l} f^l(c_i^\alpha)}{R_l}, \quad l = 1, 2.$$

The entire procedure is repeated for all  $c_i$ ,  $1 \leq i \leq N$  to build the two data bases,  $l = 1$  for chalcopyrite and  $l = 2$  for sphalerite. Fig. 4.2 above summarises the essential steps of the algorithm. For fixed  $c$ , the found average values represent the two minima  $f^1(c)$  and  $f^2(c)$  that are used to compute the tangent to  $\chi$  in the modified Allen-Cahn equation (4.5).

Even though this method works out nicely, it has one disadvantage. Since all atoms are placed manually in the supercell (set up in accordance to the space group), GULP cannot use the lattice symmetry to accelerate the computations. Hence the calculations are time consuming. For the generated data base with discrete  $c$  values with partitions  $M_2 = M_4 = 30$ ,  $M_3 = 40$ , the above calculations took 6 weeks of computations on a SUN workstation cluster.

We want to comment on the logic of the file builder and on the entire GULP approach. A supercell as a conglomerate of 3 subdivisions (=the unit cell) in each space coordinate is generated, hence a collection of 27 unit cells.

The implicitly made assumptions of this GULP ansatz are hence:

- There are no interactions over more than 3 cells.
- The influence of impurities on the free energies are neglected.
- The lattice is in electric equilibrium. Electric potentials in the computation of the free energy are not taken into account.
- It is assumed that the lattice structure changes from sphalerite to chalcopyrite in the way predicted above (i.e. there is no intermediate lattice state with a different spatial geometry) or where other mechanisms (for instance 'wall pinning' or polarons) play a role. More on this topic can be found in the article [62].
- The heuristic potentials reflect the physical situation well enough.  $E_{\text{anharm}}$  and quantum effects are small.
- Only vectors  $c$  that are stoichiometric concentrations w.r.t. the supercell can be represented.

The last restriction is not very severe. There are 216 atoms within the  $3 \times 3 \times 3$  supercell of sphalerite and 648 atoms within the larger supercell of chalcopyrite. Hence,  $c_1$  and  $c_3$  can for the supercell of sphalerite be resolved with  $1/216 \approx 0.46\%$  and with  $1/648 \approx 0.15\%$  for the supercell of chalcopyrite. Finally, the supercell geometry yields natural bounds for the concentrations,  $c_1, c_3 \leq 54/216 = 1/4$  and  $c_4 \leq 0.5$ .

## 4.5 Molecular dynamics computations of the free energy

The principle of molecular dynamics (MD) computations is to set up a huge ensemble of  $N$  atoms in a box (commonly a supercell consisting of  $5 \times 5 \times 5$  unit cells), including start positions  $(r_i(t = 0))_{1 \leq i \leq N}$  and momenta of all particles depending on the prescribed temperature (see (4.19) below), defining the atom interactions in terms of potentials, and then letting the system evolve.

In our application and based upon the analysis with GULP, no four-body potentials are defined nor angle and dihedral contributions. The complete configurational energy of the molecular system is therefore given by the formula

$$\begin{aligned}
 U(r_1, \dots, r_N) &:= \sum_{i_{\text{bond}}=1}^{N_{\text{bond}}} U_{\text{bond}}(i_{\text{bond}}, r) + \sum_{i=1}^{N-1} \sum_{j=i+1}^N U_{\text{pair}}(i, j, |r_i - r_j|) \\
 &+ \sum_{i=1}^{N-2} \sum_{j=i+1}^{N-1} \sum_{l=j+1}^N U_{3\text{body}}(i, j, l, r_i, r_j, r_l) + \sum_{i=1}^N U_{\text{ext}}(i, r_i, v_i),
 \end{aligned}$$

where  $U_{\text{bond}}$  is a heuristic potential for the chemical bonding energy,  $U_{\text{pair}}$  and  $U_{3\text{body}}$  are pair- and three body potentials, and  $U_{\text{ext}}$  represents an external field (gravitational or magnetic). For the pair- and three body terms the GULP potentials (4.11) and (P2) respectively (P5) are reused.

The new positions and velocities of the molecules are obtained by a simple forward integration in time using a leap-frog algorithm. The velocities are defined at time steps  $t + \frac{1}{2}\Delta t$  and  $t - \frac{1}{2}\Delta t$  and the positions  $r_i$  at  $t$  and  $t + \Delta t$ .

The system temperature is defined by the Boltzmann law

$$T(t) = \sum_{i=1}^N \frac{m_i v_i^2(t)}{k_B \tilde{d}}, \quad (4.19)$$

where  $(m_i)_{1 \leq i \leq N}$  are the masses of the atoms with velocities  $(v_i)_{1 \leq i \leq N}$  and  $\tilde{d}$  denotes the degrees of freedom, i.e.  $\tilde{d} = 3N - 3$  for the cubic box with periodic boundary conditions.

In order to provide an isothermal situation, the so-called Berendsen thermostat is used. Key of this approach is to scale the velocities according to Relation (4.19) in order to satisfy the correct  $T$ . By this formalism, the total momentum is conserved, but not the energy. Additionally, reflecting boundary conditions are used at the boundary of the  $5 \times 5 \times 5$  supercell.

After a certain number of iteration steps in which the system evolves towards an equilibrium, the state of the ensemble is read off. The free energy of the system is available by summing up the momenta of all atoms in the cell:

$$F(t) = k_B T(t) \ln \left( \sum_{i=1}^N m_i(t) v_i(t) \right).$$

Figure 4.3 illustrates the configuration of the MD-computations.

We can comment on this method. First of all, the number of atoms  $N$  of a computation is restricted by computer capacities and the numerical effort grows

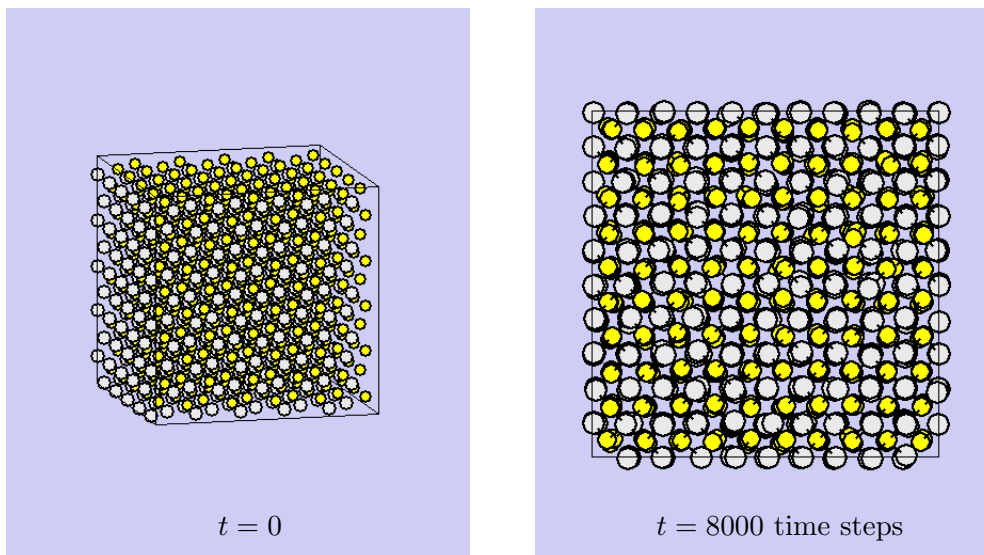


Figure 4.3: Ensemble of cubic ZnS with 500 S (yellow) and 500 Zn (gray) atoms contained in a cube with 125 unit cells. Left at  $t = 0$  and right after 8000 time steps. The right picture also shows that the lattice layers differ slightly with atoms having different positions and momenta.

exponentially with  $N$ . A typical range for  $N$  is  $10^3$  to  $10^6$  atoms. Hence, this number is very far away from the actual number of atoms which is in the range of the *Avogadro number*  $N_A = 10^{23}$ . Despite this gap the method gives in practice surprisingly good results as long as  $T > 100^\circ\text{K}$ . For low temperatures close to the zero point, quantum effects give large contributions and it is reasonable why the method yields wrong results.

Beside the question of valid temperature ranges and the influence of quantum mechanics there are two other main issues that should be clarified with regard to MD simulations:

- If more than two atoms collide, there is no way to predict the velocities and momenta of these atoms AFTER the collision. No reliable estimates are known for the number of collisions of triples (quadruples, quintuples, ...) of atoms.
- Error estimates of the relative error (in particular of the free energy) as a function of the number of atoms of the numerical computation do not exist. The asymptotic approximation of the calculated free energy towards a certain value as the number of atoms increases is only a necessity but of course no proof of convergence.

## 4.6 Quantum mechanical computations

In order to approximately solve the Schrödinger equation, we will apply the local-density approximation within the framework of density function theory, [43], [47],

[57]. This is a generally applicable black box method and yields sufficiently precise results. Scattering theory would be an alternative, in particular the coupled cluster method might ultimately lead to even better results. For the representation of the electron-atom-interactions the Troullier-Martins pseudopotentials, [70], will be used. We give here a very brief sketch of the method, the theory is developed more systematically (but unfortunately nowhere comprehensively!) within the articles cited above.

We follow the well-known Born-Oppenheimer or adiabatic approximation that assumes the atoms to have fixed positions (the mass of a nucleus is about 2000 times the mass of an electron) and solve the Schrödinger equation only for the electrons. Even with this approximation, the task remains delicate.

The Hamiltonian of the Schrödinger equation is given by

$$\mathcal{H} := \sum_i \left( -\frac{\hbar^2}{2m} \Delta_i - \sum_l \frac{Z_l e^2}{4\pi\epsilon_0 |r_i - R_l|} \right) + \frac{e^2}{4\pi\epsilon_0} \sum_{ij} \frac{1}{|r_i - r_j|}$$

where  $l$  runs over all atoms,  $i$  over all electrons,  $Z_l$  is the number of electrons of atom  $l$ ,  $R_l$  the position vector of atom  $l$ ,  $r_i$  the position vector of electron  $i$ ,  $m$  the electron mass and  $e$  the electron charge.

Let  $\psi = \psi(r, t)$  denote a wave function and  $E$  an energy. Solving the Schrödinger equation consists in finding a solution to the energy balance equation

$$\mathcal{H}\psi = E\psi$$

equipped with periodic boundary conditions. This equation can be solved exactly only for one electron, otherwise the Hartree term causes problems. To find at least approximate solutions to the Schrödinger equation, the following four main steps are pursued.

#### A: Density function theory (DFT)

In [47] it is shown that the total energy of an electron gas is uniquely determined by the electron density. In [47] it is also shown how the multi-electron problem can be mapped to a self-consistent system of equations for one electron, where all electrons are non-interacting and moving in the potentials of all other electrons.

After introducing the electron density  $\varrho(r)$  for electron position  $r$ ,

$$\int_{\mathbb{R}^3} \varrho(r) dr = N,$$

where  $N$  denotes the number of electrons, we have to solve

$$\left[ -\frac{\hbar}{2m} \Delta + V_{\text{ion}}(r) + V_H(\varrho, r) + V_{\text{XC}}(r) - \varepsilon_i \right] \psi_i(r) = 0. \quad (4.20)$$

In this formulation,  $\varepsilon_i$  denotes the energy or an eigenvalue of the Hamiltonian,

$$V_H(\varrho, r) := e^2 \int_{\mathbb{R}^3} \frac{\varrho(r')}{|r - r'|} dr'$$

is the electrostatic or Hartree potential,  $V_{\text{ion}}$  the static electron-ion potential, for an atom typically

$$V_{\text{ion}}(r) := \int_{\mathbb{R}^3} \frac{Z}{r} \varrho(r) dr,$$

and the exchange and correlation energy is given by

$$V_{\text{XC}} := \frac{\delta E_{\text{XC}}(\varrho(r))}{\delta \varrho(r)}.$$

(The wave-function of a many-electron system is antisymmetric w.r.t. exchange of two electrons due to the Pauli exclusion principle. This antisymmetry produces a spatial separation between electrons with the same spin and thus reduces the Coulomb energy of the electronic system. This energy reduction is the exchange and correlation energy.)

It is worth to notice that up to the present day no precise theoretical justification for the DFT exists. DFT was justified a posteriori by the remarkable computational results which often are only a few per cent off the measured values.

### B: Local density approximation (LDA)

The LDA theory assumes that the exchange and correlation energy per electron  $\varepsilon_{\text{XC}}(r)$  is purely local and equals the exchange and correlation energy per electron of a homogeneous electron gas with the same density as the electron gas at point  $r$ . Therefore

$$E_{\text{XC}}(\varrho(r)) = \int_{\mathbb{R}^3} \varepsilon_{\text{XC}}(r) \varrho(r) dr$$

with  $\varepsilon_{\text{XC}}(r) = \varepsilon_{\text{XC}}^{\text{hom}}(\varrho(r))$ .

LDA theory provides one unique and well-defined global minimum of the energy of a non-spin-polarised system of electrons. This suggests LDA to yield possibly wrong results whenever more than one global minimum of the electronic energy is present.

### C: Radial symmetry and lattice periodicity

By Bloch's theorem, [8], [28], the electronic wave functions in a periodic lattice have the representation

$$\psi_i(r) = \sum_G c_{i,G} \exp(i(k + G) \cdot r) \quad (4.21)$$

where  $G$  and  $k$  are reciprocal lattice vectors. Bloch's theorem is nothing but the solution formula for the wave equation by using Fourier theory and the periodicity of the functions.

For a radially symmetric solution, the Kohn-Sham equations (4.20) in dimensionless form become

$$\left[ -\frac{1}{2} \frac{d^2}{dr^2} + \frac{l(l+1)}{2r^2} + V(\varrho, r) \right] \psi_{nl}(r) = 0,$$

where  $V(\varrho, r) := -\frac{Z}{r} + V_H(\varrho, r) + V_{\text{XC}}(\varrho, r)$  and  $\psi_{nl}$  is the radially-symmetric wave function of shell  $nl$ .

By Bloch's theorem, every electron wave function can be expanded in terms of a countable family of plane-wave basis functions. By neglecting the wave functions with kinetic energy above a given truncation level, one can retract to the case of a finite-dimensional basis of wave functions.

#### D: Pseudopotentials for electron-ion-interaction

In order to dramatically decrease the needed basis functions and to increase the order of convergence, pseudopotentials are introduced. The general idea is to replace the all-electron potential that oscillates very rapidly close to the atom core due to the strong ionic potential by a pseudopotential that is much weaker in the core region  $r \leq r_c$  and identical to the original potential for  $r > r_c$ , see Fig. 4.4. Here,  $r_c$  is a chosen core cutoff radius.

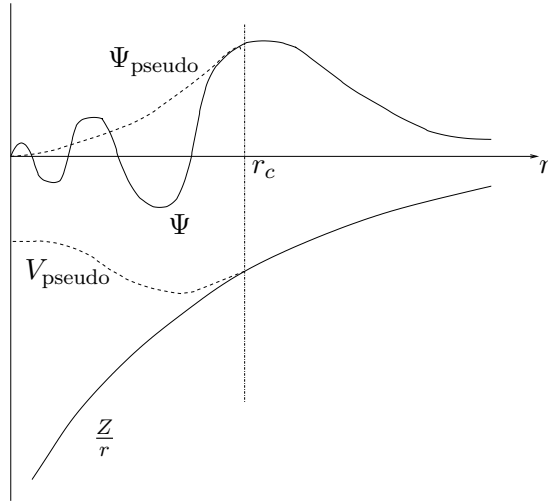


Figure 4.4: All-electron potential(solid line) and electronic pseudopotential (dashed line)

Troullier-Martins pseudopotentials belong to the class of norm-conserving pseudopotentials. These are characterised by the following five properties:

- (a) The pseudo wavefunction is twice continuously differentiable and fulfills

$$\lim_{r \searrow 0} \psi_l^{\text{pseud}}(r) \approx r^{l+1}.$$

- (b)  $\psi_l^{\text{pseud}}$  has the same eigenvalue as the all-electron wavefunction  $\psi_l$ .

- (c) Pseudo wavefunction and all-electron wave function coincide outside the core region:

$$\psi_l^{\text{pseud}}(\varepsilon_l^{\text{pseud}}, r) = \psi_{nl}(\varepsilon_{nl}, r) \quad \text{for } r \geq r_c.$$

- (d) The pseudo wave function is normalised,

$$\int_0^\infty |\psi_l^{\text{pseud}}(\varepsilon_l^{\text{pseud}}, r)|^2 dr = \int_0^\infty |\psi_{n,l}(\varepsilon_{n,l}, r)|^2 dr = 1.$$

- (e) The logarithmic derivatives (which act as boundary conditions for the numerical computations) are the same for the all-electron wave function and the pseudo

wave function:

$$\frac{d}{dr} \ln \psi_l^{\text{pseud}}(\varepsilon_l^{\text{pseud}}, r) = \frac{d}{dr} \ln \psi_{nl}(\varepsilon_{nl}, r).$$

Additional to these properties, the Troullier-Martins pseudopotentials are characterised by two further constraints, namely that all first derivatives of the electron potential and of the pseudopotential coincide at  $r = r_c$  and that  $\frac{\partial^2}{\partial r^2} V^{\text{pseud}}(r)|_{r=0} = 0$ .

After the general discussion of the theoretical background, we will now focus on the implementation details with the goal to compute essential properties of sphalerite and chalcopyrite from quantum mechanics. The calculations are carried out with ABINIT, [40], a program package developed and distributed by the Université Catholique de Louvain (<http://www.abinit.org>).

After simple convergence tests, the energy cutoff  $e_{\text{cut}}$  was set to  $20Ha \approx 544.23eV$  (one has  $e_{\text{cut}} = \frac{1}{2}[2\pi(k + G_{\text{max}})]^2$ , and  $G_{\text{max}}$  is the largest reciprocal lattice vector included in the Expansion (4.21) of the wave function) yielding a relative error of 0.4% in the total energy. The macroscopic dielectric constant  $\varepsilon_{\text{diel}}$  (a number between 1 for a perfect insulator and  $10^6$  for metal) of ZnS is preset to 8.32, the physical value found in literature. For the self-consistent energy minimisation cycle within ABINIT, the conjugated gradient method is chosen. In order to obtain satisfying results, the Brillouin zone is sampled with 182 k-points.

The following picture shows the binding energy for cubic ZnS as a function of the lattice constant.

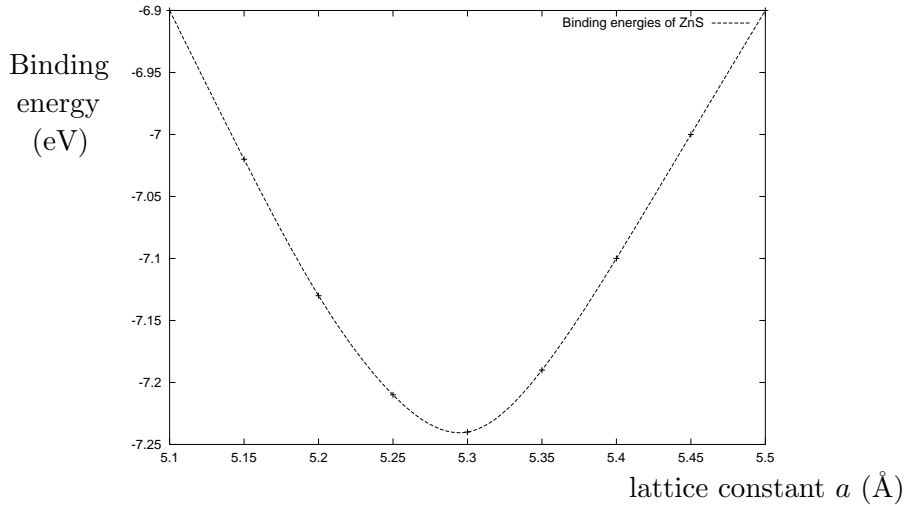


Figure 4.5: Binding energy in eV for different lattice constants  $a$  and cubic ZnS

The minimal value  $-7.22\text{eV}$  is obtained at  $a = 5.317\text{\AA}$  (the binding energy computed by GULP for  $a = 5.419$  is  $-7.676\text{eV}$ ). A slight underestimate of the lattice constant and an overestimate of the binding energy are typical of well-converged local-density calculations.

Figure 4.6 displays the densities of state for cubic ZnS as a function of energy. The densities of state are computed using 182 k-points to cover the reciprocal lattice and with a tetrahedron method.

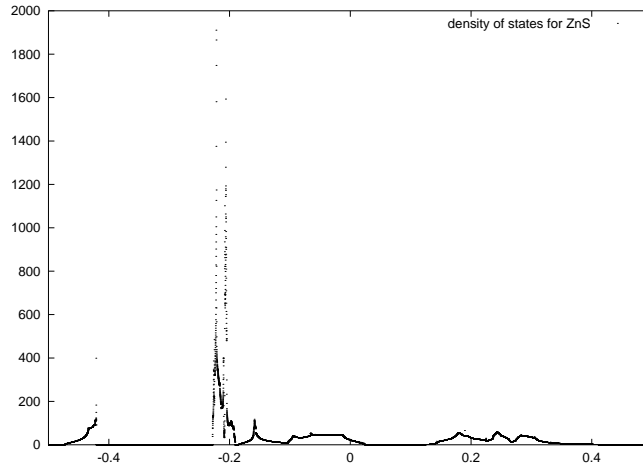


Figure 4.6: Density of states vs. energy in Hartree ( $1Ha \approx 27.211eV$ ) for ZnS

The computations for chalcopyrite are similar to those of ZnS. After convergence studies the energy cutoff  $e_{cut}$  was set to  $30Ha \approx 816.35eV$  resulting in a relative error of 0.3%. Unfortunately,  $\epsilon_{diel}$  is unknown for chalcopyrite, so that for the first computations of the relaxed geometry the ZnS-value is taken for chalcopyrite, too. Numerical tests have shown the results for chalcopyrite to change by less than 0.1% for different values of  $\epsilon_{diel}$ . As in the case of sphalerite a good sampling of the Brillouin zone is essential for the quality of the results. After some tests, the value of 182 k-points appeared to be a reasonable compromise between numerical costs and quality of the results.

Figure 4.7 displays the density of states for chalcopyrite. The minimal binding energy  $-19.7eV$  is obtained at  $a = b = 5.061\text{\AA}$  and  $c = 9.969\text{\AA}$ . The binding energy for chalcopyrite computed by GULP is  $-20.57eV$ . Comparing with the lattice vectors computed by GULP, it appears probable that the constants  $a$ ,  $b$  and  $c$  computed by DFT are as in the case of ZnS slightly too small.

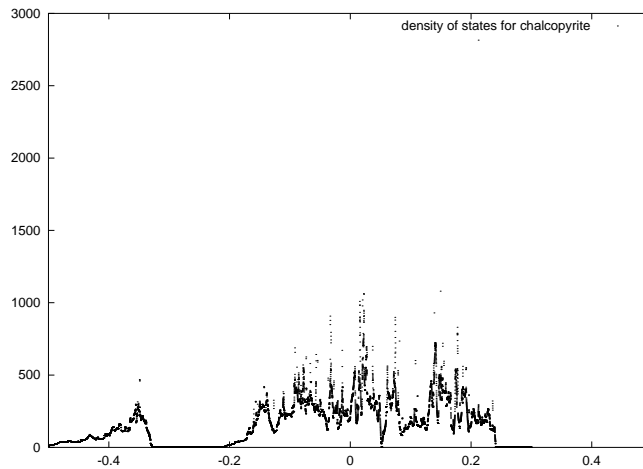


Figure 4.7: Density of states vs. energy in Hartree for chalcopyrite

There is no automatic procedure to compute the elastic constants  $C_{ij}$  within ABINIT (nor with any other quantum mechanical software package). Hopefully this will change in the future.

In the sequel we develop and compare two algorithms to determine  $C_{ij}$ . As explained above, the elastic constants are needed to gauge the interatomic potentials within GULP. The elastic constants for sphalerite serve as comparison and validation of the method.

### I Computation of $C_{ij}$ by lattice deformations

This is the direct and seemingly most natural approach. We are going to exploit the Cauchy-Born rule and apply a deformation to the lattice, determine the energy difference between undeformed and deformed state (without initial lattice relaxation!) and take advantage of the formulas

$$\begin{aligned} E &= \frac{1}{2} \sum_{i,j,k,l} C_{ijkl} \varepsilon_{ij} \varepsilon_{kl}, \\ \varepsilon_{ij} &= \frac{1}{2} \left( \frac{\partial u_i}{\partial x_j} + \frac{\partial u_j}{\partial x_i} \right). \end{aligned} \quad (4.22)$$

Here,  $\varepsilon$  denotes the strain,  $E$  the deformation energy and  $u = (u_1, u_2, u_3)$  a displacement. The computations have to be redone for deformations with respect to all three coordinate axis. In the next step, we rewrite  $C_{ijkl}$  by remembering the Voigt notation (which takes advantage of the symmetries of  $C_{ijkl}$ ), where pairs of indices are replaced by single indices:

$$\begin{array}{lll} 11 \rightarrow 1, & 22 \rightarrow 2, & 33 \rightarrow 3, \\ 12, 21 \rightarrow 6, & 13, 31 \rightarrow 5, & 23, 32 \rightarrow 4. \end{array}$$

This goes along with a reformulation of the strain tensor as a vector,

$$\begin{aligned} \varepsilon &= \begin{pmatrix} \varepsilon_{11} & \varepsilon_{12} \\ \varepsilon_{21} & \varepsilon_{22} \end{pmatrix} \rightarrow \begin{pmatrix} \varepsilon_{11} \\ \varepsilon_{22} \\ \varepsilon_{12} \end{pmatrix}, \quad \text{if } D = 2, \\ \varepsilon &= \begin{pmatrix} \varepsilon_{11} & \varepsilon_{12} & \varepsilon_{13} \\ \varepsilon_{21} & \varepsilon_{22} & \varepsilon_{23} \\ \varepsilon_{31} & \varepsilon_{32} & \varepsilon_{33} \end{pmatrix} \rightarrow \begin{pmatrix} \varepsilon_{11} \\ \varepsilon_{22} \\ \varepsilon_{33} \\ \varepsilon_{12} \\ \varepsilon_{13} \\ \varepsilon_{23} \end{pmatrix}, \quad \text{if } D = 3. \end{aligned}$$

The final entries of  $C_{ij}$  are determined by the lattice geometry, see [56]. The elastic properties of cubic ZnS are determined by 3 parameters,

$$C_{11} = C_{22} = C_{33}, \quad C_{44} = C_{55} = C_{66}, \quad C_{21} = C_{13} = C_{23}$$

and the elastic properties of tetragonal chalcopyrite by 6 values,

$$C_{11} = C_{22}, \quad C_{12}, \quad C_{33}, \quad C_{13} = C_{23}, \quad C_{44} = C_{55}, \quad C_{66}. \quad (4.23)$$

All other  $C_{ij}$  are zero. Using the symmetry of  $C_{ij}$ , this defines  $C$  completely.

The quality of the results is increased by interpolation formulas, i.e. 3 deformations are used to estimate the response of the energy functional w.r.t. variations in each direction. We spare the description of the (simple) details.

This method has the disadvantage that the lattice symmetry is lost after applying a displacement. Therefore the computations consume much time and computer memory and tend to have a low precision. Furthermore several runs have to be done for all the deformations. (The response function feature of future ABINIT versions will probably overcome this.) The second method to compute  $C_{ij}$  is therefore preferable.

## II Computation of $C_{ij}$ via acoustical modes

This method is the numerical analogon of the way how elastic constants are determined in experiment.

Travelling waves in crystals (as waves in general) can be represented by

$$u(r, t) = \tilde{u} \exp(i(k \cdot r - \omega t)). \quad (4.24)$$

Here,  $u$  is the atomic elongation,  $\tilde{u} = (\tilde{u}_1, \tilde{u}_2, \tilde{u}_3)$  is the amplitude vector,  $k = (k_1, k_2, k_3)$  the wave vector,  $r = (r_1, r_2, r_3)$  the position vector and  $\omega$  the angular frequency.

With ABINIT we compute *dispersion curves*, i.e. curves that describe the relationship  $k \mapsto \omega(k)$ . More precisely we estimate with interpolation formulas the slopes  $\omega'(0)$  of the acoustic phonon dispersion curves at the origin (acoustic phonon modes in contrast to optical phonon modes fulfill  $\omega(k=0) = 0$ ). Using Representation (4.24) in (4.22) yields

$$\begin{aligned} \varepsilon_{ij}(t) &= \frac{i}{2} (u_i(t)k_j + u_j(t)k_i) \\ &= \frac{i}{2} (\tilde{u}_i k_j + \tilde{u}_j k_i) \exp(i(k \cdot r - \omega t)). \end{aligned}$$

From Newton's equation of motion

$$\rho \partial_t^2 u_n = -\rho \omega^2 u_n$$

we get

$$\rho \omega^2 \tilde{u}_n = \sum_{jlm} C_{njlm} k_j k_l \tilde{u}_m$$

or

$$\rho \omega^2 \tilde{u} = M(k) \cdot \tilde{u}.$$

The values on the left hand side are provided by ABINIT. Suitable  $k$ -points can be gained by densifying the  $k$ -point mesh (with `dsifkpt`). It remains to compute the matrix  $M$  which is straightforward using the Voigt notation again. For the cubic ZnS lattice we find

$$M(k) = \begin{pmatrix} C_{11}k_1^2 + C_{44}(k_2^2 + k_3^2) & (C_{12} + C_{44})k_1k_2 & (C_{12} + C_{44})k_1k_3 \\ (C_{12} + C_{44})k_1k_2 & C_{11}k_2^2 + C_{44}(k_1^2 + k_3^2) & (C_{12} + C_{44})k_2k_3 \\ (C_{12} + C_{44})k_1k_3 & (C_{12} + C_{44})k_2k_3 & C_{11}k_3^2 + C_{44}(k_1^2 + k_2^2) \end{pmatrix}$$

and for tetragonal chalcopyrite we find

$$M(k) = \begin{pmatrix} C_{11}k_1^2 + C_{66}k_2^2 + C_{44}k_3^2 & (C_{12} + C_{66})k_1k_2 & (C_{13} + C_{44})k_1k_3 \\ (C_{12} + C_{66})k_1k_2 & C_{66}k_1^2 + C_{11}k_2^2 + C_{44}k_3^2 & C_{44}k_2k_3 \\ (C_{13} + C_{44})k_1k_3 & C_{44}k_2k_3 & C_{44}(k_1^2 + k_2^2) + C_{33}k_3^2 \end{pmatrix}.$$

The following Table 4.5 shows the results of the computations for ZnS and extends the results of Table 4.1. As before, EXP1 refers to the experimental results in [54], EXP2 to [14], PS2 to GULP results, QM1 is the quantum mechanical data where  $C_{ij}$  have been computed by Method I, QM2 quantum mechanical data with  $C_{ij}$  gained by Method II. As can be seen, Method II gives superior results (and is significantly faster). Therefore, Method II was used to generate reference values for  $C_{ij}$  and chalcopyrite and Table 4.3 was fitted with these results.  $B_0$  denotes the bulk modulus.

	EXP1	EXP2	QM1	QM2	P2
$a/\text{\AA}$	5.41	5.41	5.32	5.32	5.403
$V/\text{\AA}^3$	158.29	158.29	150.36	150.36	157.77
$B_0/GPa$	76.6	-	82.8	82.8	71.55
$C_{11}/GPa$	9.42	9.76	9.77	9.63	9.37
$C_{12}/GPa$	5.68	5.9	6.02	5.89	6.16
$C_{44}/GPa$	4.36	4.51	4.91	4.87	4.03
$\epsilon_{\text{stat}}$	7.9	-	-	-	7.21
$\epsilon_{\text{hf}}$	5.8	-	-	-	4.56

Table 4.5: Comparison of experimental and calculated data for ZnS

LDA tends to overbind and produces elastic constants larger than experiment. This might be corrected by the generalised gradient approach (GGA).

In Table 4.6, the results for chalcopyrite are listed. The computed lattice constants are about 6% off the experimental values. Probably, the Troullier-Martins pseudopotentials are too soft.

The found elastic constants were used in Section 4.4 to fit the GULP potentials.

	Exp2	QM	P5
$a/\text{\AA}$	5.2864	5.061	5.59
$b/\text{\AA}$	5.2864	5.061	5.59
$c/\text{\AA}$	10.4102	9.969	10.70
$V/\text{\AA}^3$	145.46	127.67	167.73
$C_{11}/GPa$	-	17.83	18.12
$C_{12}/GPa$	-	5.81	5.64
$C_{13}/GPa$	-	6.27	6.59
$C_{33}/GPa$	-	13.15	14.25
$C_{44}/GPa$	-	13.19	18.93
$C_{66}/GPa$	-	4.93	8.70

Table 4.6: Comparison of experimental/calculated data for chalcopyrite



## Chapter 5

# Numerical Simulations

### 5.1 Verification of the algorithms

We present several tests for the correctness of the computational methods.

#### 5.1.1 Two simple analytic tests for Model I

For all program runs in two space dimensions, let  $\Omega := [0, 2] \times [0, 1] \subset \mathbb{R}^2$ . In order to test the finite element method and the solution to System (2.29), we think up a vector  $(c, \chi) = (c_1, c_2, c_3, c_4, \chi) : \Omega_{T_0} \rightarrow \mathbb{R}$  that is to become a solution and plug this sought up solution into the equations.

We want to assume for (2.29)  $L_{ij} = \delta_{ij}$ , and set artificially  $b^1 = b^2 := 1$ . The last implies

$$\omega(c, \chi) = W'(\chi),$$

as a look to (2.28) reveals.

Let  $K_1, \dots, K_4$  be positive real numbers with  $(K_1, K_2, K_3, K_4) \in \Sigma$  (according to Definition (3.3) this means  $\frac{3}{2}K_1 + K_2 + K_3 + K_4 = \frac{1}{2}$ ). We set

$$\begin{aligned} c_{20} &:\equiv K_2, \quad c_{30} :\equiv K_3, \quad c_{40} :\equiv K_4, \\ \chi_0 &:\equiv \frac{1}{2}. \end{aligned}$$

With

$$\kappa := \frac{K_2^2}{K_1 K_3}$$

and due to  $\omega(\chi) = W'(\frac{1}{2}) = 0$  we find at once that

$$(c_1, c_2, c_3, c_4, \chi) \equiv (K_1, K_2, K_3, K_4, \frac{1}{2}) \tag{5.1}$$

solves (2.29) with the above initial values and choices on  $L$ ,  $\kappa$  and  $b^1, b^2$ , as

$$\mu_i \equiv \frac{1}{2} \left( \frac{\partial f_1}{\partial c_i} + \frac{\partial f_2}{\partial c_i} \right) (K_1, K_2, K_3, K_4) =: M_i \quad \text{in } \Omega_{T_0}$$

for suitable constants  $M_i \in \mathbb{R}$  and where the boundary data  $g_i$  and  $h_i$  are of course set to  $g_i \equiv K_i$  and  $h_i \equiv M_i$ .

It was found that the error between the computed and the predicted solution (5.1) in  $\|\cdot\|_{L^2}$  and  $\|\cdot\|_{L^\infty}$  is exactly 0 for all refinement levels. This is not surprising as the interpolation error for constant values is 0 independent of the level of numeric resolution.

This first test mainly checks the algorithms to compute the reaction terms, but the computational routines for the fluxes, i.e. for calculating  $\text{div}(L\nabla\mu)$  and  $\Delta\chi$ , are not adequately tested. Therefore, as second test case, we once more set  $L_{ij} = \delta_{ij}$ ,  $b^1 = b^2 := 1$ , choose  $r(c, \chi) := (w, 0, 0, 0)$  with a function  $w = w(x, t)$  to be determined later and verify the code by artificially replacing Eq. (2.29c) by

$$\mu_j = c_j, \quad 1 \leq j \leq 4$$

which is the same as writing

$$F(c, \chi) := \int_{\Omega} \left( \frac{1}{2} \sum_{j=1}^4 c_j^2 + \frac{\gamma}{2} |\nabla\chi|^2 + W(\chi) \right)$$

instead of the correct free energy. This leads to a decoupled system of the standard elliptic equation

$$\Delta c_1 = w \quad \text{in } \Omega_{T_0}, \quad (5.2)$$

an ordinary heat equation for  $\tilde{c} := (c_2, c_3, c_4)$  and standard Allen-Cahn equation. For (5.2) in two space dimensions with  $(x, y) \in \Omega$  we prescribe the solution  $c_{1,\text{ref}}(x, y) = x(2-x)y(1-y)$  which fulfills  $c_{1,\text{ref}} = 0$  on  $\partial\Omega$ , whence  $g_1 := 0$  is the first Dirichlet condition. The choice of  $c_{1,\text{ref}}$  implies

$$w = w(x, y) = 2x(x-2) + 2y(y-1)$$

as right hand side of (5.2). The solution vector  $\tilde{c}$  of the heat equations is compared with the on  $\mathbb{R}^D$  analytic solution

$$\tilde{c}_{\text{ref}}(\xi, t) = \frac{1}{(4\pi t)^{-D/2}} e^{-|\xi|^2/(4t)} * c_0(\xi)$$

gained for instance by Fourier transformation for given initial values  $c_0$ . Since  $\tilde{c}$  is the analytic solution for the whole of  $\mathbb{R}^2$  and as  $\Omega$  is bounded here, we set  $\tilde{c} = (g_2, g_3, g_4) := u_{\text{ref}}$  on  $\partial\Omega$ .

Table 5.1 shows the errors  $\|c_1 - c_{1,\text{ref}}\|_{L^2(\Omega)}$ ,  $\|c_1 - c_{1,\text{ref}}\|_{H^{1,2}(\Omega)}$  and  $\|\tilde{c} - \tilde{c}_{\text{ref}}\|_{L^\infty(L^2)}$  for both the elliptic equation and the three heat equations where  $T_0 := 1$ .

Refinement	Triangles	Vertices	$\ c_1 - c_{1,\text{ref}}\ _{L^2}$	$\ c_1 - c_{1,\text{ref}}\ _{H^1}$	$\ \tilde{c} - \tilde{c}_{\text{ref}}\ _{L^\infty(L^2)}$
2	16	15	$2.1 \cdot 10^{-2}$	$8.3 \cdot 10^{-2}$	$2.4 \cdot 10^{-2}$
4	64	45	$6.8 \cdot 10^{-3}$	$4.4 \cdot 10^{-2}$	$7.2 \cdot 10^{-3}$
6	256	153	$1.8 \cdot 10^{-3}$	$2.2 \cdot 10^{-2}$	$2.1 \cdot 10^{-3}$
8	1024	561	$4.6 \cdot 10^{-4}$	$1.1 \cdot 10^{-3}$	$4.8 \cdot 10^{-4}$
10	4096	2145	$1.1 \cdot 10^{-4}$	$5.6 \cdot 10^{-3}$	$1.16 \cdot 10^{-4}$
12	16384	8385	$2.9 \cdot 10^{-5}$	$2.7 \cdot 10^{-3}$	$2.97 \cdot 10^{-5}$
14	65536	33153	$7.3 \cdot 10^{-6}$	$1.4 \cdot 10^{-3}$	$7.35 \cdot 10^{-6}$

Table 5.1: Computed errors of the test problem for different refinement levels

The results of the Allen-Cahn equation can be checked by the well-known behavior of the solution (nucleation and interface motion by mean curvature).

The second test can be used as a benchmark to analyse the behavior of the Newton-Krylov solver and to adjust the parameters. The critical value is  $n_{it}$  which determines the number of iterations for solving the linear system inside the loop of the Newton solver. We will not discuss the quite uninteresting details but remark that the linear GMRES is only 'conditionally convergent'. This means that if one chooses  $n_{it}$  too large, the algorithm will diverge. This is not surprising as the convergence of the linear GMRES does not rely on the Banach fixed point theorem. A thorough discussion of this topic can be found in [21], [45].

### 5.1.2 Analysis of the different parts of the entropy

We compare for certain reference configurations the results of the harmonic approximation and of MD simulations. In particular this provides useful information how well the system entropy is captured. GULP can only compute the harmonic part of the system entropy. The anharmonic vibrational contributions to the system entropy are not captured.

For  $T < 1^\circ K$  we will find that both methods yield almost identical results (even though due to quantum mechanical effects both are wrong). One part of this section serves hence as a direct validation of GULP and DLPOLY. The used interatomic potentials are not verified by this comparison because they are the same in both applications (taken from Table 4.2 and Table 4.4).

#### Parameters of MD simulations: (Keywords of DLPOLY)

Cubic boundary conditions (`imcon 1`); overall 4000 steps, 2000 calibration steps; use of Berendsen thermostat with thermostat relaxation time 0.1ps and barostat relaxation time 2ps (`ensemble npt berendsen 0.1 2`); atom velocities are rescaled in every step (`scale 1`); `ewald precision 10-6`; Verlet neighbour width 1Å (`delr width 1A`); `timestep 0.001 ps`; `pressure 0 kbar`; `cutoff 12A`; the interatomic potentials are defined by Table 4.2.

Sphalerite	$T$	$a = b = c(\text{\AA})$	$F(eV)$	$F_{V_{ref}}(eV)$
GULP	$1^\circ K$	5.4243	-133.519	-836.58
	$500^\circ C$	5.4412	-135.37	-840.32
	$700^\circ C$	5.4473	-136.20	-842.61
DLPOLY	$0^\circ K$	5.4243	-133.52	-836.59
	$500^\circ C$	5.4409	-132.72	-823.99
	$700^\circ C$	5.4493	-132.29	-817.53

Chalcopyrite	$T$	$a = b(\text{\AA})$	$c(\text{\AA})$	$F(eV)$	$F_{V_{ref}}(eV)$
GULP	$1^\circ K$	5.577	10.68	-138.491	-832.63
	$500^\circ C$	5.598	10.701	-139.95	-832.08
	$700^\circ C$	5.606	10.705	-140.635	-835.85
DLPOLY	$0^\circ K$	5.577	10.68	-138.493	-832.65
	$500^\circ C$	5.602	10.708	-139.09	-827.83
	$700^\circ C$	5.61	10.73	-139.37	-825.41

Table 5.2: Lattice geometry and free energy for GULP and DLPOLY

The results of DLPOLY are converted from data of a  $5 \times 5 \times 5$  supercell. The

original data for sphalerite and  $T = 0^\circ K$  is  $\bar{a} = 27.1215\text{\AA}$  (edgelenlength of the supercell) and  $\bar{F} = -16690\text{ eV}$  (total free energy of the supercell). For the last column,  $F$  is reconverted to  $V_{\text{ref}} = 1000\text{\AA}^3$  thereby taking the volume of the computed unit cell into account.

As can be seen, the agreement for  $T = 0^\circ K$  (GULP only accepts  $T > 0^\circ K$  for computations of the free energy) is extremely good when there is (almost) no entropic contribution to  $f$ . Further tests were made for selected atomistic configurations that arise during the phase transition from sphalerite to chalcopyrite always with a negligible difference in the energy. We omit the presentation of the figures. This test is the for-mentioned validation of GULP and DLPOLY against each other in a special case.

Having another look at Table 5.2, there is also bad news. We see that the energy difference between GULP and DLPOLY data increases as  $T$  becomes larger. We observe that this difference exceeds for  $T = 700^\circ C$  the driving force of the segregation process as computed by GULP which is the energy difference between the two phases.

Conclusion: *Numerical experiments based on MD simulations can show a different behavior of the solution as simulations based on the harmonic approximation!*

## 5.2 The dependence of GULP data on atomistic lattice configurations

For given lattice geometry  $l = 1, 2$  we want to analyse the variation of the free energies as computed by GULP for  $R_l$  atomistic configurations that all represent one concentration vector. The aim is to find an empirical heuristic to control  $R_l$ .

This analysis is closely related to Section 4.4. Let  $c_i$  be the  $i$ -th selected entry in the list of concentration vectors which is kept fixed in the following. Firstly, we compute admissible atom configurations  $c_i^j$ ,  $1 \leq j \leq 20$  of a  $3 \times 3 \times 3$  supercell (for both the lattice structures of sphalerite( $l = 2$ ) and of chalcopyrite( $l = 1$ )) that represent  $c_i$ , then invoke GULP to compute the free energies  $f^l(c_i^j)$ ,  $l = 1, 2$ . It is possible that  $c_i^j = c_i^k$  for  $j \neq k$  and  $j, k \in \{1, 2, \dots, 20\}$ , for instance if only one atomistic configuration exists to represent  $c_i$ .

The values  $(f^l(c_i^j))_{1 \leq j \leq 20}$  are used to sample the distribution. We calculate the mean value (or expectation value)

$$\bar{f}_l := \frac{1}{20} \sum_{j=1}^{20} f^l(c_i^j)$$

and the variance

$$s_l := \sqrt{\frac{\sum_{j=1}^{20} (f^l(c_i^j) - \bar{f}_l)^2}{20}}.$$

Figure 5.1 shows the fraction  $s_l/\bar{f}_l$  for  $l = 2$  of the sample  $(f^2(c_i^j))_{1 \leq j \leq 20}$  for different configurations of the sphalerite-supercell.  $s_2/\bar{f}_2$  is plotted as a function of two arguments, the number of Cu atoms on the  $x$ -axis and the number of Fe atoms on the  $y$ -axis, both numbers between 0 and 54. As there are overall 108 positions which are not occupied by S atoms, the remaining are still filled by Zn.

The lattice order of sphalerite is located at the origin ( $x = y = 0$ ) of the diagram, the lattice order of chalcopryite is placed at the right corner ( $x = y = 54$ ). For these two geometries, the deviation of  $f^2$  is exactly zero because only one atom configuration may be chosen.

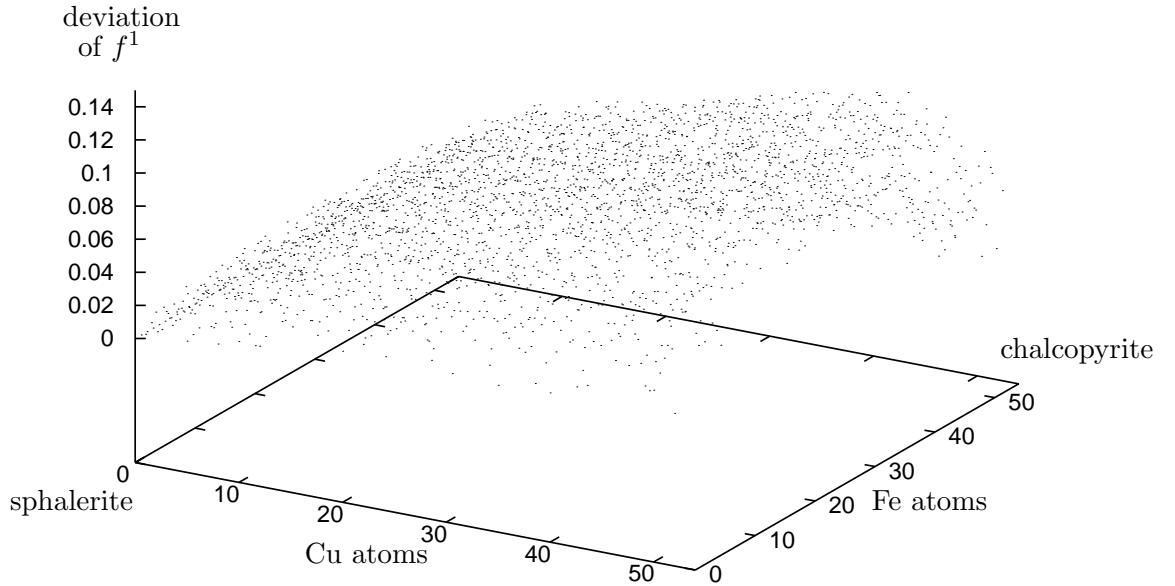


Figure 5.1: Deviation of GULP data for ZnS as a function of lattice configuration

From Figure 5.1 we learn that the deviation of  $f^2$  grows considerably stronger in  $x$ -direction than in  $y$ -direction indicating that the Cu atoms have a much larger impact on the geometry of the sphalerite-supercell than Fe has.

The variation of  $f^1$  is not displayed, but it is very similar to Figure 5.1 with larger values as the superstructure of chalcopryite has almost doubled its length in the  $z$ -direction.

As the perspective in Figure 5.1 may be misleading, two cuts through the graph are displayed in Figure 5.2. The first is parallel to the  $y$ -axis for  $x = 45$  Cu atoms, the second parallel to the  $x$ -axis for  $y = 45$  Fe atoms.

The information of the sample with 20 computed free energies is now used to estimate  $R_l$ . We assume that  $X_l := (f^l(c_i^j))_j$  is normally distributed where we put  $\sigma_l := s_l$  for the variance of  $X_l$ . The transformed distribution  $U_l := \frac{X_l - \bar{f}_l}{\sigma_l}$  has mean value 0 and variance 1. Now, for a given number  $\varrho > 0$  we determine a confidence interval of length  $\varrho$  which contains  $\bar{f}$  with a probability of at least 95%. Let  $\Phi$  denote the (tabulated) function of the normal distribution with variance 1 and mean value 0. In order to fulfill the 95% niveau and due to symmetry we choose  $u_0 := 1.96$  (we have  $\Phi(u_0) \approx 0.975$ ). From the formula

$$|X_l - \bar{f}_l| \leq \frac{\varrho}{2} = u_0 \frac{\sigma}{\sqrt{R_l}}$$

which implies

$$R_l := \frac{4u_0^2\sigma^2}{\varrho^2}$$

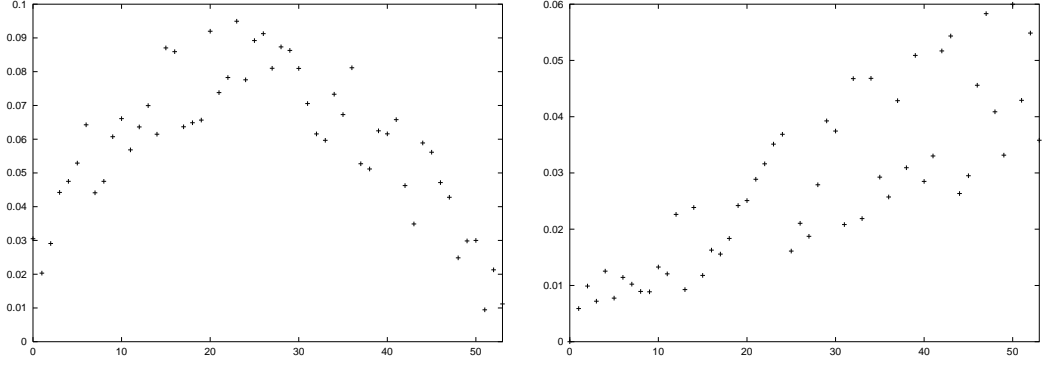


Figure 5.2: Cut through deviation data for  $x = 45$  Cu atoms as a function of Fe atoms (left) and for  $y = 45$  Fe atoms as a function of Cu atoms (right)

we infer the setting

$$R_l := \min \left\{ 50, \left\lceil \frac{4u_0^2 s^2}{\varrho^2} \right\rceil \right\}.$$

The cutoff value of 50 is introduced to bound the computational effort.

### 5.3 Numerical results for Model I

Now we want to illustrate the behavior of the model (2.29) equipped with the free energy (2.24). In all numerical simulations, the underlying uniform triangulation of  $\Omega$  as well as the time step  $\Delta t$  were not adapted during the computation. The simulations were performed in two space dimensions. System (2.29) was solved in its dimensional form as explained in Section 2.5.

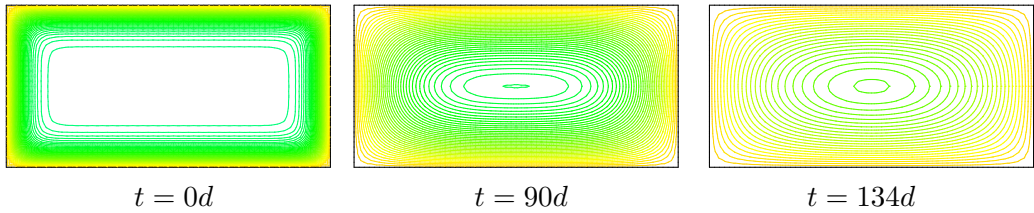


Figure 5.3: Diffusion of  $\text{Cu}^+$ . The density of the level sets indicates the steepness of the copper gradient. At  $t = 0$ , the initial datum falls from 0.2 at the boundary to 0.001 in the center.

**Physical Parameters:**  $\Omega = [0, 0.2\text{m}] \times [0, 0.1\text{m}]$  (i.e.  $D = 2$ ),  $T = 500^\circ\text{C}$ ,  $k = 1$ ,  $\kappa = 0.06$ ,  $\gamma = 3 \cdot 10^{-9}\text{m}$ ,  $D_{\text{Cu}} = 2.6 \cdot 10^{-4}\text{m/s}$ ,  $D_{\text{Fe}} = 1.26 \cdot 10^{-4}\text{m/s}$ ,  $D_{\text{Zn}} = 1.85 \cdot 10^{-7}\text{m/s}$ ,  $\alpha_1 = 0.555$ ,  $\alpha_2 = 0.66$ ,  $\alpha_3 = 0.635$ ,  $\alpha_4 = 0.64$ .

**Triangulation Data:** 6521 points, 12800 triangles,  $h = 10^{-8}$ .

**General Parameters:**  $\epsilon_{\text{GMRES}} = \Delta t = 0.004$ ,  $\eta = 10^{-8}$ ,  $b^1 = 1$ ,  $b^2 = 0.8$ .

**Initial Conditions:**  $c_3 \equiv 0.001$ ,  $c_2 \equiv 0.245$ ;  $\chi$  a small random deviation of 0.5.

**Boundary conditions:**  $\partial_\nu c_1 = 0$ ,  $\partial_\nu c_2 = 0$ ,  $c_3 = 0.2$  and  $\partial_\nu \chi = 0$  on  $\partial\Omega$ .

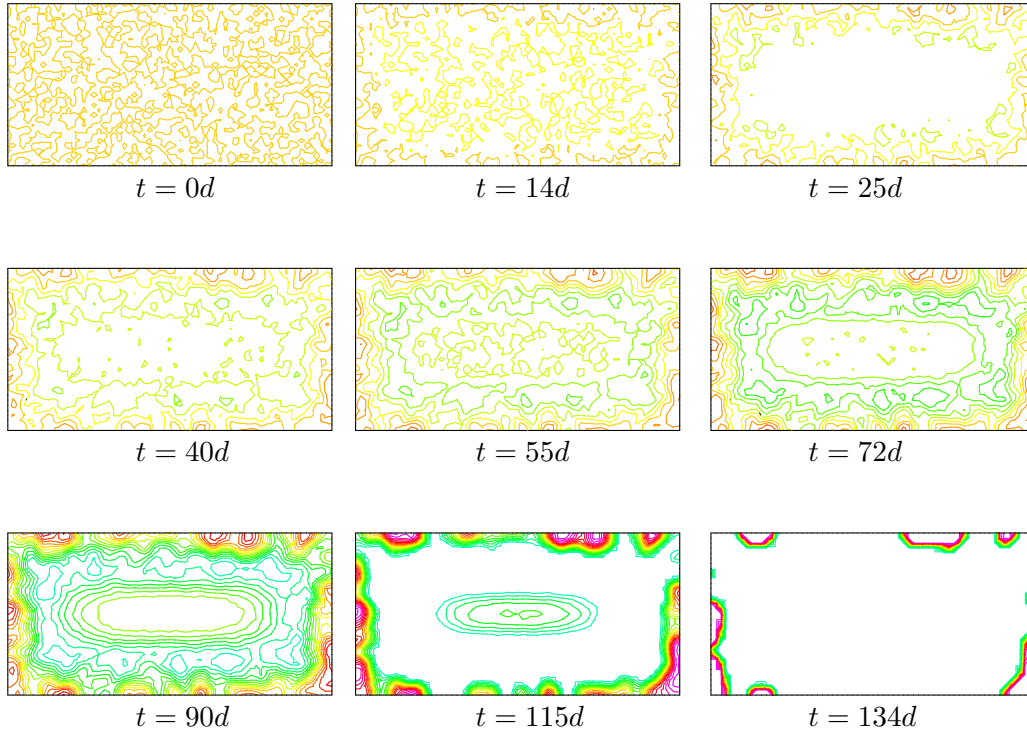


Figure 5.4: Time evolution of the chalcopyrite phases. The first picture for  $t = 0d$  shows the random distribution of  $\chi$  around 0.5. Phase formation takes place until for  $t = 134d$  the chalcopyrite phases concentrate near the boundary as a consequence of the copper gradient and the diffusion of copper into the crystal.

Some parameters like  $b^1$ ,  $b^2$  cannot be obtained from physical considerations. They are chosen in such a way that conditions (2.49), (3.35) and (2.50) hold and hence  $\partial_t F(c(t), \chi(t)) \leq 0$ .

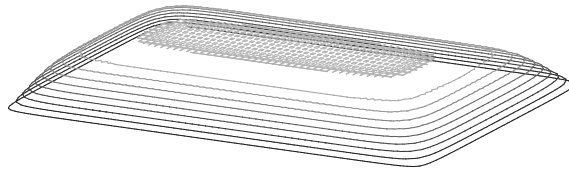


Figure 5.5: Typical plot of  $\text{Fe}^{3+}$ . The graph of  $\text{Fe}^{3+}$  grows slightly towards the center and is convex. The graph of  $c_1$  is very flat due to the maximum content of  $\text{Fe}^{3+}$  on the iron concentration. The display is magnified, the maximum of  $c_1$  being 0.05 and the minimum 0.001.

During the computation, the graph of  $\text{Fe}^{3+}$  is flattening even more. The graph of Zn behaves opposite to that of  $\text{Cu}^+$  and decreases near the boundary. The concentration of  $\text{Fe}^{3+} + \text{Fe}^{2+}$  is not displayed, it is a perfect constant in time and space. Hence, Fig. 5.5 also tells us about the distribution of the free electrons as predicted by Model I.

The diffusivity constants were taken from [55]. From the measurements we learn the relationship  $D_{\text{Zn}} \approx D_{\text{Fe}} \approx 10^3 \cdot D_{\text{Cu}}$ .

The presented phenomenon depends critically upon the time scales, the diffusion parameter  $D_{\text{Cu}}$  of Cu and the relaxation parameter  $\tau$  of the Allen-Cahn equation.

## 5.4 Extension of Model I to linear elasticity

In this section we shall discuss a generalisation of Model (2.29) that includes linear elasticity.

Let  $\Omega$  be a reference configuration of the crystal. We denote by

$$\Phi(t) : \Omega \rightarrow \mathbb{R}^D \text{ for } t > 0$$

the time dependent deformation of the crystal. In particular we postulate

$$\Phi \in H^{1,D+\delta}$$

for some  $\delta > 0$  to guarantee that  $D\Phi$  exists and that  $\Phi$  is invertible with  $\det(D\Phi) > 0$ . We assume the deformations to be small and use a standard linearised theory, the displacement  $u$  given by the formula

$$\Phi(t) := \text{Id} + u(t). \quad (5.3)$$

With the help of  $u$  the local strain can be written as

$$\varepsilon(u) := \frac{1}{2}(\nabla u + \nabla u^t)$$

or equivalently

$$\varepsilon_{ij}(u) = \frac{1}{2}(\partial_i u_j + \partial_j u_i).$$

The elastic properties of the crystal are determined by the symmetric positive definite tensor  $C$ . Using the reduced vector representation

$$\varepsilon = \begin{pmatrix} \varepsilon_{11} & \varepsilon_{12} \\ \varepsilon_{12} & \varepsilon_{22} \end{pmatrix} \approx (\varepsilon_{11}, \varepsilon_{22}, \varepsilon_{13})^t \text{ for } D = 2 \quad (5.4)$$

and

$$\varepsilon = \begin{pmatrix} \varepsilon_{11} & \varepsilon_{12} & \varepsilon_{13} \\ \varepsilon_{21} & \varepsilon_{22} & \varepsilon_{23} \\ \varepsilon_{31} & \varepsilon_{32} & \varepsilon_{33} \end{pmatrix} \approx (\varepsilon_{11}, \varepsilon_{22}, \varepsilon_{33}, \varepsilon_{12}, \varepsilon_{13}, \varepsilon_{23})^t \text{ for } D = 3, \quad (5.5)$$

we may write for the cubic lattice geometry of sphalerite

$$C^2 \varepsilon = \begin{pmatrix} C_{11}^2 & C_{12}^1 & 0 \\ C_{12}^2 & C_{11}^1 & 0 \\ 0 & 0 & C_{44}^2 \end{pmatrix} \begin{pmatrix} \varepsilon_{11} \\ \varepsilon_{22} \\ \varepsilon_{12} \end{pmatrix} \text{ for } D = 2 \quad (5.6)$$

and

$$C^2 \varepsilon = \begin{pmatrix} C_{11}^2 & C_{12}^2 & C_{12}^2 & 0 & \dots & 0 \\ C_{12}^2 & C_{11}^2 & C_{12}^2 & 0 & & 0 \\ C_{12}^2 & C_{12}^2 & C_{11}^2 & 0 & & 0 \\ 0 & \dots & 0 & C_{44}^2 & 0 & 0 \\ 0 & & & 0 & C_{44}^2 & 0 \\ 0 & \dots & \dots & \dots & 0 & C_{44}^2 \end{pmatrix} \begin{pmatrix} \varepsilon_{11} \\ \varepsilon_{22} \\ \varepsilon_{33} \\ \varepsilon_{12} \\ \varepsilon_{13} \\ \varepsilon_{23} \end{pmatrix} \quad \text{for } D = 3 \quad (5.7)$$

and this is the form of  $C\varepsilon$  commonly used in literature. The last two equations are valid for sphalerite. The analogous formula for  $C^1$  and the tetragonal chalcopyrite is supplied in (4.23).

Due to a well-known work by Eshelby [30], we write the elastic energy of phase  $l$  in the form

$$Q^l(u, c_4) := \frac{1}{2}(\varepsilon(u) - \bar{\varepsilon}(c_4)) : C^l(\varepsilon(u) - \bar{\varepsilon}(c_4)), \quad l = 1, 2. \quad (5.8)$$

In this formula it is assumed that the energy of the unstressed solid at rest is determined by the concentration  $c_4$  of  $\text{Zn}^{2+}$ . This can be motivated by considering the replacement mechanism during the reorganisation of the lattice geometry from sphalerite to chalcopyrite and from mineralogical measurements, [54], [66].

In (5.8),  $C^1$  is defined by Eq. (5.6) or (5.7). Next we assume that the elastic energy is the convex combination of the elastic energies of both lattice geometries:

$$Q(\varepsilon, c_4, \chi) := \chi Q^1(\varepsilon, c_4) + (1 - \chi) Q^2(\varepsilon, c_4).$$

The crystal is in elastic equilibrium if for the stress  $\sigma = \partial_\varepsilon Q(\varepsilon, c_4, \chi)$

$$\operatorname{div} \sigma = \operatorname{div}((\chi C^1 + (1 - \chi) C^2)(\varepsilon(u) - \bar{\varepsilon}(c_4))) = 0. \quad (5.9)$$

Eq. (5.9) is coupled with the natural boundary conditions

$$\partial_\nu \sigma = 0 \quad \text{on } \partial\Omega. \quad (5.10)$$

With the knowledge of the local strain we are in the position to find a more precise formula for the free energy of the single phases. For the free energy of the bulk phase we write

$$f_l(c, u) = b^l \sum_{i=1}^4 c_i \ln c_i + Q^l(\varepsilon(u), c_4), \quad l = 1, 2. \quad (5.11)$$

In Section 2.3 the approximation  $(\sum_i \alpha_i c_i)^2$  instead of  $Q^l(\varepsilon, c_4)$  for the elastic part of the free energy had been used.

For convenience it is assumed that the minimal strain  $\bar{\varepsilon}(c_4)$  is a multiple of the identity:

$$\bar{\varepsilon}(c_4) = \varrho c_4 \operatorname{Id} \quad (5.12)$$

with the lattice misfit  $\varrho$ .

The remaining modifications to the model are straightforward. The density of the mixing entropy  $s_M$  is defined as in Section 2.3. To avoid ambiguities we denote by  $s$  the entropy density and by  $\sigma$  the stress. Due to the thermodynamic relation

$f = e - Ts$ , with the concentration vector  $c = (c_1, c_2, c_3, c_4)$ , the free energy density of the system has the form (2.8).

For the numerical treatment, it is suitable to eliminate the equation for  $c_4$ . For the computation of  $\mu_j$  we remember  $c_4 = \frac{1}{2} - \frac{3}{2}c_1 - c_2 - c_3$  and write with the chain rule

$$\frac{\partial Q(\varepsilon, c_4)}{\partial c_j} = \frac{\partial Q(\varepsilon, c_4)}{\partial c_4} \frac{\partial c_4}{\partial c_j}, \quad 1 \leq j \leq 3.$$

A simple calculation yields

$$\frac{\partial Q(\varepsilon, c_4)}{\partial c_4} = -(\chi C^1 + (1 - \chi)C^2)(\varepsilon(u) - \bar{\varepsilon}(c_4)) : \frac{\partial \bar{\varepsilon}}{\partial c_4} = -\sigma : \frac{\partial \bar{\varepsilon}}{\partial c_4}.$$

For  $\bar{\varepsilon}(c_4) = \rho c_4 \text{Id}$  we find

$$\frac{\partial Q(\varepsilon, c_4, \chi)}{\partial c_4} = -\rho \text{tr}(\sigma).$$

Replacing (2.9), for  $\omega$  we make the ansatz

$$\omega(c, \chi) = \ln \chi - \ln(1 - \chi) - \chi + m(c) - \sum_{ij} \xi_{ij} \varepsilon_{ij} \chi. \quad (5.13)$$

This is a bilinear coupling between strain and order parameter. The numbers  $\xi_{ij}$  are determined by the symmetry group and cannot be chosen arbitrarily, see [64].

Finally, for the resulting model, we obtain the coupled equations (2.29), (5.13), (5.9), (5.10), where Relation (2.8) determines the free energy density  $f$ .

When numerically solving the equations one faces the problem that Eq. (5.9) determines uniquely the strain  $\varepsilon$ , but not the displacement  $u$ . This is due to the fact that the differential operator  $\varepsilon(u)$  has the non-trivial kernel

$$\ker(\varepsilon) = \{f : \mathbb{R}^D \rightarrow \mathbb{R}^D \mid f(x) = a \wedge x + b; a, b \in \mathbb{R}^D\}.$$

To overcome this difficulty, in each step of GMRES one projects to the orthogonal complement of the matrix corresponding to Eq. (5.9).

In order to be able to show existence of solutions to this model, the following additional assumptions are needed:

(A6) The elastic energy  $Q \in C^1(\mathbb{R}^{D \times D} \times \mathbb{R} \times \mathbb{R}; \mathbb{R})$  fulfills

(A6.1)  $Q(\varepsilon, c_4, \chi)$  only depends on the symmetric part of  $\varepsilon \in \mathbb{R}^{D \times D}$ , i.e.

$$Q(\varepsilon, c_4, \chi) = Q((\varepsilon)^t, c_4, \chi) \quad \text{for all } \varepsilon \in \mathbb{R}^{D \times D}, \text{ all } c_4 \in \mathbb{R} \text{ and all } \chi \in \mathbb{R}.$$

(A6.2)  $\partial_\varepsilon Q(\cdot, c_4, \chi)$  is strongly monotone uniformly in  $c_4$  and  $\chi$ , i.e. there exists a constant  $C_2 > 0$  such that for all symmetric  $\varepsilon^1, \varepsilon^2 \in \mathbb{R}^{D \times D}$

$$(\partial_\varepsilon Q(\varepsilon^1, c_4, \chi) - \partial_\varepsilon Q(\varepsilon^2, c_4, \chi)) : (\varepsilon^1 - \varepsilon^2) \geq C_2 |\varepsilon^1 - \varepsilon^2|^2 \quad \text{for all } c_4 \in \mathbb{R}, \chi \in \mathbb{R}.$$

(A6.3) There exists a constant  $C_3 > 0$  such that for all symmetric  $\varepsilon \in \mathbb{R}^{D \times D}$ , all  $0 < c_4 < 1$  and all  $0 \leq \chi \leq 1$

$$\begin{aligned} |Q(\varepsilon, c_4, \chi)| &\leq C_3(|\varepsilon|^2 + |c_4|^2 + 1), \\ |\partial_{c_4} Q(\varepsilon, c_4, \chi)| &\leq C_3(|\varepsilon|^2 + |c_4|^2 + 1), \\ |\partial_\varepsilon Q(\varepsilon, c_4, \chi)| &\leq C_3(|\varepsilon| + |c_4| + 1). \end{aligned}$$

Assumption (A4.2) is extended by

(A4.2)<sup>+</sup> The lattice misfit  $\varrho > 0$  in (5.12) is sufficiently large. This guarantees  $\text{tr}(\sigma) < 0$  and hence

$$\int_{\Omega} \left( \frac{\partial Q}{\partial c_1} - 2 \frac{\partial Q}{\partial c_2} + \frac{\partial Q}{\partial c_3} \right) = \int_{\Omega} \frac{\varrho}{2} \text{tr}(\sigma) < 0.$$

Combining the results of Chapter 3 and the crucial estimates of [38], the proof of the following theorem is now straightforward:

**Theorem 5.1:** (*Global existence and uniqueness for the extended model*)

Let the assumptions of Section 3.9 and (A6) hold. Then there exists a unique weak solution  $(c, \mu, \chi)$  of Formulation (3.1) with logarithmic free energy and elasticity such that

- (i)  $c \in C^{0, \frac{1}{4}}([0, T_0]; L^2(\Omega; \mathbb{R}^4))$ ,
- (ii)  $\partial_t c \in L^2(0, T_0; (H_0^1(\Omega; \mathbb{R}^4))')$ ,
- (iii)  $\chi \in C^{0, \frac{1}{2}}([0, T_0]; L^2(\Omega))$ ,
- (iv)  $\partial_t \chi \in L^2(0, T_0; (H_0^1(\Omega))')$ ,
- (v) there exists a  $p > 2$  such that  $u \in L^\infty(, 0, T; H^{1,p}(\Omega))$ ,
- (vi) there exists a  $q > 1$  such that  $\ln c_j \in L^q(\Omega_{T_0})$  for  $1 \leq j \leq 4$ ,  $\ln \chi, \ln(1 - \chi) \in L^2(\Omega_{T_0})$  and in particular  $0 < \chi, c_j < 1$  a.e.

After stating the theory, we have a look at the numerical solutions. First, we consider the time evolution of the chalcopyrite phases in the new model, see Fig. 5.6. The results are similar to those without elasticity, we still observe an accumulation of chalcopyrite phases near  $\partial\Omega$  as a consequence of the penetrating  $\text{Cu}^+$ . But now the phases are slightly stretched.

**Physical Parameters:**  $\Omega = [0, 0.2\text{m}] \times [0, 0.1\text{m}]$ ,  $T = 500^\circ\text{C}$ ,  $\kappa = 0.06$ ,  $k = 1$ ,  $\gamma = 3 \cdot 10^{-9}\text{m}$ ,  $D_{\text{Cu}} = 2.6 \cdot 10^{-4}\text{ms}^{-1}$ ,  $D_{\text{Fe}} = 1.26 \cdot 10^{-4}\text{ms}^{-1}$ ,  $D_{\text{Zn}} = 1.85 \cdot 10^{-7}\text{ms}^{-1}$ ,  $C_{11} = 9.42\text{GPa}$ ,  $C_{12} = 5.68\text{GPa}$ ,  $C_{44} = 4.36\text{GPa}$ .

**Triangulation Data:** 6521 points, 12800 triangles,  $h = 10^{-8}$ .

**General Parameters:**  $\epsilon_{\text{GMRES}} = \Delta t = 0.004$ ,  $\eta = 10^{-8}$ ,  $b^1 = 1$ ,  $b^2 = 0.8$ .

**Initial Conditions:**  $c_3 \equiv 0.001$ ,  $c_2 \equiv 0.245$ ;  $\vec{u} \equiv 0$ ;  $\chi$  a random deviation of 0.5.

**Boundary conditions:**  $\partial_\nu c_1 = \partial_\nu c_2 = \partial_\nu \chi = \partial_\nu S = 0$  and  $c_3 = 0.2$  on  $\partial\Omega$ .

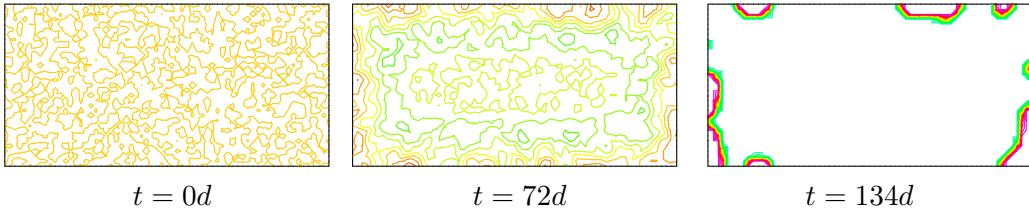


Figure 5.6: Time evolution of the chalcopyrite phases. Initial values are a random distribution of  $\chi$  with small deviation around 0.5.

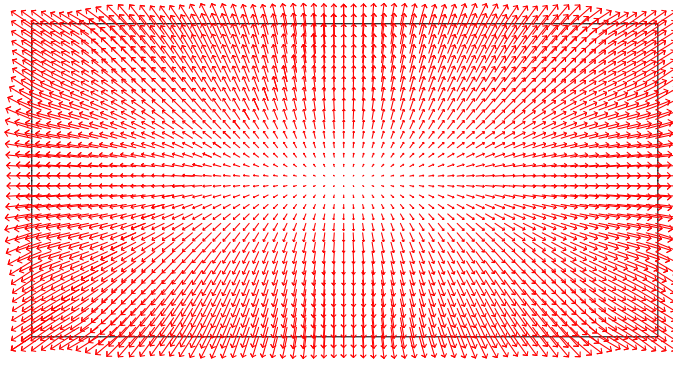


Figure 5.7: Typical plot of the local strain  $u$ , here for  $t = 72d$ . The length of the vector  $u$  mainly depends on the gradient of  $c_4$  and is hence largest near  $\partial\Omega$ .

To illustrate the stretching effect, Fig. 5.8 displays a subsection of  $\Omega$  and shows the influence of elasticity to the shape of the chalcopyrite phase. The two pictures are taken at identical time from two calculations with identical physical parameters and initial data.

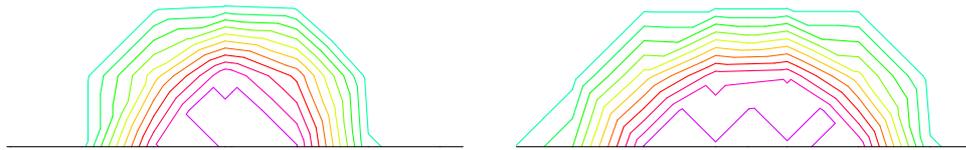


Figure 5.8: Enlargement of a section located at the left bottom of  $\partial\Omega$ . The straight line is part of the boundary. Left the shape of the chalcopyrite phase without elasticity (Model I), right with elasticity.

The following picture illustrates the effect of elasticity in more clarity.

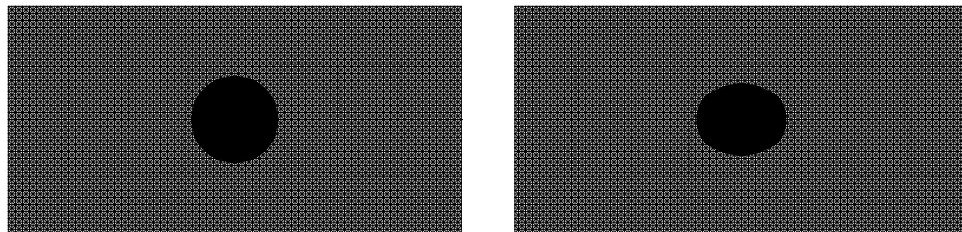


Figure 5.9: Comparison of the shape of the transition layer between sphalerite and chalcopyrite. Left without elasticity, right with elasticity. In the background, the underlying triangulation is rendered.

## 5.5 Finite element computations with the tabulated free energy

In the following we present some finite-element computations in  $2D$ . The free energy is computed beforehand by the harmonic approximation. The results will depend on the number of sub-divisions  $M_2 = M_4 = 30$ ,  $M_3 = 40$  of the free energy data bases w.r.t.  $c_j$ , see Section 4.2, on the cutoff value 50 that bounds the maximal number of generated atomistic configurations, see Section 5.2, and finally on the number of 27 unit cells that form the supercell. As mentioned before, larger values for these parameters would be desirable.

The following Fig. 5.10 illustrates the development of the phase parameter  $\chi$  for Model II and free energy gained by GULP computations. The main effect is that  $\chi$  flips over from the sphalerite to the chalcopyrite phase as Cu penetrates the domain.

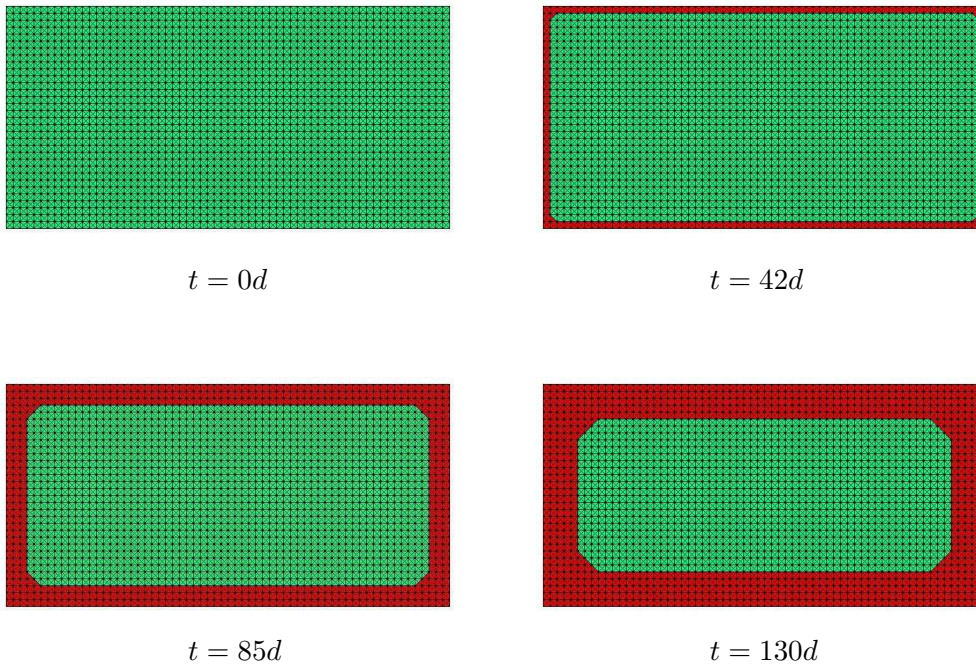


Figure 5.10: Evolution of  $\chi$  for Model III with constant surface energy and free energy computed by the harmonic approximation

The plots of Figure 5.10 do not show the delicate interplay between chalcopyrite phases and sphalerite phases close to the boundary as observed in nature (documented by Figure 1.1) and in experiment, but are quite regular. The complicated shape of the chalcopyrite phases close to the crystal boundary is a consequence of a competition between surface energy and volumetric free energy. This effect is captured neither by Model II nor by Model III. Even if we calculated the surface energy correctly for the different configurations that occur in the model (instead of setting it to the constant  $\int_{\Omega} \gamma |\nabla \chi|^2$  for Model II respectively to  $\int_{\Omega} \gamma |\nabla \chi|$  for Model III) the situation sketched in Figure 5.10 would not change significantly. This is due to a perfect symmetry with respect to the circular level sets of  $c_3$ .

Rather, the impurities play an important role as nucleation centers.

In order to demonstrate this effect, we make the following test. We decompose  $\Omega$  in two disjoint subsets,  $\Omega := \Omega_1 \cup \Omega_2$ , where  $\Omega_1, \Omega_2$  are invariant w.r.t. time, and set artificially  $\chi := 1$  in  $\Omega_1$  for  $t \geq 0$ . The set  $\Omega_1$  is not simply connected and consists of randomly chosen elements of the triangulation  $\mathcal{T}_h$  that do not touch  $\partial\Omega$ . The elements in  $\Omega_1$  will play the role of impurities. In case of Model III, the mathematical formulation reads now:

Find for  $t \geq 0$  the vector  $c = (c_2, c_3, c_4)$  and  $\chi$  such that in  $\Omega \subset \mathbb{R}^D$  for  $t > 0$

$$\begin{aligned} \partial_t c_i &= \operatorname{div} \left( \sum_{j=2}^4 L_{ij} \nabla \mu_j \right), \quad i = 2, 3, 4, \\ \mu_i &= \chi \frac{\partial f^1}{\partial c_i}(c) + (1 - \chi) \frac{\partial f^2}{\partial c_i}(c), \quad i = 2, 3, 4, \\ F(c, \chi) &= \min_{\tilde{\chi} \in \tilde{V}} F(c, \tilde{\chi}), \\ \tilde{V} &:= \{ \tilde{\chi} \in BV(\Omega) \mid \tilde{\chi}(1 - \tilde{\chi}) = 0 \text{ a.e. in } \Omega, \chi = 1 \text{ a.e. in } \Omega_1 \} \end{aligned}$$

and for  $t = 0, x \in \Omega$

$$c_i(x, 0) = c_{0i}(x), \quad i = 2, 3, 4; \quad \chi(x, 0) = \chi_0(x)$$

and for  $t > 0, x \in \partial\Omega$

$$\begin{aligned} \partial_\nu \chi &= 0, \\ c_i &= g_i, \quad 2 \leq i \leq 4, \\ \mu_i &= h_i, \quad 2 \leq i \leq 4. \end{aligned}$$

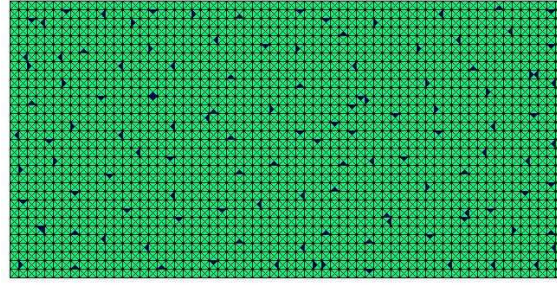
In order to have a consistent formulation, we demand  $\chi_0 \equiv 1$  in  $\Omega_1$ .

Figure 5.11 shows the evolution of the phase parameter for this modification. Due to the constraint  $\chi := 1$  in  $\Omega_1$ , those elements  $T_i \in \mathcal{T}_h$  with  $\overline{T_i} \cap \overline{\Omega_1} \neq \emptyset$  can flip over more easily because this shortens the interface between sphalerite phase and chalcopyrite phase. This introduces unsymmetry into the model.

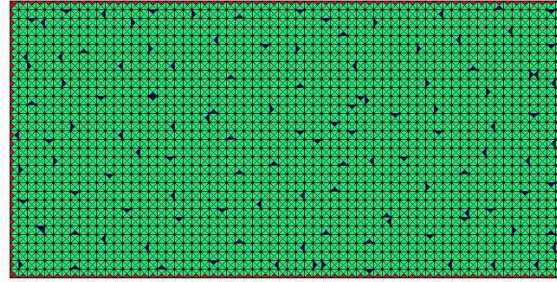
As is of course well understood, the resolution of the computations is rather poor in comparison to the size of impurities in experiment and in nature. The computations only serve as a demonstration of the principle.

Finally we want to formulate a list of fundamental differences between Model I with order-disorder logarithmic free energy and Model II, Model III.

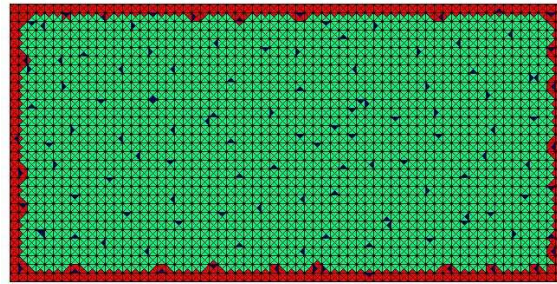
- In Model I the initial datum  $\chi_0$  of  $\chi$  significantly governs the behavior of  $\chi$  for  $t > 0$ . Depending upon  $\operatorname{sgn}(\chi - 0.5)$ , the solution will tend to one of the local minima of  $f$ . By  $m(c_3)$  it is only controlled which of the minima is more favorable.
- Once Model I has reached a local minimum of the free energy, the solution stays in this minimum forever. This means in particular that no flipping from sphalerite phase to chalcopyrite phase is possible in Model I. Changes of  $\chi$  during the late stages of the computation to 5.3 are only due to diffusion (with flux  $\gamma \nabla \chi$ ). This also puts new light on the initial random datum  $\chi_0$  in Fig. 5.3. When starting with the physically correct initial datum  $\chi_0 \approx 0$  for sphalerite, no chalcopyrite could ever form!



$t = 0d$



$t = 19d$



$t = 45d$

Figure 5.11: Evolution of  $\chi$  for Model III with constant surface energy, free energy computed by the harmonic approximation, and 'Impurities'

- For certain values of the copper concentration  $c_3$ , with Model III and Model II there will be no formation of chalcopyrite whereas some quantity of chalcopyrite will always form for Model I due to the random initial values of  $\chi$  (but a much smaller amount than sphalerite).

It remains to explain how the minimisation process corresponding to Eq. (2.32) is implemented numerically. This part logically belongs to Chapter 4, but can be better understood after the applications with Figure 5.11 and Figure 5.10 have been introduced.

## 5.6 Free energy minimisation for Model III

The algorithm presented here is a simple variant of the *Fast Marching Method*, extensively discussed in [67]. We want to assume that at  $t = 0$  a transition layer  $\Gamma(t = 0)$  between sphalerite phase and chalcopyrite phase exists.

This transition layer is implicitly given as zero level set of a function  $\Phi : \Omega_{T_0} \rightarrow \mathbb{R}$ ,

$$\Gamma(t) = \{x \in \Omega \mid \Phi(x, t) = 0\}.$$

If  $v \in \mathbb{R}$  denotes the speed of the front  $\Gamma$ , the front motion can be formulated within the framework of hyperbolic conservation laws,

$$\Phi_s + v|\nabla\Phi| = 0. \quad (5.14)$$

A new time variable  $s \geq 0$  is introduced here because the propagation of  $\Gamma$  has to be done for each time step  $t$  of the full system (2.31) as an inner loop. The mapping  $s \mapsto \Phi(\cdot, s)$  defines a time evolution independent of  $t$ .

The original fast marching method consists in restricting to a small band of triangles belonging to the triangulation  $\mathcal{T}_h$  of  $\Omega$  close to  $\Gamma(t)$  with nodes  $(x_j)_{j \in J}$  and updating  $\Phi|_{x_j}$  in 'upwind direction' from smaller values of  $\Phi$  to larger values of  $\Phi$ . This goes along with the direction of the characteristics of the hyperbolic problem (5.14), hence with the way information is transported in the corresponding physical problem.

There is one simplification to the original fast marching method at hand here because the diffusion induced segregation process is not time-reversal. This means that an element  $T_i \in \mathcal{T}_h$  once it has switched from sphalerite to chalcopyrite never flips back at later time. Hence, the front speed  $v$  is always positive and the small band close to  $\Gamma$  can be placed in only one direction of the two normal directions  $\pm \vec{n}$  to  $\Gamma$ . The minimisation problem (2.32) is now solved by propagating  $\Gamma$  for  $s > 0$  due to the Hamilton-Jacobi equation (5.14) and flipping an element  $T_i$  adjacent to  $\Gamma$  whenever this decreases the free energy  $F$  defined in Eq. (2.34).

The algorithm for every discrete time step  $t_k = k\Delta t > 0$  consists hence of the following steps:

1. Set  $\tilde{\Gamma}(s = 0) := \Gamma(t_{k-1})$ , where  $\Gamma(t_{k-1})$  denotes either the front computed at the end of time step  $t_{k-1}$  or is given as the starting front at  $t = 0$ . For the computations of Figure 5.10 we set  $\Gamma(t = 0) := \partial\Omega$  and for the computations of Figure 5.11 we have  $\Gamma(t = 0) := \partial\Omega \cup \partial\Omega_1$ .
2. Evolve  $\tilde{\Gamma}(s)$  as explained above for small constant front speed  $v > 0$  by flipping an element  $T_i$  whenever this decreases  $F$ .
3. Set  $\Gamma(t_k) := \lim_{s \rightarrow \infty} \tilde{\Gamma}(s)$ .

For the computations of Figure 5.10 without 'impurities' where a simple front starting from  $\partial\Omega$  moves inward it would be possible to define  $\tilde{\Gamma}(s = 0)$  in terms of a suitable level set of  $c_3$ . The difficulty with this variant is that such a level set of  $c_3$  first has to be projected to the triangulation  $\mathcal{T}_h$ .

## Chapter 6

# Discussion of the Results and Outlook

The first main topic of the present work is an analysis of the nature of reactions in the context of phase change problems and the correlation of reactions to the free energy estimate or the second law of thermodynamics. It could be shown how common formulas to describe reactions have to be modified in order to account for the introduced order parameter. In particular Condition (2.17) plays a key role to characterise reactions.

The treatment of the reaction term in the existence proof is quite instructive. In the semi-implicit scheme (3.7), in particular in (3.7a), the reaction term is treated explicitly. The proof of the a-priori estimate Lemma 3.3, see Eq. (3.20), indicates that this is the canonical formulation of the problem and goes along with the estimation  $\int_{\Omega} \sum_i r_i \mu_i \leq 0$  and the structure expressed in Formula (2.17). Hence there is a natural connection between the free energy estimate (or entropy estimate in the non-isothermal case) and the semi-implicit time discretisation. We remark that the reaction term cannot be written as minimum of an energy functional (hence the explicit treatment in the time-discrete scheme). It rather fulfills a saddle point condition w.r.t. concentration and chemical potential.

Beside the reaction term, these other aspects of Model I deserve a remark:

- The free energy  $f$  and the function  $m(c)$  were gained theoretically and have no direct connection to the sphalerite-chalcopyrite-system.
- There is no analysis of micro structure.
- The control mechanism to the phase parameter only enables us to represent the generation of chalcopyrite in the early stages of the simulation. A flipping over from sphalerite phase to chalcopyrite phase is not possible for the model. This goes along with unphysical initial values for  $\chi$ .
- The set of variables  $d$  with  $d_i = c_i$  for  $i \neq 2$  and  $d_2 = c_1 + c_2$ , as introduced in page 26, is the most natural way to formulate the mathematical system. The reason is that for fixed  $d_2 = c_1 + c_2$  the variable  $d_1 = c_1$  also describes the free electrons. Nevertheless it was decided to prefer Formulation (2.29), because it allows to handle more easily the investigations of existence and uniqueness as well as the numerical simulations. A transformation between the two formulations is of course trivial.

The introduction of

$$\int_{\Omega} \lambda |\nabla c|^2$$

as a term in the free energy functional in the beginning of Chapter 3 is necessary to estimate  $\frac{1}{2h} \|c - c^{m-1} - hr^{m-1}\|_L$ , as Estimate (3.4) underlines. Without this additional surface term, Lemma 3.1 will be wrong, i.e. one cannot proof the existence of a minimiser with the methods of Chapter 3, at least as long as one considers solutions in  $H^{1,2}(\Omega)$  and not in  $L^2(\Omega)$ . For the case of solutions  $c \in L^2(\Omega)$  the techniques developed in [1] are well suited.

The smallness condition (A4.2) on  $\lambda$  indicates that the approximation scheme of Chapter 3 is unphysical. Probably, the reaction term should be modified in order to account for  $\int_{\Omega} \lambda |\nabla c|^2$  in the free energy. The same difficulty is encountered in Section 2.8 where it is shown that constant, i.e. non-solution-dependent, surface energy terms as for instance

$$\int_{\Omega} \left( \frac{1}{2} \Lambda \nabla c : \nabla c + \frac{\gamma}{2} |\nabla \chi|^2 \right) \quad (6.1)$$

are wrong in the context of reactive systems. It is mandatory that the interfacial energy must depend on  $\chi$  and  $c$ , even though it is common practice in simpler models to introduce constant coefficients in the surface energy.

Solution-dependent tensors  $\Lambda$  are not new but are commonly used to model anisotropic diffusion, i.e.  $\gamma(\chi) = \gamma_0 \cos(\alpha)$ , where  $\gamma_0 > 0$  is a constant and  $\alpha$  denotes the angle between  $\nabla \chi \neq 0$  and a preferred direction, e.g. a fixed canonical basis vector of  $\mathbb{R}^D$ . In the physical derivation of the standard segregation models, e.g. the Cahn-Hilliard model [22], the surface tensor is set up correctly as non-constant quantity.

As second main issue of this work it was tried to simulate diffusion induced segregation closer to reality. As could be seen, the simulations were able to capture some of the properties of DIS, but several open questions remain.

Let us collect here the main physical restrictions and simplifications that Model I and Model II have in common.

- The diffusivities of  $\text{Cu}^+$ ,  $\text{Zn}^{2+}$  and of the Fe-ions are assumed to be constant.
- Impurities by other elements like Indium or Selen are not taken into account.
- The attachment of  $\text{S}^{2-}$  ions and the growth of the crystal surface is not incorporated.

A realistic representation of the diffusion process appears to be rather difficult. The diffusing  $\text{Cu}^+$  dramatically perturbs the regular lattice structure of sphalerite. Hence, diffusion will depend on additional parameters as the lattice geometry on the micro scale. A way to overcome this might be to find a description of the mechanism on the smaller scales and then to apply homogenisation techniques.

Little is known about the actual influence of impurities, but it is believed that they play a crucial role as nucleation centers in the early stages of segregation.

The mathematical models of homogeneous nucleation are not yet satisfying and further research in this direction (e.g. by analysing many-particle-models of Ising type) will hopefully yield some progress.

For the modification of Model I with linear elasticity as discussed in Section 5.4 it should be mentioned that instead of Condition (5.10) there should be a jump of  $\partial_n \sigma$  along the transition layer in accordance with the Gibbs-Thomson law (this is well known for the Stefan problem with kinetic undercooling).

It follows a list of problems that arise with regard to Model II.

- MD and harmonic computations can only compute states in electronic equilibrium. Consequently, for the computations of Chapter 5, electric equilibrium is assumed. Quantum effects are neglected for the generation of the free energy data base as quantum mechanical computations are very time consuming.
- The harmonic approximation does not capture well the vibrational parts of the entropy. As the analysis of Section 5.1.2 reveals, the free energies computed with the harmonic approximation and with MD simulations may differ significantly and this effect increases as  $T$  increases. With the computer power available today it does not seem likely to use MD simulations on a large scale in the way the harmonic approximation is used in this work.
- The static and high frequency dielectric constants  $\epsilon_{\text{stat}}$  and  $\epsilon_{\text{hf}}$  as well as the elastic constants of chalcopyrite are not known from experiment. At least the elastic parameters are needed to fit the GULP potentials. Therefore, the GULP potentials had to be fitted to quantum mechanical computations in the hope that this provides satisfying data until experimental results are at hand.
- The numerical resolution of the finite element approach is quite poor when considering the spatial scale needed to satisfyingly resolve transition layers, nucleation and impurities. This situation will not change in the near future.
- Identical intermolecular potentials were used for GULP and DLPOLY.
- There exists no a-priori justification of the density function theory used in Section 4.6. The method can only be justified a-posteriori. No absolute bounds exist for the errors of the free energy approximations gained by quantum mechanical/ab-initio computations.

The problem of resolving the electron-electron interaction is already inherent in the Schrödinger equation itself which cannot be solved for three or more particles. Hartree-Fock models (with corrections of the correlation energy) do not seem to improve the situation.

- For practical implementation reasons, the numerical effort is limited and three artificial restrictions are introduced: the size of the supercell ansatz in Section 4.4, the number of subdivisions  $M_j$  for the free energy databases in Section 4.2 and the maximal number of computed atomistic configurations per concentration vector (here 50) in Section 5.2. It is not known how the solution depends on these choices.

- Assumptions are made on the geometry of the lattice during the phase transition.
- In the Allen-Cahn equation, there appears a term

$$\alpha(\ln(\chi) - \ln(1 - \chi))$$

in order to guarantee  $0 < \chi < 1$  in  $\Omega_{T_0}$ . Every positive  $\alpha > 0$  can be used, but  $\chi$  will depend on this arbitrary parameter. It is not possible to avoid this logarithmic term in order to ensure  $0 < \chi < 1$  as long as an evolution equation for  $\chi$  is used. Cutting off the solution if  $\chi < \varepsilon_c$  or  $\chi > 1 - \varepsilon_c$  is no alternative, since this gives unrealistic kinks in the graph of  $\chi$  and the choice of the cut level  $\varepsilon_c$  strongly and artificially influences the solution. Therefore, choosing functions of bounded variation for  $\chi$  and searching the minimum of the free energy, see (2.32), is preferable.

- In the Allen-Cahn equation a constant surface energy  $\int_{\Omega} |\gamma \nabla \chi|^2$  is employed. Similarly,  $\int_{\Omega} \gamma |\nabla \chi|$  in Equation (2.32) defines a constant surface energy. The correct physical surface energy  $F_S$  is not a constant but depends on  $c$  and the atomistic configurations. In order to correctly compute  $F_S$ , pairs of atomistic configurations for both lattice geometries have to be plugged in and the surface energy has to be computed by averaging or by reasoning which configurations are unphysical.
- The numerical results for Model I, Model II and Model III stress that a satisfying theory for nucleation is needed.

One might hope to incorporate stochastic terms to the free energy of Model I and thereby introduce a way for the model to change (at least with low probability) from one phase to the other. This might be also a way towards a better understanding of nucleation. But so far, work in this direction has not been very promising, see [25].

The presented approach for chalcopyrite disease within sphalerite can certainly be transferred to simulate other phenomena of solid state physics. Yet, for metals, quantum mechanical effects cannot be neglected and the harmonic approximation will fail and yield wrong numbers.

# Appendix A

## Notations

Symbol	Meaning	Introduced
$T$	temperature	p.1
$t$	time, $t \geq 0$	p.5
$x$	coordinate of a point in physical space	p.5
$\Omega \subset \mathbb{R}^D$	bounded Lipschitz domain, representing the crystal	p.5
$T_0$	stop time of simulation	p.5
$\Omega_{T_0}$	cylinder in space time, $\Omega_{T_0} := \Omega \times (0, T_0) \subset \mathbb{R}^{D+1}$	p.5
$c_1$	concentration of $\text{Fe}^{3+}$	p.5
$c_2$	concentration of $\text{Fe}^{2+}$ (Model I)/overall Fe concentration	p.5, p.14
$c_3$	concentration of $\text{Cu}^+$	p.5
$c_4$	concentration of $\text{Zn}^{2+}$	p.5
$c_5$	vacancy concentration	p.5, p.6
$c_e$	electron concentration	p.5
$c_S$	(constant) sulphur centration	p.5
$c$	concentration vector, $c = (c_1, \dots, c_4)$	p.10
$\Sigma$	simplex of feasible concentration vectors $c$	p.26
$d_i, 1 \leq i \leq 4$	natural variables for the reaction term	p.10
$L = (L_{ij})_{1 \leq i, j \leq 4}$	positive definite mobility tensor	p.5
$\mu_i$	chemical potential of $i$ -th substance	p.6
$\mu$	vector of chemical potentials, $\mu = (\mu_1, \dots, \mu_4)$	p.6
$\nabla \mu$	$\nabla \mu = (\frac{\partial \mu_i}{\partial x_j})_{1 \leq i \leq 4, 1 \leq j \leq D}$	p.6
$\partial_i a$	$\partial_i a = \frac{\partial a}{\partial x_i}, 1 \leq i \leq D$ for a function $a : \mathbb{R}^D \rightarrow \mathbb{R}$	p.16
$J = L \nabla \mu$	mass flux	p.6
$\text{div} j$	divergence of a function $j : \mathbb{R}^D \rightarrow \mathbb{R}, \text{div} j = \sum_{i=1}^D \partial_i j$	p.5
$\Delta a$	Laplacian of a function $a : \mathbb{R}^D \rightarrow \mathbb{R}, \Delta a = \sum_{i=1}^D \frac{\partial^2 a}{\partial x_i^2}$	p.19
$\vec{\nu}$	unit outer normal to $\partial \Omega$	p.19
$a \cdot b = \sum_{i=1}^D a_i b_i$	inner product of vectors $a, b$	p.19
$A^t$	transpose of a linear mapping $A$	p.87
$A : B$	inner product, $A : B := \text{tr}(A^t B) = \sum_{ij} A_{ij} B_{ij}$	p.23
$\text{diag}(\lambda_i)$	tensor with $\lambda_i \in \mathbb{R}$ as diagonal entries	p.23
$f_l$	theoretical free energy density of phase $l, l = 1, 2$	p.6
$f^l(c)$	free energy density of phase $l$ taken from data-base	p.15
$f^l(c, \chi)$	decomposition of $f$ in convex ( $f^1$ ) and sublinear part ( $f^2$ )	p.28
$f$	free energy density	p.7

$F$	total free energy, $F = \int_{\Omega} f$	p.11
$s_M$	density of mixing entropy	p.7
$s$	entropy density	p.7
$e$	internal energy density	p.7
$\gamma$	square of thickness of boundary chalcopyrite-sphalerite	p.7
$W$	double-well potential in definition of $s_M$	p.7
$\alpha_i$	energy coefficient related to the ion radius of substance $i$	p.6
$\beta_i^l$	factors in definition of $f^l$ , $l = 1, 2$	p.6
$b^l$	normalisation of coefficients $\beta_i^l$ , $l = 1, 2$	p.11
$b_{\chi}$	factor in free energy, $b_{\chi} = \chi b^1 + (1 - \chi)b^2$	p.11
$\bar{\alpha} > 0$	additive constant in the driving force for $\chi$	p.12
$\chi$	volume fraction of chalcopyrite phase	p.7
$\tau$	time scale adjustment in the Allen-Cahn equation	p.7
$\omega$	driving force in the Allen-Cahn equation	p.7, p.28
$r_i$	reaction terms	p.9
$k, \kappa k$	reaction rates of Fe-reaction	p.9
$c_{0i}$	initial values for $c_i$	p.13
$g_i$	Dirichlet data for $c_i$	p.13
$h_i$	Dirichlet data for $\mu_i$	p.13
$Q(c)$	quadratic approximation for elastic energy	p.19
$V$	$V := \{\chi \in BV(\Omega) \mid \chi(1 - \chi) = 0 \text{ a.e. in } \Omega\}$	p.15
$\text{\AA}$	length scale Angström, $1\text{\AA} = 10^{-10}m$	p.18
$\hbar$	Planck's constant, $\hbar \approx 6.63 \cdot 10^{-34}Js$ ,	p.59
$J$	Joule	p.18
$eV$	electron volt, $1eV \approx 1.60 \cdot 10^{-19}J$	p.18
$Ha$	Hartree, $1Ha \approx 27.211eV$	p.74
$\varepsilon_0$	electric field constant, $\varepsilon_0 \approx 8.85 \cdot 10^{-12}AsV^{-1}m^{-1}$	p.58
$k_B$	Boltzmann constant, $k_B \approx 1,38 \cdot 10^{-23}JK^{-1}$	p.6
$\sigma_1, \sigma_2, \sigma_3$	constants defining the sup/inf of $c_i$ in $\Omega_{T_0}$	p.20
$C, \text{const}$	generic constants that can change from line to line	p.26
$\lambda$	small parameter for surface energy term in $F$	p.26
$\lambda_0$	maximal value for $\lambda$ with $\partial_t F(c(t), \chi(t)) \leq 0$	p.29
$X_1, X_2$	solution spaces	p.26
$Y$	space of test functions, $Y := H_0^{1,2}(\Omega; \mathbb{R}^4)$	p.26
$\mathcal{D}$	dual of $Y$ , $\mathcal{D} := H^{-1,2}(\Omega)$	p.27
$r^{m-1}$	abbreviation for reaction term, $r^{m-1} = r(c^{m-1}, \chi^{m-1})$	p.28
$\mathcal{G}$	Green's operator, inverse of $-\text{div}(L\nabla\mu)$ in a weak sense	p.27
$(\cdot, \cdot)_{L^2}$	inner product in $L^2(\Omega)$ , $(v_1, v_2)_{L^2} := \int_{\Omega} v_1(x)v_2(x) dx$	p.27
$(\cdot, \cdot)_L$	$L$ scalar product, $(v_1, v_2)_L := (L\nabla\mathcal{G}v_1, \nabla\mathcal{G}v_2)_{L^2}$	p.27
$\ \cdot\ _L$	$L$ -norm, $\ v\ _L := \sqrt{(v, v)_L}$	p.27
$\eta$	small parameter for GMRES	p.54
$\delta_{ij}$	Kronecker delta, $\delta_{ij} = 1$ for $i = j$ , $\delta_{ij} = 0$ for $i \neq j$	p.55
$M_j$	dimension of free energy data base w.r.t. $c_j$	p.56
$R_l$	no. of atomistic samples representing $c_i^j$ to compute $f^l(c_i)$	p.66
$\varepsilon_{\text{stat}}$	static dielectric constant	p.61
$\varepsilon_{\text{hf}}$	high-frequency dielectric constant	p.61
$\Omega_1$	subset of $\Omega$ preset to chalcopyrite phase	p.92
$\Omega_2$	subset of $\Omega$ without 'impurities', $\Omega_2 := \Omega \setminus \Omega_1$	p.92
$D_{Zn}$	diffusivity constant of Zn	p.86
$D_{Fe}$	diffusivity constant of Fe	p.86

$D_{\text{Cu}}$	diffusivity constant of Cu	p.86
$\beta$	parameter in the Boltzmann distribution, $\beta = (k_B T)^{-1}$	p.59
$Q$	elastic energy	p.87
$\sigma$	stress tensor	p.87
$u$	displacement vector $u = (u_1, \dots, u_D)$	p.86
$\varepsilon$	(linearised) strain tensor, $\varepsilon(u) = \frac{1}{2}(\nabla u + \nabla u^t)$	p.75, p.87
$a, b, c$	lattice constants of unit cell	p.61
$C_{ij}$	elastic constants	p.61
$V$	volume of unit cell	p.61

# Appendix B

## Mathematical Symbols

### B.1 Function spaces

Let  $\Omega \subset \mathbb{R}^d$  be open,  $1 \leq d \leq 3$ ,  $1 \leq p \leq \infty$ ,  $m \in \mathbb{N}_0$ , and let  $\mathcal{L}^d$  denote the Lebesgue measure in  $\mathbb{R}^d$ . We define the following spaces:

1.  $C_0^\infty(\Omega)$  denotes the space of infinitely often differentiable functions with compact support in  $\Omega$ .
2.  $C^m(\overline{\Omega})$  is the space of  $m$ -times continuously differentiable functions over  $\Omega$  such that  $D^\alpha f$  can be continuously extended for  $|\alpha| \leq m$  to  $\overline{\Omega}$ .  $C^m(\overline{\Omega})$  is a Banach space with the norm

$$\|f\|_{C^m(\overline{\Omega})} := \sum_{|\alpha| \leq m} \sup_{x \in \Omega} |D^\alpha f(x)|.$$

3.  $L^p(\Omega)$  denotes the space of Lebesgue measurable and  $p$ -integrable functions over  $\Omega$ , equipped with the norm

$$\begin{aligned} \|f\|_{L^p(\Omega)} &:= \left( \int_{\Omega} |f(x)|^p dx \right)^{\frac{1}{p}}, \quad p < \infty, \\ \|f\|_{L^\infty(\Omega)} &:= \operatorname{ess\,sup}_{x \in \Omega} |f(x)| := \inf_{\mathcal{L}^d(N)=0} \sup_{x \in \Omega \setminus N} |f(x)|, \quad p = \infty. \end{aligned}$$

4.  $H^{m,p}(\Omega)$  is introduced as the Sobolev space of functions in  $L^p(\Omega)$  that possess weak derivatives up to order  $m$  in  $L^p(\Omega)$ .  $H^{m,p}(\Omega)$  is a Banach space. For  $p < \infty$  the corresponding norm is

$$\|f\|_{H^{m,p}(\Omega)} := \left( \sum_{k=0}^m \|D^k f\|_{L^p(\Omega)} \right)^{\frac{1}{p}}$$

where

$$\|D^k f\|_{L^p(\Omega)}^p := \sum_{|\alpha| \leq k} \|D^\alpha f\|_{L^p(\Omega)}^p, \quad D^\alpha f := \frac{\partial^{|\alpha|} f}{\prod_{i=1}^d \partial_i^{\alpha_i}} \quad \text{for } \alpha \in \mathbb{N}_0^d.$$

5. With  $H_0^{m,p}(\Omega)$ ,  $1 \leq p < \infty$  we denote the closure of  $C_0^\infty(\Omega)$  in  $H^{m,p}(\Omega)$  w.r.t.  $\|\cdot\|_{H^{m,p}}$ . Frequently we write  $H^m(\Omega)$  instead of  $H^{m,2}(\Omega)$  and  $H_0^m(\Omega)$  for  $H_0^{m,2}(\Omega)$ .
6. For  $T_0 > 0$  and functions  $u : \Omega \times (0, T_0) \rightarrow \mathbb{R}$  we define  $L^p(0, T_0; H^q(\Omega))$  as the set of functions for which the expression

$$\begin{aligned} \|u\|_{L^p(0, T_0; H^q)} &:= \left( \int_0^{T_0} \|u(s)\|_{H^q(\Omega)}^p ds \right)^{1/p} && \text{if } p < \infty, \\ \|u\|_{L^\infty(0, T_0; H^q)} &:= \operatorname{ess\,sup}_{t \in (0, T_0)} \|u(t)\|_{H^q(\Omega)} && \text{if } p = \infty \end{aligned}$$

is finite.

7. For a function  $u \in L^1(\Omega)$  let

$$\|Du\| := \sup \left\{ \int_{\Omega} u \operatorname{div} \varphi \mid \varphi = (\varphi_1, \dots, \varphi_d) \in C_0^\infty(\Omega, \mathbb{R}^d), \|\varphi\|_{\infty, \Omega} \leq 1 \right\}$$

and define

$$\|u\|_{BV(\Omega)} := \|u\|_{L^1(\Omega)} + \|Du\|.$$

A function of bounded variation is now characterised by  $\|u\|_{BV(\Omega)} < \infty$ .

Alternatively,  $u \in BV(\Omega)$  if and only if there exist (signed) Radon measures  $\mu_1, \dots, \mu_d$  in  $\Omega$  such that  $|D\mu_i|(\Omega) < \infty$  and

$$\int_{\mathbb{R}^d} u D_i \varphi = - \int_{\mathbb{R}^d} \varphi d\mu_i \quad \forall \varphi \in C_0^\infty(\Omega).$$

Hence, the partial derivatives of BV-functions are measures with finite total variation.

Additional definitions and background knowledge concerning the spaces just introduced can for instance be found in [4], [76], [34].

## B.2 Vector- and tensor notations

Let  $a$  and  $b$  be vectors.  $a \otimes b$ , the tensor product of vectors  $a$  and  $b$  is the tensor defined by the equality  $(a \otimes b) : c = (b \cdot c)a$  for all vectors  $c$ . For a matrix  $A = (A_{ij})_{ij}$  let  $A^t := (A_{ji})_{ij}$  be the transposed of  $A$ .

With  $\partial_j := \frac{\partial}{\partial x_j}$  we denote the  $j$ -th partial derivative w.r.t. coordinate  $j$ . Divergence, gradient and Laplace operator of a scalar field  $\chi$  are denoted by  $\nabla \chi$ ,  $\operatorname{div} \chi$  and  $\Delta \chi$ . For a vector field  $u(x)$  let  $\nabla u(x)$  be the tensor with entries  $(\partial_i u_j)_{ij}$ ,  $i$ =line index,  $j$ =column index. Let  $A = A_{ij}$  and  $B = B_{ij}$  be two tensor fields. The divergence of  $A$  is the vector with components  $\sum_j \partial_j A_{ij}$  and  $A : B$  is the scalar function defined by  $\sum_{ij} A_{ij} B_{ji}$ .

The derivative of a scalar function  $f$  is denoted by  $f'$ , the Fréchet derivative of a field  $u(x)$  by  $Du(x)$ .

# Bibliography

- [1] S. Arnrich, T. Blesgen and S. Luckhaus "A mathematical model for Phase Transitions in Crystals", Preprint of the DFG priority programme 1095 "Analysis of Multiscale Problems", 2002
- [2] S.M. Allen, J.W. Cahn, "A microscopic theory for antiphase boundary motion and its application to antiphase domain coarsening", *Acta Metallurgica* **27**, pp. 1085-1095, 1979
- [3] D. Alfe, G.D. Price and M.J. Gillan, "Thermodynamics of hexagonal-close-packed iron under Earth's core conditions", *Journal of Comp. Phys.* **7** 2002
- [4] H.W. Alt, "Lineare Funktionalanalysis", 2nd Edition, Springer 1992
- [5] H.W. Alt, I. Pawlov, "A mathematical model of dynamics of non-isothermal phase separation" *Physica D*, **59**(1992), pp. 389-416
- [6] H.W. Alt, S. Luckhaus, "Quasilinear elliptic parabolic differential equations", *Math. Z.*, **183**(1983), pp. 311-338
- [7] H. Aman, "Ordinary Differential Equations: An introduction to nonlinear analysis", de Gruyter 1990
- [8] Ashcroft, Mermin, "Solid State Physics", Saunders College Pub. 1976
- [9] H. Attouch, "Variational convergence for functions and operators", Pitman Boston 1984
- [10] Barton, Toulmin, *Econ. Geol.* **61**(1966),pp. 815-849
- [11] M.S. Bazaraa, H.D. Sherali and C.M. Shetty, "Nonlinear programming, theory and algorithms", Wiley 1993, 638p.
- [12] K. Bente, T. Doering, *Eur. J. Mineral.* **10**(1993):465
- [13] K. Bente, T. Doering, *Min. Petrol* **53**(1995) pp. 285-305
- [14] K. Bente, P. Lepetit, private communication
- [15] T.Blesgen, "A Generalisation of the Navier-Stokes equations to Two-Phase Flows", *Journal of Phys. D* **32**(1999), pp. 1119-1123
- [16] T.Blesgen, "A fluid mechanical model and numerical computations of two-phase flows", *Ass. Mechanics and Eng. Sci.* **7**(2000), pp. 403-412
- [17] T. Blesgen, U. Weikard, "A sharp interface Model for Phase Transitions in Crystals with Linear Elasticity", *Comm. Part. Diff. Eq.*, to appear

- [18] R. Blink and B. Zeks, "Soft modes in Ferroelectrics and Antiferroelectrics", North-Holland, Amsterdam 1974
- [19] H. Brézis, "Analyse Fonctionnelle, théorie et applications", Mason 1983
- [20] M.O. Bristeau, R. Glowinski and J. Periaux, "Numerical methods for the Navier-Stokes equations: Applications to the simulation of compressible viscous flows", Computer Physics Report, Research Report UH/MD 4, Univ. of Houston, 1987
- [21] P. N. Brown, SIAM J. Num. Anal. **24**(1987) pp. 407-434
- [22] J.W. Cahn, J.F. Hilliard, "Free energy of a non-uniform system I. Interfacial energy", J.Chem. Phys. **28**(1958), pp. 258-267
- [23] P.G. Ciarlet, "The Finite Element Method for Elliptic Problems", Soc. Ind. and Appl. Math., 2002
- [24] B. Dacorogna, "Direct Methods in the Calculus of Variations", Springer New York 1989
- [25] N. Dirr, S. Luckhaus, "Mesoscopic limit for nonisothermal phase transitions", Markov Processes **7**, 3 (2001), pp. 355-382
- [26] B.G. Dick and A.W. Overhauser, "Theory of the dielectric constants of alkali halide crystals", Phys. Rev. **112**(1958), pp. 90-103
- [27] M.T. Dove, "Introduction to Lattice Dynamics", Cambridge University Text, 1993
- [28] M.T. Dove, "Structure and Dynamics: an atomic view of materials", Oxford Univ. Press 2003
- [29] C.M. Elliott and S. Luckhaus, "A generalised diffusion equation for phase separation of a multi-component mixture with interfacial free energy", preprint SFB 256, University Bonn (1991)
- [30] J.D. Eshelby, "Elastic inclusions and inhomogeneities", Prog. Solid Mech. **2**, (1961), pp. 89-140
- [31] C.M. Elliott und Z. Songmu, "'On the Cahn-Hilliard Equation'", Arch. Ration. Mech. Anal. **96** (1986), pp. 339-357
- [32] L.C. Evans and R.F. Gariepy, "Measure Theory and Fine Properties of Functions", CRC Press, Boca Raton, Ann Arbor, London 1992
- [33] P.P. Ewald "Die Berechnung optischer und elektrostatischer Gitterpotentiale", Ann. Phys. **64**(1921), pp. 253-287
- [34] H. Federer, "Geometric Measure Theory", Springer, Berlin, Heidelberg, New York 1996
- [35] P. Fletcher, "Chemical Thermodynamics", Longman Scientific, Essex 1993
- [36] D. Frenkel and B. Smit, "Understanding Molecular Simulation", Academic Press, San Diego 1996

- [37] J.D. Gale, "GULP-A Computer program for the symmetry adapted simulation of solids", *JCS Faraday Trans.*, **93**(1997), p. 629
- [38] H. Garcke, "On mathematical models for phase separation in elastically stressed solids", habilitation thesis, Bonn (2001)
- [39] D. Gilbarg und N.S. Trudinger, "Elliptic Partial Differential Equations of Second Order", 2nd Edition, Springer 1998
- [40] X. Gonze, J.-M. Beuken, R. Caracas, F. Detraux, M. Fuchs, G.-M. Rignanese, L. Sindic, M. Verstraete, G. Zerah, F. Jollet, M. Torrent, A. Roy, M. Mikami, Ph. Ghosez, J.-Y. Raty, D.C. Allan, "First-principles computation of material properties : the ABINIT software project", *Computational Materials Science* **25** (2002), pp. 478-492
- [41] P. Grindrod, "The theory and application of reaction-diffusion equations, patterns and waves", 2nd Edition, Clarendon Press, Oxford 1996
- [42] M.E. Gurtin, "On a nonequilibrium thermodynamics of capillarity and phase", *Quart. Appl. Math.*, **47**(1989), pp. 129-145
- [43] P. Hohenberg, W. Kohn, *Phys. Rev. B* **136**(1964), p.136
- [44] O'Keefe, "Structure and Bonding in Crystals", Academic Press 1981.
- [45] C.T. Kelley, "Iterative Methods for Linear and Nonlinear Equations", SIAM Frontiers in Appl. Math., Philadelphia 1995
- [46] R. Kobayashi, "Modeling and numerical simulations of dendritic crystal growth", *Physica D* (1993), pp. 410-423
- [47] W. Kohn, L.J. Sham, *Phys. Rev. A* **140**(1965), p.1133
- [48] T. Kratz, H. Fuess, *Z. Kristall.***186**(1989), p.167-169
- [49] P.H. Leo, J.S. Lowengrub and H.J. Lou, "A diffuse interface model for microstructural evolution in elastically stressed solids", *Acta Metall.*, **37**(1989), pp. 3119-3138
- [50] J. Leray, "Essai sur les mouvements plans d'un liquide visqueux que limitent des parois", *J. Math. Pures Appl.*, **13**(1934), pp.331-418
- [51] S. Luckhaus, A. Visintin, "Phase transitions in multicomponent mixtures", *Manuscripta Math.* **43**(1983), pp.261-288
- [52] S. Luckhaus, "The Stefan problem with the Gibbs Thompson law" Report 591 of the Dipartimento di Matematica de Pisa, 1991
- [53] J.J. Mahoney and J. Norbury, "Asymptotic location of nodal lines using geodesic theory", *J. Austr. Math. Soc. Ser. B*, **27**(1986)
- [54] E.H. Nickel, Information Circular IC 170, Department of Mines
- [55] P. Nelkowski and S. Bollman, *Min. Petrol.* 27 (1969) Technical Surveys, Ottawa 1965
- [56] J.F. Nye, "Physical Properties of Crystals", Clarendon Press, Oxford 1964

- [57] M.C. Payne, M.P. Teter, D.A. Allan, T.A. Arias and J.D. Joannopoulos, "Iterative minimization techniques for ab initio total-energy calculations: molecular and conjugate gradients", *Rev. Mod. Phys.* **64**(1992), p.1045-1097
- [58] K. Pitzer "Thermodynamics", 3rd Edition, Mc Graw Hill 1995
- [59] M.H. Protter, H.F. Weinberger, "Maximum Principle in Differential Equations", 2nd Edition Springer 1999
- [60] J. Rubinstein, P. Sternberg, J. Keller, "Fast reaction, slow diffusion, and curve shortening", *SIAM J. Appl. Math.* **49**(1989), pp. 116-133
- [61] Y. Saad, *Iterative Methods for Sparse Linear Systems*, PWS Pub. Boston 1996
- [62] E.K.H. Salje and J. Novak, "Surface structure of domain walls", *J. Phys: Condens. Matter*, **10** (1998) p.359-366
- [63] E.K.H. Salje and J. Novak, "Simulated mesoscopic structures of a domain wall in a ferroelastic lattice", *European Phys. J. B*, **4** (1998), p. 279-284
- [64] E.K.H. Salje, V.Devarajan, *Phase Transitions* **6** (1986) p.235
- [65] M.J. Saunders, M. Leslie and C.R.A. Catlow, *Journ. Chem. Soc., Chem. Comm.* 1984, p.1271
- [66] E.A. Secco, *Journal of Chem. Phys.* **29**(1958), p.406
- [67] J.A. Sethian, "Level Set Methods and Fast Marching Methods", Cambridge University Press, 2nd Edition 1999
- [68] L. Simon, "Lectures on Geometric Measure Theory", *Proc. of the Centre for Math. Analysis, Vol. 3*, ANU Canberra 1983
- [69] V. Thomeè, "Galerkin Finite Element Methods for Parabolic Problems", Springer Heidelberg 1984
- [70] N. Troullier, J.L. Martins, *Phys. Rev. B* **43**(1993), p.1991
- [71] A. Visintin, "Models of Phase Transitions", Birkhäuser Boston 1996
- [72] W. Walter, "Gewöhnliche Differentialgleichungen", 6.Edition, Springer 1996
- [73] U. Weikard "Numerische Lösungen der Cahn-Hilliard-Gleichung unter Einbeziehung elastischer Materialeigenschaften", diploma thesis, University Bonn, 1998
- [74] U. Weikard, T. Blesgen "The numerical analysis of a sharp interface model for phase transitions in crystals", *Interfaces and Free Boundaries*, to appear
- [75] K. Wright, R. Jackson, "Computer Simulation of the Structure and Defect Properties of Zinc Sulfide", *J. Mater. Chem.* **5**(11)1995, pp. 2037-2040
- [76] W.P. Ziemer, "Weakly differentiable functions", Springer New York 1989